University of California
Santa Barbara

Area/Entropy Laws, Traversable Wormholes, and the Connections Between Geometry and Entanglement

A dissertation submitted in partial satisfaction
of the requirements for the degree

Doctor of Philosophy
in
Physics

by

Brianna Michelle Grado-White

Committee in charge:

Professor Donald Marolf, Chair
Professor Gary Horowitz
Professor Claudio Campagnari

September 2020

The Dissertation of Brianna Michelle Grado-White is approved.

Professor Gary Horowitz

Professor Claudio Campagnari

Professor Donald Marolf, Committee Chair

August 2020

Area/Entropy Laws, Traversable Wormholes, and the Connections Between Geometry and Entanglement

by

Brianna Michelle Grado-White

Acknowledgements

Firstly, I would like to thank my advisor, Don, for not only providing guidance, support, and ideas, but also filling the halls of the sixth floor of Broida with the sounds of echoing laughter.

Of course I am also grateful to the larger community of friends and colleagues at UCSB as a whole – Seth, Gabriel, and Alex for our little high energy theory community at UCSB; Marija for a final year of friendship and physics; and Eric Jones (and the rest of UDIP and WIP) for always caring about and improving the larger world around you.

Finally, I would like to thank my family for always being the just the right amount of crazy and passing it along to me, as it seems to be a prerequisite for studying physics.

This work was supported in part by National Science Foundation's Graduate Research Fellowship.

Curriculum Vitæ

Brianna Michelle Grado-White

Education

2020	Ph.D. in Physics (Expected), University of California, Santa Barbara.
2018	M.A. in Physics, University of California, Santa Barbara.
2015	B.A. in Physics, Mathematics, & Astrophysics, University of California, Berkeley

Publications

B. Grado-White, D. Marolf, and S. J. Weinberg, "Radial Cutoffs and Holographic Entanglement ," arXiv:2008.07022 [hep-th].

Z. Fu, B. Grado-White, and D. Marolf, "Traversable Asymptotically Flat Wormholes with Short Transit Times," Class. Quant. Grav. 36no. 24 (2019), 245018 arXiv:1908.03273 [hep-th].

Z. Fu, B. Grado-White, and D. Marolf,"A Perturbative Perspective on Self-Supporting Wormholes," Class. Quant. Grav.36no. 4, (2019) 045006, arXiv:1807.07917 [hep-th].

B. Grado-White and D. Marolf, "Marginally Trapped Surfaces and AdS/CFT," JHEP02(2018) 049, arXiv:1708.00957 [hep-th].

M. Akashi-Ronquest [and 29 others, including B. Grado-White] "Triplet Lifetime in Gaseous Argon," arXiv:1903.06706 [physics.ins-det]

Abstract

Area/Entropy Laws, Traversable Wormholes, and the Connections Between Geometry and Entanglement

by

Brianna Michelle Grado-White

We study the relationship between the geometry of spacetime and quantum information. This is motivated by recent insights which suggest that geometry is an emergent phenomenon in quantum gravity, and in particular that geometry is built from quantum entanglement.

Part I of this thesis is focused on the relationship between area and entropy. Area/entropy relations are ubiquitous in gravitating systems. One manifestation of this relationship comes from the AdS/CFT correspondence, which posits a duality between quantum gravity in asymptotically Anti-de Sitter space and certain quantum field theories that can be thought of as living on the boundary of the Anti-de Sitter spacetime. When the field theory has a large number of strongly coupled fields, the dual quantum gravity spacetime is described to good approximation by classical General Relativity. In this limit, the Hubeny-Rangamani-Takayanagi (HRT) formula relates the area of surfaces in the bulk spacetime to the entanglement entropy of associated subregions in the dual field theory. A second potential incarnation of the relationship between area and entropy comes in the form of black hole area laws and a more locally-defined generalization known as a holographic screens. We explore connections between these different notions of area and entropy by studying the properties of holographic screens in Anti-de Sitter space. We also study a (modified version) of HRT like surfaces attached to arbitrary boundaries (that need not be an Anti-de Sitter boundary).

Part II of this thesis involves the study of traversable wormholes. Physicists have long believed that wormholes that could be crossed by an observer or signal would be impossible to build. In fact it can be shown that, with only classical matter, traversable wormholes cannot exist. While it remained possible that subtle quantum effects might be able to provide the negative energy needed to build them, there were no successful attempts at doing so. Recently, however, examples were constructed in AdS that relied on putting interactions in the dual, entangled quantum systems, and thus illustrated the intimate relation between quantum entanglement and spacetime geometry. Below, we describe a general method by which to construct traversable wormholes that can be applied to any spacetime, including asymptotically flat space. We explicitly construct several examples in AdS and in flat space, and generalize the result to construct multi-mouthed wormholes. We further use these multi-mouthed wormholes to study the entanglement structure of the spacetime they reside in.

Contents

Curriculum Vitae **v**

Abstract **vi**

1 Introduction **1**
1.1 Area/Entropy Relations 3
1.2 Traversable Wormholes 10
1.3 Permissions and Attributions 18

Part I Area/Entropy Relations **19**

2 Marginally Trapped Surfaces and AdS/CFT **20**
2.1 Introduction 20
2.2 Preliminaries 22
2.3 Ordering of Surfaces 31
2.4 Divergences 38
2.5 Thermodynamics 45
2.6 Discussion 48

3 Radial Cutoffs and Holographic Entanglement **52**
3.1 Introduction 52
3.2 Introduction 52
3.3 Preliminaries 57
3.4 Main Results 66
3.5 Discussion 79

Part II Traversable Wormholes **83**

4 A Perturbative Perspective on Self-Supporting Wormholes **84**
4.1 Introduction 84

4.2 $\mathbb{Z}_2$-quotient wormholes and their Hartle-Hawking states 90
4.3 Simple traversable AdS_3 wormholes from Hartle-Hawking states 98
4.4 Rotating traversable wormholes with Kaluza-Klein zero-brane orbifolds . 112
4.5 Discussion 119

5 Traversable, Asymptotically Flat Wormholes with Short Transit Times 126
5.1 Introduction 126
5.2 Stress-energy on the horizon 134
5.3 Back-reaction and Stability 142
5.4 Discussion 148

6 Multi-mouth Wormholes 153
6.1 Introduction 153
6.2 Review of two-mouth traversable wormhole models 156
6.3 Gravitational Construction 161
6.4 Discussion 169

A $\mathrm{Mm}_\gamma(A)$ is mostly contained in the interior of $D(\gamma)$ and in γ itself 173

B First-order traversability requires a stationary horizon 175

C Counterpoint: Negative Energy causes collapse of cosmological wormholes 177

D Constructing the wormhole 181

Bibliography 185

Chapter 1

Introduction

Within their own respective regimes of validity, quantum mechanics and general relativity have offered eloquent descriptions of physics on the smallest and largest observable scales, and each theory has been experimentally verified to extremely high accuracy. While these theories are separately successful, arguably the most important unresolved problem in theoretical physics is to understand how they combine into a consistent, agreed upon theory of quantum gravity. In particular, both the early stages of the universe and the interiors of black holes intertwine the large energies governed by general relativity and the small length scales governed by quantum mechanics. Moreover, questions surrounding black hole information and entropy, for example, have often led to paradoxes and potential violations of central tenants of at least one theory, underscoring the tension between them.

While string theory offers a viable candidate theory of quantum gravity, calculations can often quickly become cumbersome (if not completely intractable), leaving many fundamental properties of our universe obscure. String theory has, however, given us a powerful tool in the form of the Anti de Sitter/Conformal Field theory (AdS/CFT) correspondence. This duality gives a nonperturbative formulation of quantum gravity by stating that a string theory living in a spacetime with asymptotically Anti-de Sit-

ter boundary conditions is dual to a Conformal Field Theory (CFT) living in one less dimension. This CFT is often thought of as living on the boundary of AdS.

To get a feel for this correspondence, we can relate parameters on each side. The 't Hooft coupling of the CFT, $\lambda = g^2 N$ (for g the gauge coupling and N the rank of the gauge theory), can be related to the string length, ℓ_s, and the radius of curvature in the asymptotically AdS spacetime, ℓ, by $\frac{\ell_s}{\ell} \propto \lambda^{-1/4}$. N can be related to the Planck length, ℓ_p, and ℓ by $\frac{\ell_p}{\ell} \propto N^{-1/4}$. We thus see that when the quantum field theory is strongly coupled and N is large, the bulk is well described by the classical gravity limit of string theory. Conversely, when the quantum field theory is weakly coupled with small N, the corresponding bulk will consist of strongly interacting strings.

In general, a purely quantum system in fewer dimensions would seem easier to understand than a higher dimensional quantum gravitational system. Indeed, studying this duality has revealed many hints about the fundamental structure of quantum gravity, and even aspects of semiclassical gravity in AdS spacetimes. One such hint has been the importance of the relationship between geometry and entanglement, and the suggestion that spacetime is not a fundamental property in quantum gravity, but instead is a property emerging from entanglement in the dual quantum system.

A caveat, however, is that these insights do not immediately translate into an understanding of the early universe or black holes that we might observe. Anti-de Sitter space is the maximally symmetric spacetime with a negative cosmological constant, whereas the apparent acceleration of the expansion of our universe means we live in a spacetime with a positive cosmological constant.

There is, however, some hope that notions of holography — the idea that certain gravitating systems can actually be described by dual systems that live in fewer dimensions — persist in general spacetimes. The first signs of this come from studying black holes, which have the surprising property that their entropy scales with the area of their event

horizon, instead of the volume inside. Various conjectures discussed in the next section have also been put forth which generalize this result to bound the entropy of general spacetime regions in terms of some characteristic area associated with the system.

The work below focuses on importing the insights about quantum gravity revealed by holography into our own universe. In particular, we focus on two particular avenues to understanding the relation between geometry and entanglement: area/entropy formulas and traversable wormholes.

1.1 Area/Entropy Relations

Though entropy is normally thought of as an extensive quantity, systems for which entropy scales with area are ubiquitous in gravity. Perhaps the most familiar example of this is a black hole, whose thermodynamic entropy scales with the area of its event horizon. AdS/CFT provides its own examples of area/entropy laws, in which entanglement entropies of the boundary quantum system can be measured by the areas of bulk surfaces. These two area/entropy relations are reviewed below, and potential connections between them are explored.

1.1.1 Black Hole Thermodynamics and Entropy Bounds

A cornerstone of gravitational physics is the realization that black holes behave as thermodynamic objects. The first hint of this came from Hawking, who showed that in physically allowed processes, the area of a black hole must increase [1]. This was shown by imposing the Null Energy Condition (a condition on the stress tensor requiring $T_{ab}k^a k^b > 0$ for k any null vector in the spacetime) which is broadly obeyed by classical matter.

While this area increase is reminiscent of the second law of thermodynamics, it was

then unclear whether this should be considered simply an analogy, or as indicative of some deeper principle. Bekenstein, however, observed that black holes could be used to apparently violate the second law of thermodynamics. To see this, note that to an outside observer, black holes can be completely characterized by their mass, charge, and angular momentum. Thus, dropping an entropic object into a black hole could effectively hide degrees of freedom behind the horizon. This led Bekenstein to conclude that, in fact, black holes themselves must carry some notion of entropy. Based on Hawking's observation, the area of the black hole's event horizon provides a natural candidate. Bekenstein proposed, in turn, that a generalized notion of entropy — the sum of the black hole's area and the entropy of matter outside — would obey the second law of thermodynamics (now deemed the Generalized Second Law) [2]. It has been further shown that black holes also satisfy an analogue of all of the laws of thermodynamics, with the surface gravity playing the role of temperature, and the mass M of the black hole playing the role of energy [3].

Here, however, another tension perhaps arises: if black holes do have a temperature given by their surface gravity, then they should radiate. The defining feature of black holes, however, is that they are regions of spacetime so curved that no information, not even light, can escape. Fortunately, this confusion was partially resolved by Hawking, who showed that once quantum effects (which can generally violate the Null Energy Condition, as discussed more below) are considered, black holes in fact radiate at a temperature proportional to their surface gravity [4]. This again underscores that black holes satisfy actual thermodynamic laws, and not some merely analogous properties.

Beyond black holes, the Generalized Second Law has motivated various conjectures bounding the information content of general spacetimes. One version of such a general bound, known as the Covariant Entropy Bound, conjectures that the entropy passing through non-expanding null sheets emanating from a surface is bound by the area of that surface [5]. In this vein, the notion of a holographic screen can also be introduced.

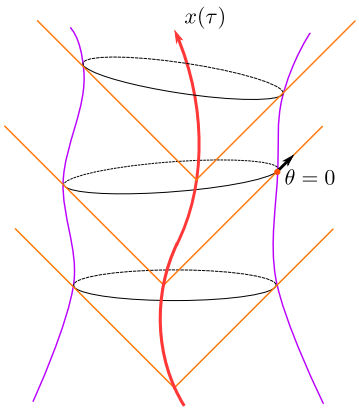

Figure 1.1: A holographic screen can be constructed by the null foliation produced by an observer's light cones. Given an spacetime path $x(\tau)$ (shown in red above), on each future lightcone emanating from that path (in orange), we can find the maximal area cross-section surface, if it exists (in black). This surface will then have non-expanding area along the lightcone (and in particular will have null expansion $\theta = 0$). Stitching together all these surfaces on all of the future lightcones associated with the observer will give us our holographic screen (in purple).

Assuming the Covariant Entropy Bound, the degrees of freedom on a light cone can be bound by the area of that lighcone's largest area cross-section (the light sheet will then have non-increasing area both to the future and past of this leaf). See figure 1.1.1. Note that when the gravitational effects are great enough for this cross-section of largest area to be compact, it is also known as a marginally trapped surface. Foliating the spacetime by the lightcones of an observer and stitching together the various largest area cross-sections (called leaves) forms a holographic screen, and the areas of its leaves would bound the degrees of freedom for the entire spacetime [6]. In [7, 8], it was shown that the areas of the leaves increase monotonically along the screen, suggesting a thermodynamic law for general spacetimes.

1.1.2 Area/Entropy Relations in AdS/CFT

While the above area/entropy relations give a vague notion of holography, as noted above the AdS/CFT correspondence gives a concrete realization of this principal, where a precise dual theory living in fewer dimensions is known. Furthermore, AdS/CFT gives rise to its own area/entropy laws, where the entanglement entropy of subregions of the boundary field theory can be measured by the area of surfaces living in the bulk.

The first proposed version of this relation was the Ryu-Takayanagi (RT) formula. Suppose we start with a static state in the dual field theory, given by a density matrix ρ. Further suppose we are interested in calculating the entanglement entropy of some spatial subregion A of a fixed time slice of the boundary. This is given by $\mathrm{Tr}\rho_A \log \rho_A$, where ρ_A is the reduced density matrix of A, formed by tracing out the degrees of freedom of the complement of A. In a quantum field theory, this quantity is UV divergent; however, if a cutoff ϵ is introduced, the leading order behavior of the entanglement entropy is given by $S_{EE}(A) = \frac{\mathrm{Area}(\partial A)}{\epsilon^{d-2}} + \mathcal{O}(\epsilon^{d-4})$, for boundary dimension $d > 2$.

If we work at large N and strong coupling, the bulk will be described by a classical, static geometry. In particular, the constant time slice of the boundary can be extended into a constant time slice in the bulk. Then, the RT formula states that entanglement entropy of A is given by the area of the minimal surface M_A on this bulk slice that contains ∂A, and is homologous to A [9],

$$S_{EE}(A) = \frac{\mathrm{Area}(M_A)}{4G_N\hbar}. \tag{1.1}$$

This formula is notably reminiscent of the Bekenstein-Hawking formula for the entropy of a black hole. As noted above, the entanglement entropy is UV divergent, and must be regulated. Likewise, the area of a minimal surface extending out to boundary is IR divergent, but can be regulated by introducing a cutoff at distance $1/\epsilon$ from the boundary.

As a consistency check, one can see that the areas of these bulk surfaces satisfy conditions known to hold for entanglement entropy. In particular, it was shown in [10] that RT surfaces satisfy Strong Subadditivity, which states that for subregions A, B and C, the corresponding entropies satisfy $S(AB)+S(BC) \geq S(ABC)+S(B)$. Additionally, the RT formula has been used to show that inequalities that need not be satisfied by general quantum systems are satisfied by holographic systems. Monogamy of Mutual information, which bounds tripartite mutual information, is one such example. Moreover, the RT formula has been derived (with certain assumptions) [11].

One major limitation of the Ryu-Takayanagi formula, however, is that it only applies to static spacetimes. In dynamical spacetimes, the bulk will not have any preferred time slicing. Without the restriction to a particular fixed time slice, minimal surfaces of arbitrarily small area can be constructed by considering slices arbitrarily close to being lightlike. Hubeny, Rangamani, and Takayanagi (HRT) proposed instead that for general spacetimes, the correct entropy measuring surface for a boundary subregion A is the bulk extremal surface anchored to ∂A, and homologous to A [12]. An equivalent formulation was given in [13], which noted that this extremal surface could be constructed by considering the minimal area surfaces on every possible spatial slice containing ∂A. Maximizing the area of these minimal surfaces over the set of spatial slices then results in the HRT surface. This procedure is known as maximin. As yet another formulation, it can also be noted that because HRT surfaces are stationary points of the area functional, they can also be characterized by the fact that the area of light sheets emanating from them are neither expanding nor contracting.

1.1.3 Holographic Screens in AdS, and Maximin in General Spacetimes

In Chapter 2, we attempt to connect the area/entropy relations of general spacetimes and those of AdS/CFT by studying the properties of holographic screens in asymptotically AdS space. Despite the apparent thermodynamic properties of holographic screens suggested by their monotonic area laws, the nature of the entropy described by holographic screens is unclear. In contrast, the HRT surfaces compute a fine grained, von Neumann entropy of the dual CFT density matrix, and thus the precise boundary quantity is well understood. However, there are no dynamical, thermodynamic properties associated with these HRT surfaces.

Note, as mentioned above however, that HRT surfaces also have non-expanding null congruences, and can thus be thought of as marginally trapped surfaces. In particular, HRT surfaces are thus compatible with being leaves of a holographic screen. In Chapter 2, we exploit this observation by exploring the properties of holographic screens anchored to the AdS boundary, and containing an HRT surface as a leaf. In particular, we generalize the results of [7, 8] to show that these non-compact, boundary anchored holographic screens also obey a monotonic area law, with the HRT surface being the leaf of smallest area. This result is consistent with a thermodynamic interpretation in which moving along the holographic screen represents a progressive coarse graining of the fine grained von Neumann entropy. In related work, [14] further showed that for black holes in AdS, the area of a marginally trapped surface associated with a black hole measures a coarse-grained entropy, where the coarse-graining is over all solutions of the interior of the black hole, keeping the geometry of the exterior fixed. Though the above properties apply to marginally trapped surfaces and holographic screens in anti-de Sitter space, studying their properties there will hopefully give way to progress in understanding these same

properties in general spacetimes.

In Chapter 3, we study the complementary problem of understanding HRT like surfaces in general spacetimes. In particular, we study HRT like surfaces anchored to an arbitrarily chosen boundary (instead of an AdS boundary). Unlike the AdS boundary, for an arbitrary boundary there is no known quantum theory living on it that is dual to its interior. Therefore, no such entropy measuring surface is guaranteed to exist. However, the question remains of whether some set of bulk surfaces could be consistent with an entropic interpretation, and in particular satisfy quantum entropy relations like Strong Subadditivity. In dynamical asymptotically AdS spacetimes, a naive application of the HRT prescription to surfaces anchored to a finite, cutoff boundary can in fact fail to satisfy Strong Subadditivity.

Thus, we consider different construction for holographic entropy in the presence of a radial cutoff. In particular, we use a restricted maximin procedure, where the spatial slices that are varied over in the maximin procedure must contain an entire, fixed codimension 2 surface, which can be thought of as a fixed time slice of the arbitrary boundary. This is in contrast to the the normal (un-restricted) maximin procedure, in which slices need only contain ∂A. While in cutoff free cases the maximin and restricted maximin procedures both provide an equivalent definition of HRT, in the case with a finite cutoff, the restricted and unrestricted formulations can generally differ. In the cutoff case, choosing the restricted prescription can be justified as follows: imposing some cutoff can be thought of as creating some open system that continues to interact with the exterior. Time evolution can then generally change the entropies being studied, so one must fix a slice of the codimension 1 boundary to obtain a well-defined entropy.

We then show that this restricted maximin prescription satisfies the requisite quantum Strong Subadditivity, in addition to the holographic Monogamy of Mutual Information inequality. Having a consistent bulk formulation for entropy in the presence of a radial

cutoff may represent a first step in understanding any potential dual quantum theory to arbitrary regions in spacetime.

With these connections between various area/entropy laws, we turn to a different potential avenue for understanding the relation between geometry and entanglement, in the form of traversable wormholes.

1.2 Traversable Wormholes

Though traversable wormholes are familiar entries in the lexicon of general relativity, their use has largely been relegated to the realm of science fiction. There, they helpfully serve as bridges allowing intrepid travelers to journey to distant or disconnected portions of the universe, often faster than light. The fantastical possibilities suggested by traversable wormholes however, from a more pragmatic perspective, seem to preclude their existence. As such, physicists have long suspected that wormholes that could be crossed by an observer or signal would be impossible to build, even theoretically.

The first attempts at a naive analysis indeed bear out this suspicion, and it can be shown that using, for example, only classical matter, wormholes cannot be made traversable. The section below reviews some of these analyses, explains how they can be circumvented, and introduces the traversable wormhole constructions to be detailed in later chapters. It further gives an overview of how these constructions could lend insight into the connection between geometry and entanglement.

1.2.1 Topological Censorship and Energy Conditions

A traversable wormhole can be defined as the set of causal curves that cannot be deformed (while remaining causal) to lie entirely in the boundary of a spacetime. In other words, a spacetime possesses a traversable wormhole if is contains some non-trivial

topology that is not hidden behind a horizon, such that an observer could start from infinitely far away, jump in, thread itself through the topologically non-trivial handle of the wormhole, and still escape back out to infinity. Topological Censorship theorems, described below, seek to rule out this possibility.

First, however, it helps to understand different energy conditions and their role in general relativity. As mentioned above, reasonable classical matter is assumed to satisfy the Null Energy Condition, $T_{ab}k^a k^b > 0$ for k any null vector. This condition guarantees that matter always causes null rays to focus, and Topological Censorship can be proven assuming it. The spirit behind this proof is that light rays will converge as they enter the wormhole throat, and any matter used to construct the traversable wormhole will ensure that light rays will only continue to focus. In particular, the light rays cannot defocus as needed to leave the wormhole throat and escape out to the other side.

While classical matter generally satisfies the Null Energy Condition, as noted above quantum fluctuations can generally violate it. However, while local, negative energy quantum fluctuations may cause a local violation of the Null Energy Condition, one might expect that these fluctuations will average out with local, positive quantum fluctuations. For example, the Casimir energy produced by two parallel conducting plates will cause a negative null stress energy to be accumulated by light rays traveling across the plates; however, this will be overcome by the positive stress energy produced by the mass of the plates themselves. On average then, light rays traveling across the plates focus. By imposing an Average Null Energy Condition

$$\int_{-\infty}^{+\infty} T_{ab}k^a k^b d\lambda > 0 \tag{1.2}$$

for λ an affine parameter, Topological Censorship theorems can again be proven.

However, even this stronger Average Null Energy Condition can be violated by quan-

tum effects, this time with the addition of nontrivial topology. For example, in a $1+1$ dimensional spacetime with the topology of a cylinder, a null geodesic that winds around the cylinder will pick up a negative Casimir energy, and now no massive plates exist to give a compensating positive stress energy.

Despite this, topological censorship theorems can still be proven using an Achronal Average Null Energy Condition, in which the Average Null Energy Condition is imposed only on those geodesics which are achronal, meaning that no two points on the null geodesic are timelike related (as they would be in a compact space). Though Topological Censorship then only applies to achronal null geodesics, we might expect the chronal geodesics to simply wind around a compact direction, and thus never escape out to infinity anyway.

More concretely, if a null geodesic between two points is the fastest curve between them, it means it must be achronal. Otherwise, there would be a timelike geodesic connecting two points, which would mean a faster curve could be found. The Average Achronal Null Energy Condition can thus be immediately used to rule out traversable wormholes connecting otherwise disconnected universes, as the only null geodesics (and therefore fastest null geodesic) connecting the two sides go through the wormhole, and thus some null geodesic through the wormhole is achronal. In the same manner, topological censorship applied to achronal null geodesics also rules out traversable wormholes which provide the fastest path between two boundary points, as this fastest path would be achronal. This limit on short wormholes in turn limits the use of traversable wormholes as time machines.

Thus, while it remained possible that quantum effects on non-trivial topology could conspire to give rise to some traversable wormhole (though one which was sufficiently slow, and connected points in the same universe), the Achronal Average Null Energy Condition proved restrictive enough that for many years none were constructed.

1.2.2 Examples of Traversable Wormholes and Their Ties to Entanglement

Despite this obstacle, recently several examples of traversable wormholes were successfully constructed in asymptotically AdS spacetimes. In particular, the example of Gao, Jafferis, and Wall [15] starts by considering a Schwarzschild black hole in a 3 dimensional asymptotically AdS spacetime. This two sided black hole looks like an almost traversable wormhole, as an observer starting in the infinitely far past in one asymptotic region will only make it to the other asymptotic region infinitely far into the future (see figure 1.2). This near traversability makes it so that a small perturbation could render the wormhole traversable. The boundary dual of this AdS black hole consists of two copies of a conformal field theory, one for each asymptotic region the wormhole. Further, the two copies will be in a highly entangled thermal state, known as the thermofield double. Just as on the gravitational side, though the quantum systems are entangled, signals cannot yet propagate from one side to the other.

On the quantum side however, standard quantum teleportation protocols tell us that signals can be made to propagate between two entangled systems, so long as classical information is transferred between the two sides (or couplings are added, as in the case below). [15] used this quantum intuition to show that indeed, adding simple couplings between the two dual quantum systems renders the bulk AdS wormhole traversable. While it is not surprising that adding a nonlocal (from the perspective of the bulk) interaction could allow information to be exchanged between distant regions, it perhaps is surprising that these simple couplings in fact modify the interior of the bulk to create a smooth, classical, geometric path for the information to travel through. However, from the bulk perspective, this interaction modifies the boundary conditions of fields propagating in the background spacetime, giving rise to a negative Casimir energy along

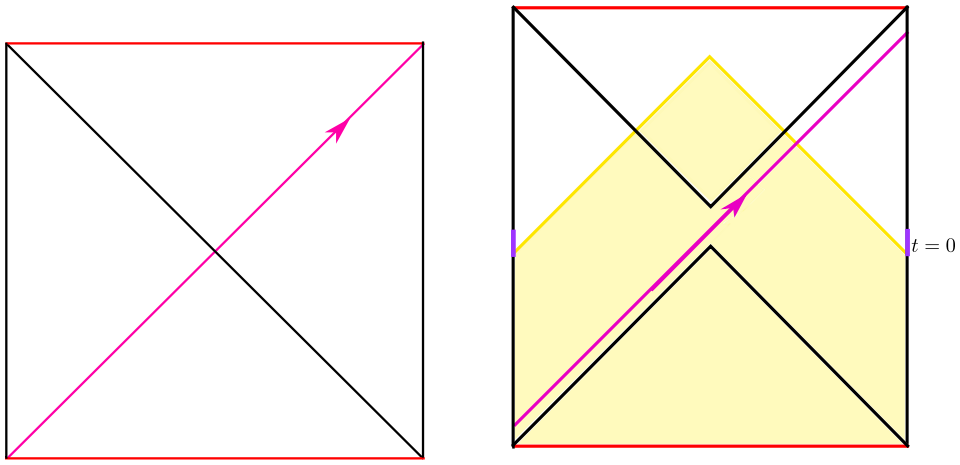

Figure 1.2: **Left:** An AdS black hole, which can be thought of as an almost traversable wormhole, as the observer (in pink) leaving infinitely far in the past in the left asymptotic region makes it to the right asymptotic region infinitely far in the future. **Right:** The traversable wormholes of [15], in which a coupling between the two boundaries is added (denoted in purple). The backreaction from quantum fields will modify this geometry (though by causality the coupling does not modify the geometry in the yellow region). Changes to the geometry outside this region cause the even horizon to recede, such that an observer can traverse to the other side.

the horizon. This interaction also modifies the causal structure of the spacetime, making it so that the geodesic that traverses the wormhole is chronal — in particular, a path passing directly through the boundary interactions can jump between asymptotic regions faster than by traveling through the wormhole.

While the construction of [15] relied heavily on the AdS/CFT duality, in Chapter 4 we argue that a broad class of wormholes in different spacetimes will become traversable after including the Casimir energy from linear quantum fields propagating on the spacetime, without the need for nonlocal interactions at infinity. As in the case of [15], we start with an *almost* traversable wormhole connecting two asymptotic regions. Performing an additional quotient that identifies points in the two asymptotic regions creates an *almost* traversable wormhole between the same asymptotic region (see figure 1.3). This quotienting creates the nontrivial topology necessary to create chronal geodesics and a negative Casimir energy.

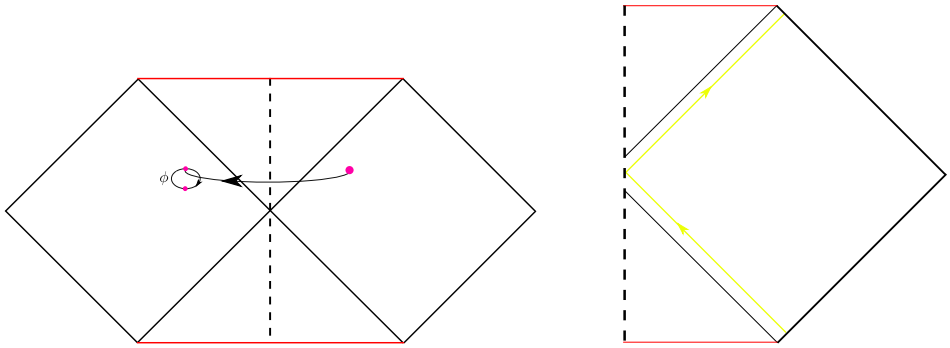

Figure 1.3: Left: A quotient of the maximally-extended Schwarzschild black hole. The quotient acts on the above conformal diagram by reflection across the dashed line, and simultaneously acts as the antipodal map on the suppressed sphere. Right: A small perturbation of maximally-extended Schwarzschild renders the quotient wormhole traversable. This results in a causal curve running between past and future null infinity that is not deformable to the boundary

In Chapter 5, we use the methods of Chapter 4 to explicitly construct an example of a traversable wormhole in asymptotically flat space in the more familiar form of a handle connecting two mouths in the same asymptotic region (see figure 5.1). This is done by noting that wormholes of this form can be formed by taking a quotient of a spacetime containing two asymptotic regions (each with a pair of two-sided black holes) that identifies a point with the point obtained in the other black hole in the other asymptotic region. A pair of cosmic strings can be used to provide a tension that keeps the black holes from falling into one another. An additional compact cosmic string that wraps around the throat of the wormhole will provide the quantum fluctuations needed to render the wormhole traversable.

Finally, in Chapter 6, we then note that the asymptotically flat wormholes constructed above can be modified to form multi-mouthed traversable wormholes, where an observer can travel through any pair of mouths. In particular, we can start with a two mouthed wormhole and perturb this solution by adding a small black hole in the throat. If this black hole is small enough, traversability can be maintained between the original two mouths. This small black hole can then be used to make an additional wormhole be-

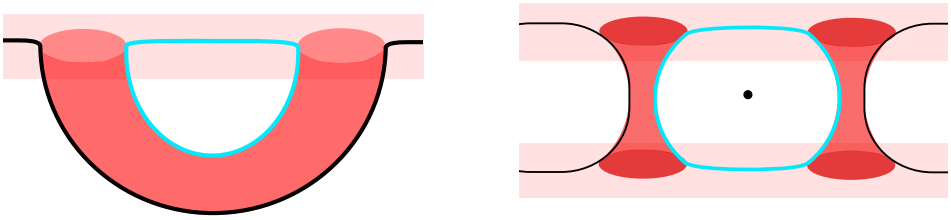

Figure 1.4: Left: A moment of time of wormhole with two mouths in the same asymptotic region. Quantum fluctuations of a compact cosmic string (blue) provide the negative Casimir energy necessary for traversability. A cosmic string that runs through the wormhole throat and stretches to infinity provides a tension that prevents the mouths from colliding (black). Right: The wormhole in the left figure can be formed by taking a quotient of the space depicted on the right, which contains a pair of two sided black holes, and three cosmic strings. In particular, the quotient identifies a point with a π rotation about the imaginary black dot in the figure.

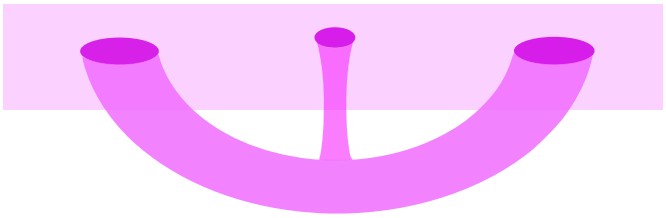

Figure 1.5: A multi-mouth wormhole, with all three mouths in the same asymptotic region, as constructed in Chapter 6. The cosmic strings necessary for stability and Casimir energy are omitted for illustrational clarity.

tween this throat and another distant region As with the two mouthed wormholes above, this three mouthed configuration can be put into mechanical equilibrium and be made traversable by the proper placement of cosmic strings.

In addition to being interesting gravitational solutions, wormholes (the traversable and non-traversable kind) are illustrative of the connection between geometry and entanglement. In particular, a useful slogan for this connection has been "ER=EPR," which roughly suggests that entangled quantum systems (like EPR pairs) are connected by a wormhole (or Einstein-Rosen bridge) [16]. In the AdS example, this relation is more or less explicit, as interactions between an entangled, dual quantum system modifies the geometry of a wormhole in the bulk.

In flat space, there is no known holographic, dual quantum system. However, knowing the structure and connections between various wormhole solutions could be used to study the underlying entanglement structure of spacetime and potential dual systems. In AdS, non-traversable multiboundary wormholes have previously been a tool for studying multipartite entanglement [17] — entanglement between more than two subregions that cannot be distilled into bell pairs between pairs of regions. In holography, while some results constraining multiparty holographic entanglement exist (including Monogamy of Mutual Information), the results and tools are limited. Thus, in Chapter 6, we use the gravitational construction of multi-mouth wormholes to study the multipartite entanglement between the mouths in flat space.

1.3 Permissions and Attributions

1. The content of Chapter 2 is the result of a collaboration with Donald Marolf, and has previously appeared in the Journal of High Energy Physics JHEP **02** (2018) 049. It is reproduced here with the permission of the International School of Advanced Studies (SISSA): `http://jhep.sissa.it/jhep/help/JHEP/CR_OA.pdf`.

2. The content of Chapter 3 and Appendix A is the result of a collaboration with Donald Marolf and Sean Jason Weinberg [18].

3. The content of Chapter 4 and Appendix B is the result of a collaboration with Zicao Fu and Donald Marolf, and has previously appeared in Classical and Quantum Gravity, Class.Quant.Grav. **36** (2019) 4, 045006, Class.Quant.Grav. **36** (2019) 24, 249501 (erratum). It is reproduced here with the permission of the Institute of Physics (IOP): `http://authors.iop.org/atom/help.nsf/LookupJournalSpecific/WebPermissionsFAQ~**`

4. The content of Chapter 5 and Appendix C is the result of a collaboration with Zicao Fu and Donald Marolf, and has previously appeared in Classical and Quantum Gravity, Class.Quant.Grav. **36** (2019) 24, 245018 (erratum). It is reproduced here with the permission of the Institute of Physics (IOP): `http://authors.iop.org/atom/help.nsf/LookupJournalSpecific/WebPermissionsFAQ~**`

5. The content of Chapter 6 and Appendix D is the result of a collaboration with Roberto Emparan, Donald Marolf, and Marija Tomašević.

Part I

Area/Entropy Relations

Chapter 2

Marginally Trapped Surfaces and AdS/CFT

2.1 Introduction

One of the central and most striking pillars of black hole thermodynamics is the Bekenstein-Hawking entropy formula, which relates the entropy of a black hole to the area of its event horizon [1, 2]. The notion that the microscopic degrees of freedom of a spacetime are controlled by degrees of freedom on a codimension-one surface is known as holography, and the area/entropy formula has been generalized in various directions. One such generalization comes from the AdS/CFT correspondence in the form of the Ryu-Takayanagi formula (or its covariant generalization by Hubeny, Rangamani, and Takayanagi [HRT]) [19, 9, 12]. This formula relates the entropy of the dual CFT in some boundary region with the area of an extremal surface through the bulk. A second generalization comes from the conjectured Covariant Entropy Bound (or Bousso bound) which states that the area of an achronal codimension-two surface having non-positive expansion ($\theta \leq 0$). As noted in [5], marginally trapped surfaces have a special status with

respect to this bound, as the two future-directed congruences have $\theta = 0$ and $\theta \leq 0$. When the Null Curvature condition holds, the bound would then apply to both congruences (and both future and past directions of the $\theta = 0$ congruence). Such surfaces can be stitched together to form a continuous codimension-one surface, called a holographic screen, in which case the marginally trapped surfaces are called leaves of the screen. It was further shown in [8, 7] that the leaves of the holographic screen obey a monotonic area law, and thus presumably a thermodynamic second law.

Despite this thermodynamic property, the nature of the entropy described by holographic screens has remained unclear.[1] In contrast, the Ryu-Takayanagi formula computes the von Neumann entropy, $\mathrm{tr}(\rho \log \rho)$, of the dual CFT density matrix ρ. A natural question, then, is whether these two notions can be connected. A first step in this direction is to notice that the extremal surface used by RT has vanishing expansions in both of its orthogonal null directions. Though the usual definitions of marginally trapped surfaces require that they be compact, if we generalize to the non-compact case the extremal surface can be thought of as a leaf of a holographic screen.[2] This suggests that it may be useful to define a general notion of non-compact holographic screen anchored to appropriate boundary sets ∂A on an asymptotically locally anti-de Sitter (AlAdS) boundary.

We explore the properties of such screens below when all leaves are anchored to the same boundary set ∂A, whereas for RT/HRT we take ∂A to be the boundary of a partial Cauchy surface A for the boundary spacetime. In contrast, as can be seen by considering screens where every leaf is an extremal surface, letting the anchor set vary from leaf to leaf would generally result in infinite area-differences of either sign between nearby

[1] During the preparation of this work, [14] appeared which further clarified this issue. See Section 6.4 for further comments on [14]

[2] The connection between AdS/CFT holography and the Covariant Entropy Bound was explored in [12]

leaves, so such screens do not appear to satisfy a useful second law of thermodynamics. However, many of our results would nevertheless apply to that case as well.

We begin in Section 3.3 with a brief review and discussion of the method we will use to construct marginally trapped surfaces anchored to the AdS boundary. Section 2.3 then shows that, with certain assumptions, a marginally trapped surface must lie inside the entanglement wedge but outside the causal wedge associated with the same boundary region. We further show that the area of the marginally trapped surface equals or exceeds that of the corresponding extremal surface, suggesting that it describes a coarse graining of the von Neumann entropy. In addition, when a marginally-trapped surface anchored at ∂A lies in the past horizon defined by an appropriate boundary region S (with $\partial S = \partial A$), a construction naturally called future causal holographic information also gives on upper bound on the marginally-trapped area. Section 2.4 studies divergences in the area of the marginally trapped surfaces associated with the region near the AdS boundary and shows that, while the leading order divergences of our marginally trapped surfaces match those of the extremal surface, the subleading divergences generally differ. Section 2.5 then generalizes the thermodynamic results of [8, 7] to holographic screens with non-compact leaves. We close with some brief discussion in Section 6.4. In particular, for surfaces on the past horizon of a boundary set S as above, we note that the results of Section 2.5 can take the form of a standard second law in that they imply non-decrease in area under arbitrary deformations of S toward the future, so long as ∂S remains fixed and the holographic screen moves in a spacelike direction.

2.2 Preliminaries

This section provides some definitions and lemmas that will be used throughout the work below. It also summarizes the method we use to construct boundary-anchored

holographic screens and thus defines the class of such surfaces to be studied.

We assume that the bulk spacetime obeys the Null Curvature Condition, $R_{ab}k^a k^b \geq 0$ for any null vector k^a and is AdS globally hyperbolic. The latter condition (see e.g. [20]) means that there is an achronal surface Σ for which the AdS-domain of dependence $D(\Sigma) = D^+(\Sigma) \cup D^-(\Sigma)$ is the entire spacetime. Here $D^+(\Sigma)$ ($D^-(\Sigma)$) is the set of points p for which all past-inextendible (future-inextendible) causal curve through p intersects either Σ or the AlAdS boundary.

Definition: A *future holographic screen* H is a smooth hypersurface which admits a foliation by marginally trapped surfaces, called *leaves*. A *marginally trapped surface* is a smooth, codimension-two achronal spacelike surface whose future directed orthogonal null congruences, k and ℓ, have expansions satisfying

$$\begin{aligned} \theta_k &= 0, \\ \theta_\ell &\leq 0. \end{aligned} \tag{2.1}$$

Similarly, we can define a *past holographic screen* as a smooth hypersurface which admits a foliation by marginally *anti-trapped surfaces*, so that $\theta_l \geq 0$. Note that an extremal surface will have $\theta_\ell = \theta_k = 0$.

Holographic screens are also known as marginally trapped tubes [21], and are a generalization of dynamical horizons and future outer trapped horizons [22], removing the restriction [8] that the surface be spacelike. Since we focus on the boundary-anchored case, we also omit the usual requirement that the marginally trapped surfaces be compact. In addition, we require such boundary-anchored marginally trapped surfaces σ to be homologous to some partial Cauchy surface A for the boundary spacetime. Here by

'homologous to A', we mean that there is a bulk AdS-Cauchy surface $\Sigma = \Sigma_1 \cup \Sigma_2$ with $\partial\Sigma = \sigma \cup A$. As a result, $\partial\sigma = \partial A$. In this work we use the symbol ∂X to denote the boundary of any set X as computed in the conformal compactification of our AlAdS spacetime; i.e., ∂X will include any limit points of X in the AlAdS boundary. In contrast, we will use the notation $\dot{X}$ to refer to the boundary of X as defined by the natural topology of the bulk spacetime in which the bulk is an open set. As a result, $\dot{X}$ cannot intersect the AlAdS boundary, but $\partial\dot{X} := \partial(\dot{X})$ contains precisely those points in the AlAdS boundary which are limit points of $\dot{X}$.

We will focus in particular on future holographic screens where, for the boundary-anchored case, we define the k, ℓ null congruences as follows: consider a boundary region A and a marginally trapped surface σ homologous to A as above. We define the k null congruence orthogonal to σ to be the one launched towards the future from the Σ_1 side of σ, while the l null congruence orthogonal to σ is the one launched toward the future from the Σ_2 side. Note that AdS-global hyperbolicity requires $\dot{D}^+(\Sigma_1)\backslash\Sigma_1 = \dot{I}^+(\Sigma_2)$, and in fact $\dot{D}^+(\Sigma_1) \setminus \Sigma_1 \subset \dot{I}^+(\sigma)$, which implies that it is generated by the k-congruence just defined.

A well known property of holographic screens is that they are highly non-unique: changing the foliation of the spacetime generally changes the holographic screen (see, e.g. [7]). Previous work has focused on generating them from null foliations (e.g. [8, 7, 23]), building the leaves of the holographic screen by finding a codimension-two surface with maximal area on each null slice (see Figure 3.6). In the case where the null foliations are taken to be the set of past or future light cones emanating from an observer's worldine, the foliation dependence of screens can be thought of as an observer dependence.

However, if we were to use this null construction in empty AdS, then the maximal cut of any null surface would lie on the AdS boundary. The holographic screen would then just be the usual conformal boundary of the spacetime. This is consistent with the

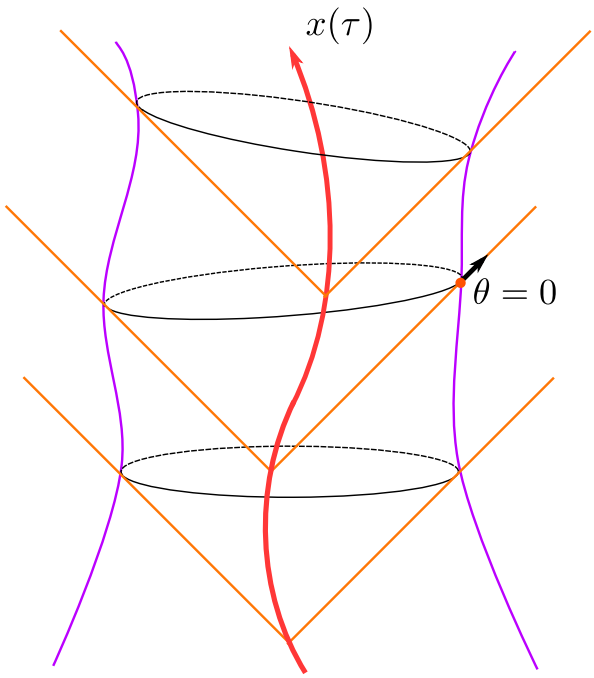

Figure 2.1: A holographic screen can be constructed by null foliation from an observer's light cones. For example, given an spacetime path $x(\tau)$, on each future lightcone emanating from that path, we can find the maximal area codimension-two surface, if it exists. This surface will then have $\theta = 0$ along the lightcone. Stitching together all these surfaces on all of the future lightcones associated with the observer will give us our holographic screen.

Bousso-bound picture, in that the degrees of freedom in the boundary CFT control the bulk degrees of freedom, but seems rather trivial. In particular, even the renormalized area is strictly infinite.

For a fixed subset A of some boundary Cauchy surface C, we instead wish to construct a marginally trapped surface through the bulk and anchored to the boundary ∂A of that region. To do so, instead of using a null foliation as above, we pick any foliation of our bulk spacetime such that each slice Σ_i contains ∂A. On Σ_i, we can then attempt to solve for a marginally trapped surface also anchored to ∂A, giving us our leaf $\sigma_i(A)$. See Figure 2.2 for a depiction. Although we leave a complete analysis for future investigation, in practice we find that solutions exist. While the leaves of the screen are required to be

spacelike, the same need not be true of the slices Σ_i used to construct them.

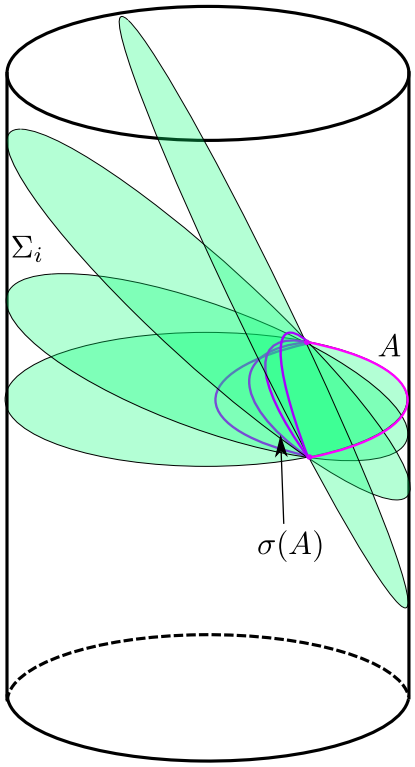

Figure 2.2: For a fixed boundary region A, we construct our holographic screens by first fixing a foliation (pictured here as green slices), such that each slice contains ∂A (where A is the pink section). Then, on each slice, we solve for the trapped surface (the purple curves). Each trapped surface is a leaf of a holographic screen, and stitched together, the collection of leaves comprises our holographic screen. In practice, we find that solutions typically exist. The figure is based on numerical results in Schwarzschild-AdS.

Indeed, we solve for our leaves in the following manner (see [12] for a similar setup): a general codimension-two surface S can be specified by two constraints,

$$\begin{aligned} F(x^\mu) &= 0, \\ G(x^\mu) &= 0. \end{aligned} \tag{2.2}$$

The gradients $\nabla_\nu F(x^\mu)$ and $\nabla_\nu G(x^\mu)$ are then vectors orthogonal to S. When they are

independent and S is spacelike, we can write the orthogonal null vectors as some linear combinations

$$n_{\nu,a} = \nabla_\nu F(x^\mu) + c_a \nabla_\nu G(x^\mu), \tag{2.3}$$

for c_a constants and $a = \ell, k$ with $k_\mu = n_{\mu,k}, \ell_\mu = n_{\mu,\ell}$. The null extrinsic curvatures are then

$$\chi_{\mu\nu,a} = \tilde{g}^\rho_\mu \tilde{g}^\lambda_\nu \nabla_\rho n_{\lambda,a}, \tag{2.4}$$

where $\tilde{g}$ is the induced metric on S:

$$\tilde{g}_{\mu\nu} = g_{\mu\nu} + \ell_\mu k_\nu + \ell_\mu k_\nu. \tag{2.5}$$

Finally, each expansion is the trace of the appropriate null extrinsic curvature:

$$\theta_a = \chi^\mu{}_{\mu,a}. \tag{2.6}$$

The extremal surface anchored to ∂A is then found by solving $\theta_k = \theta_\ell = 0$ to find F and G. But for our marginally trapped surfaces, only θ_k need vanish so the solution is underdetermined. We may hope to specify a unique solution by taking $G(x^\mu) = t - \hat{G}(x^i) = 0$, for some particular $\hat{G}$ (with $\{x^\mu\} = \{t, x^i\}$), and to then solve $\theta_k = 0$ for F.

Once we have found our holographic screen, we will want to compare it to both the causal wedge and entanglement wedge as defined below (following [12]).

Definition: For a given boundary region A, we will denote the boundary domain of dependence by $D_{bndy}(A)$. The *causal wedge* is then defined as the intersection of the bulk past and future of this domain of dependence, $\mathcal{C}(A) = I^-(D_{bndy}(A)) \cap I^+(D_{bndy}(A))$. The

causal information surface or *causal surface* Ξ_A lies on the boundary of this region, and is given by the intersection of the past and future bulk horizons of the boundary domain of dependence of A, $\Xi_A = \dot{I}^-(D_{bndy}(A)) \cap \dot{I}^+(D_{bndy}(A))$.

Definition: Let the HRT surface $m(A)$ be the codimension-two surface with extremal area in the bulk, anchored to the boundary ∂A of A. We also require that $m(A)$ be homologous to A in the sense discussed above for marginally trapped surfaces. If there are multiple extremal surfaces satisfying this constraint, take the one with least area. The entanglement wedge $\mathcal{E}(A)$ is then the bulk AdS-domain of dependence $D(\Sigma)$ of any partial AdS-Cauchy surface Σ satisfying $\partial\Sigma = A \cup m(A)$.

We can also define a similar wedge $\mathcal{M}(\sigma)$ associated with any marginally trapped surface.

Definition: For any marginally trapped surface σ homologous to A we define the *marginally trapped wedge* $\mathcal{M}(\sigma)$ to be the bulk domain of dependence $D(\Sigma)$ of any partial AdS-Cauchy surface Σ satisfying $\partial\Sigma = \sigma \cup A$.

In addition to the above definitions, we will repeatedly use the following Lemma.

Lemma 2.1: (From [13]) Suppose N_1 and N_2 are two null hypersurfaces that are tangent at some point x on some slice Σ. Then if there exists some neighborhood of x on Σ, such that N_2 is nowhere to the past of N_1, then $\theta_{N_2} \geq \theta_{N_1}$ at p.

This Lemma is especially useful when combined with the following result (often left implicit in applications of Lemma 2.1).

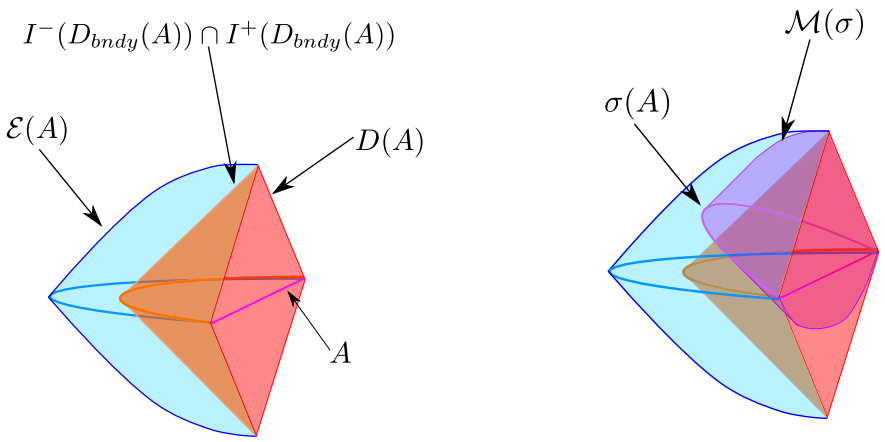

Figure 2.3: Left: Depiction of the Entanglement Wedge (blue) and Causal Wedge (orange). The entanglement wedge $\mathcal{E}(A)$ is the domain of dependence lying between the extremal surface $m(A)$ and the boundary. In contrast, the causal wedge $I^-(D_{bndy}(A)) \cap I^+(D_{bndy}(A))$ is defined as the intersection of the bulk past and future of the domain of dependence $D_{bndy}(A)$ in the boundary. The intersection of the past and future horizons defines the causal surface. Right: Depiction of the marginally trapped surface $\sigma(A)$ which (as shown in Section 2.3) must lie in the entanglement wedge but above the future horizon of $D_{bndy}(A)$. The associated marginally trapped wedge $\mathcal{M}(\sigma)$ is also shown (purple).

Lemma 2.2 If a smooth spacelike curve γ intersects the boundary of the future $I^+(S)$ of some set S at a point p, then either i) γ enters the chronological future $I^+(S)$ or ii) all null generators of $\dot{I}^+(S)$ through p intersect γ orthogonally.

Proof: By e.g. Theorem 8.1.6 of [3], p lies on a null geodesic λ (perhaps with a past endpoint) that (at least to the past of p) lies entirely in $\dot{I}^+(S)$. Let k^a and ζ^a be vectors respectively tangent to λ and γ at p. Since k^a is null and ζ^a is spacelike, then either a) k^a and ζ^a span a timelike plane or b) k^a and ζ^a span a null plane, and are orthogonal. So if any null generator λ through p fails to intersect γ orthogonally, case (a) must hold for that generator. We can then find a local Lorentz frame where $k^a \partial_a \propto \partial_t + \partial_x$ and $\zeta^a \propto \partial_x$, so γ clearly enters $I^+(S)$.

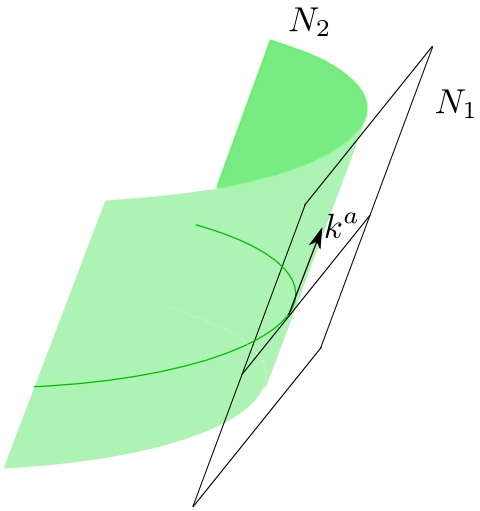

Figure 2.4: The lines depict intersecting spacelike cuts of null congruences N_1 and N_2. N_2 is nowhere to the past of N_1 and is thus expanding faster by Lemma 2.1.

Combining Lemmas 2.1 and 2.2 gives us the following:

Corollary 2.3 If a codimension-two surface σ intersects $\dot{I}^+(S)$ at p then either σ enters $I^+(S)$ or every generator λ of $I^+(S)$ at p has a well-defined expansion $\theta^\lambda(p)$ that is equal to or greater than the expansion $\theta^\sigma(p)$ along the same null geodesic as defined by the associated null congruence orthogonal to σ.

Proof: If σ fails to enter $I^+(S)$, then by Lemma 2.2, all null generators of $I^+(S)$ at p intersect σ orthogonally. Consider such a generator λ, together with the nearby generators in $\dot{I}^+(S)$. Unless λ has a conjugate point at p, at least in a neighborhood of p these generators define a smooth null surface $\mathcal{N}$ nowhere to the past of σ. As a result, in a neighborhood of p the orthogonal null congruence to σ containing λ is also smooth and lies nowhere to its future. Thus $\theta^{\mathcal{N}}(p) \geq \theta^\sigma(p)$ by Lemma 2.1. Furthermore, if the expansion along λ at p is ill-defined (i.e. if p is a conjugate point of λ), then any point $q \in \lambda$ to the future of p also lies in the chronological future of geodesic generators λ' of $I^+(S)$ close to λ, and which differ from λ only to first order in $q - p$. As a result, such

geodesics λ' also lie in front (i.e. to the past) of the infinitesimal null plane $\mathcal{N}$ defined by λ by an amount that is first order[3] in the separation $\delta\lambda$ between λ and λ'. But since σ is smooth, it can bend in front of this null plane only at second order. Thus σ enters the future of some λ' and thus enters $I^+(S)$.

2.3 Ordering of Surfaces

The RT and HRT surfaces measure the fine-grained entropy of the dual CFT in the associated domain. In addition, the Causal Surface has been conjectured to give a coarse-grained measure of the entropy known as the Causal Holographic Information [24]; see related discussion in [25, 26, 27]. The idea that the latter is a coarse-graining of the former is associated with the fact that the causal surface lies closer to the boundary and has larger area than the extremal surface anchored to the same region [12, 13].

In this section, we argue that any marginally trapped surface σ anchored to the boundary at ∂A lies in some sense between the above two surfaces. Specifically, we show it to lie inside the entanglement wedge but above the future horizon associated with A. We also show the area of σ to be bounded below by the area of the extremal surface and – in certain cases– bounded above by the area of a cut of the causal horizon associated with future causal holographic information (fCHI). So in such cases we expect the area of σ to describe a coarse-grained entropy for the dual CFT that is finer than the coarse-graining associated with fCHI.

The proofs regarding the ordering of wedges are similar to proofs in [3, 13]. For arguments in Section 3.2, we assume that our marginal surface σ can be approximated

[3]We believe this to be true. What is straightforward to argue rigorously is that if the expansion of $\dot{I}^+(S)$ remains bounded when approaching p from any direction, then we may argue just as in the case where p is not a conjugate point. If a direction-dependent limit diverges along some spacelike cut, then the cut must deviate from $\mathcal{N}$ strictly faster than quadratically. Furthermore, it must do so by lying in front (to the past) of $\mathcal{N}$ so that λ can enter its future immediately after the conjugate point at p. As a result, since σ is tangent to $\mathcal{N}$, it also lies to the past of σ. I.e., σ enters $I^+(S)$.

by a sequence σ_i of surfaces anchored to the same ∂A, lying in a common AdS-Cauchy surface Σ in which all of the surfaces σ, σ_i are homologous to A, and maintaining $\theta_\ell \leq 0$ but having $\theta_k > 0$. We can call such σ *deformable*, indicating that they may be deformed to cases with $\theta_k > 0$, $\theta_\ell \leq 0$.

2.3.1 Leaves Lie Outside of the Causal Wedge

Our first result generalizes the well-known theorem that apparent horizons lie to the future of event horizons [3].

Theorem 3.1.1: Let σ be a marginally trapped surface, anchored to a boundary region A. Then it will lie above the future horizon of $D_{bndy}(A)$, and in particular outside the causal wedge $\mathcal{C}(A)$.

Proof: We assume A to be connected, as otherwise we can simply work with each connected component. If σ fails to lie above the future horizon of $D_{bndy}(A)$, then some $p \in D_{bndy}(A)$ lies in the future of σ. But by the homology constraint, σ lies on a Cauchy surface Σ containing A, so A is not in the future of Σ. Thus, there are points in $D_{bndy}(A)$ that are not to the future of σ. But since A is connected, so is $D_{bndy}(A)$, and so some $q \in D_{bndy}(A)$ must lie on the boundary of the future of σ. Since q is in the interior of $D_{bndy}(A)$, there is an open set $U \ni q$, $U \subset D_{bndy}(A)$ that does not intersect the future of ∂A. As a result, the closure K of the set of points $r \in \sigma$ that can send future-directed timelike curves to U is compact.

Thus q lies on the boundary of the future of K. Since K is compact, this means there is a null generator λ of $\dot{I}^+(K)$ that reaches q, and which in particular reaches the AlAdS boundary. Thus λ maintains $\theta = 0$ for infinite affine parameter. It follows that adding any perturbation which makes all null generators of the k-congruence from σ satisfy the generic condition (i.e. that there exists non-vanishing null-curvature or shear

along any segment of any null congruence) moves $\partial I^+(\sigma)$ off of $D_{bndy}(A)$. For example, we can throw null particles into the bulk from $D_{bndy}(A)$ just below every point of $\partial I^+(\sigma)$. Then, however, such particles clearly intersect the generators of $\dot{I}^+(\sigma)$ near the AlAdS boundary and can only move $\partial I^+(\sigma)$ by a small amount. But this contradicts the fact that $D_{bndy}(A)$ is an open set, so a small change in $\partial I^+(\sigma)$ cannot in fact remove the intersection with $D_{bndy}(A)$. We thus conclude $I^+(\sigma) \cap D_{bndy}(A) = \emptyset$ so that no part of σ is below the future horizon.

For a certain class of extremal surfaces, we can also use a cut of the causal horizon to bound the area of the marginally trapped surface in the following sense:[4]

Theorem 3.1.2: Suppose a marginally trapped surface σ anchored to ∂A lies on the boundary of $I^+(S)$ of some S in the AlAdS boundary for which $\partial S = \partial A$. Then the boundary of $I^+(S)$ will also intersect the future causal horizon defined by $D_{bndy}(A)$ in some cut Y, and the generators of $\dot{I}^+(S)$ define a map from σ into Y under which the local area element is everywhere non-decreasing.

Proof: Note that since the expansion of $\dot{I}^+(S)$ vanishes on the AlAdS boundary it is negative or zero everywhere on $\dot{I}^+(S)$. By Theorem 3.1.1, any generator of $\dot{I}^+(S)$ that reaches σ does so after (or simultaneously with) passing through Y. Thus the map defined by these generators from σ to Y cannot decrease local areas.

The surface Y that gives the bound was introduced in [26] as a modification of causal holographic information conjectured to be associated with the future boundary domain of dependence $D^+_{bndy}(Y)$. The quantity $A/4G$ for Y is thus naturally called future causal holographic information.

Now, Theorem 3.1.2 provides a sense in which the area of σ is bounded below by

[4]We thank Aron Wall for a discussion regarding this point.

that of Y. But one should be careful to ask to what extent the local non-decrease of area guaranteed by this theorem implies non-decrease of meaningful measures of the total area. The subtlety is that since both σ and Y have infinite area, comparing them requires some process of regularization. Specifically, we impose that one must regularize the areas using a cut-off $z = z_0$ in terms of some Fefferman-Graham coordinate z. We then consider the difference between the areas in the limit $z_0 \to 0$ in which the regulator is removed[5]. One should thus ask to what extent the map of Theorem 3.1.2 can take some piece of σ that is before the cutoff (i.e., with $z > z_0$) into the part of Y beyond the cutoff (i.e., with $z < z_0$). If this effect is large enough as $z_0 \to 0$, Theorem 3.1.2 might still allow the regulated area to decrease even at leading order in z_0.

To analyze this issue, we must understand how many generators of $\dot{I}^+(S)$ cross the regulator surface $z = z_0$ between Y and σ in the limit $z_0 \to 0$. The limiting flux of such generators is known to be finite [28] when the boundary of $D_{bndy}(S)$ is a boundary Killing horizon, but extrapolating those results to the more general case suggests that the flux generally diverges as $z_0^{-(d-2)}$ and that this divergence can take either sign. Indeed, the total area of $\dot{I}^+(S)$ lost through the $z = z_0$ regulator surface takes the form

$$\text{Lost Area} \sim \int_Y^\sigma d\lambda \int_{\partial A_{z_0}} l^{d-2} z^{-(d-2)} \sqrt{\tilde{q}^0} \frac{1}{z} \frac{\partial z}{\partial \lambda}, \tag{2.7}$$

where l is the AdS scale, ∂A_{z_0} is a regulated version of ∂A located at $z = z_0$, $\sqrt{\tilde{q}^{(0)}}$ is the area element on ∂A of the finite-but-unphysical metric on the AlAdS conformal boundary (see Section 2.4.1), and λ is a smooth parameter along each geodesics between Y and σ. If Y and σ admit power series expansions in z (perhaps with possible log terms at order z^d) we generally have $\frac{1}{z}\frac{\partial z}{\partial \lambda} \sim 1$, and also $\int_Y^\sigma d\lambda \sim z$ since Y and σ both intersect

[5]One may also attempt to renormalize each quantity by subtracting an appropriate set of counter-terms. However, since both intersect the boundary in the same set ∂A, any counter-terms locally constructed from boundary information at ∂A will cancel when computing the area difference between σ and Y.

the AlAdS boundary at ∂A. The lost area is then $O(z^{-(d-3)})$, so we learn that if the areas of Y and σ differ by a term more divergent than $z^{-(d-3)}$, then the regulated area of Y does indeed exceed that of σ. In particular, the bound applies to the coefficient of the leading divergence at $O(z^{-(d-2)})$. However, if the areas are already known to coincide to higher order, then Theorem 3.1.2 tells us nothing further.

On the other hand, we expect the case of most interest to occur when both Y and σ coincide asymptotically with the extremal surface $m(A)$ anchored at ∂A. Consider then the renormalized areas of Y and σ defined by subtracting the known counter-terms for extremal surfaces areas. Since the regulated areas (before subtracting counter-terms) are of the form

$$\text{Regulated Areas} \sim \int_{z_0} \frac{dz}{z} \int_{\partial A_{z_0}} l^{d-2} z^{-(d-2)} \sqrt{\tilde{q}^{(0)}}, \tag{2.8}$$

the renormalized areas of Y and σ are generally finite only when these surfaces coincide with $m(A)$ up to corrections vanishing faster than z^{d-2} by some power law. Comparing with (2.7) immediately yields the following result:

Theorem 3.1.3: Suppose σ and Y in theorem 3.1.2 both agree with $m(A)$ up to corrections vanishing faster than z^{d-2} by some power law. Then the renormalized areas of σ and Y are finite, and the renormalized area of Y equals or exceeds that of σ.

2.3.2 Leaves Lie Inside of the Extremal Wedge

We now show that boundary anchored marginally trapped surfaces lie inside the extremal wedge $\mathcal{E}(A)$, as long as there is an appropriate region through which we can deform extremal surfaces while keeping them extremal. This condition is related to the absence of extremal surface barriers as defined in [20].

Theorem 3.2.1 Let σ be a deformable marginally trapped surface anchored to ∂A,

with a sequence of approximating surfaces σ_i. All σ_i lie in some AdS-Cauchy surface Σ, such that $\partial\Sigma \supset A$. Suppose there is a one parameter family $m(I)$ of extremal surfaces[6] anchored to the boundary on non-overlapping sets $\partial A_I \subset \partial\Sigma$ such that i) m(I) is continuous in I for $I \in [0,1]$, ii) $m(I=0) = m(A)$ but $\partial A_I \subset \partial\Sigma \setminus \overline{A}$. for $I > 0$, iii) each σ_i is contained in the extremal wedge associated with $m(I=1)$, and iv) each ∂A_I is the boundary of some boundary set A_I homologous to $m(I)$. Then σ lies in the closure of the entanglement wedge $\mathcal{E}(A)$.

Proof: Define Σ_{1i}, Σ_{2i} to be the regions in Σ such that $\Sigma_{1i} \cup \Sigma_{2i} = \Sigma$ and $\partial\Sigma_{1i} = \sigma_i \cup A$. For $m(I)$, we similarly define Σ_I, Σ_{1I}, and Σ_{2I}. Note that we may choose Σ_{1I} to be continuous in I.[7] We can also define the wedges associated to each of the surfaces of interest: $\mathcal{E}(I) = D(\Sigma_{1I})$, and $\mathcal{M}(\sigma_i) = D(\Sigma_{1i})$. Let I_i be the smallest I for which the closure $\overline{\mathcal{E}(I)}$ of $\mathcal{E}(I)$ contains $\mathcal{M}(\sigma_i)$; see figure 2.5. Then, since $\mathcal{E}(I)$ is continuous in Σ_{1I} (and thus in I), if $I_i \neq 0$ there must be some point p that lies in the boundaries of both $\mathcal{E}(I_i)$ and $\mathcal{M}(\sigma_i)$. Note that in this case the point p cannot lie on the AdS boundary since $\partial A_{I_i} \subset \partial\Sigma \setminus \bar{A}$.

Now, since $p \in \dot{\mathcal{M}}(\sigma_i)$, it is connected to σ_i by a null geodesic $\lambda \subset \overline{\mathcal{M}(\sigma_i)} \subset \overline{\mathcal{E}(I_i)}$. But no point of λ can lie in the interior of $\mathcal{E}(I_i)$, as then p would also lie in the interior of $\mathcal{E}(I_i)$ and not on the boundary of $\mathcal{E}(I_i)$. So if q is the past endpoint of λ on σ_i we must also have q lying in the boundary of $\mathcal{E}(I_i)$. Furthermore, it is clear that the k-congruence from σ_i is the one that locally does not enter $I^+(\Sigma_{2I_i})$. By the null convergence condition and Corollary 2.3 we then have that the expansions through q defined by the orthogonal null congruences from $m(I_i)$ and σ_i satisfy $0 \geq \theta^{m(I_i)} \geq \theta^{\sigma_i} > 0$. This is a contradiction, so $I_i = 0$ for all i. In particular, $\sigma_i \subset \mathcal{E}(A)$ and thus $\sigma \subset \overline{\mathcal{E}(A)}$ as desired.

[6]Note that a general $m(I)$ need not be an HRT surface, as it need not be the extremal surface of minimal area.

[7]This continuity is automatic unless there is a connected component of the bulk spacetime that does not have an AdS boundary; i.e. the bulk contains a closed cosmology in addition to the asymptotic AdS piece. Such cases do not appear to be allowed in AdS/CFT, but for completeness we include them here.

Note that condition (iii) that each σ_i be contained in the wedge associated with $m(I = 1)$ is realized whenever we can deform the boundary region ∂A to a point through $\Sigma \setminus \bar{A}$.

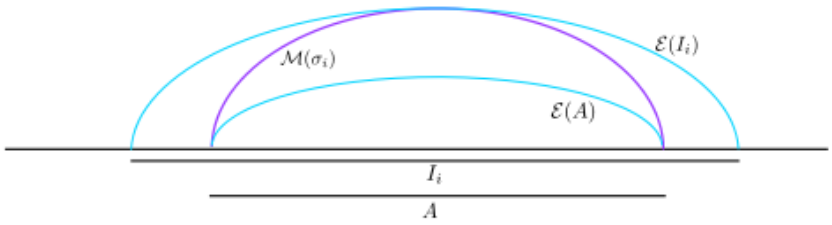

Figure 2.5: If a marginally trapped surface (or one of its approximating curves) $\sigma_i(A)$ lies outside the corresponding entanglement wedge $\mathcal{E}(A)$, we can continuously deform our boundary to larger regions, until at some point the entanglement wedge just touches the wedge associated with σ_i. This results in a contradiction.

We can also use the extremal surface anchored at ∂A to bound the area of appropriate similarly-anchored marginally trapped surfaces. The useful notions of 'appropriate' are defined by issues involving the regulator surfaces $z = z_0$ as in the discussion of Theorems 3.1.2 and 3.1.3.

Theorem 3.2.2: Given a marginally-trapped surface σ and an HRT surface $m(A)$ both anchored to ∂A, the renormalized area Area_{ren} of σ equals or exceeds that of $m(A)$ if i) ∂A lies on a Killing horizon of the boundary or ii) σ coincides with $m(A)$ up to corrections vanishing faster than z^{d-2} by some power law. More generally, the coefficient of the leading divergence in the area of σ equals or exceeds that for $m(A)$.

Proof: We can use the maximin construction of HRT surfaces [13] to find an AdS-Cauchy surface Σ on which $m(A)$ is the minimal surface. Let N be the surface formed by following the ℓ-orthogonal null congruence from σ toward the future and by also following the k-orthogonal null congruence from σ toward the past, with the convention that a given geodesic remains in N only so long as it lies on the boundary of the future/past of σ. Define $\tilde{\sigma}$ as the intersection of N with Σ, $N \cap \Sigma$. Now, the future directed portion of N has $\theta \leq 0$ at σ, while the past directed portion has $\theta = 0$ at σ. The null curvature condition

implies that null rays can only focus as they move away from σ, decreasing the the total area of N. As in the discussion of theorems 3.1.1 and 3.1.2, either condition (i) or (ii) suffices to guarantee that the flux of area through any regulator surface $z = z_0$ vanishes as $z_0 \to 0$, and otherwise we discuss only the coefficient of the leading divergence. Since $m(A)$ is minimal on Σ we thus find $\text{Area}_{\text{ren}}(\sigma) \geq \text{Area}_{\text{ren}}(\tilde{\sigma}) \geq \text{Area}_{\text{ren}}(m(A))$.

2.4 Divergences

Entanglement entropy and Causal Holographic Information are both infinite, as are the areas of the boundary anchored surfaces that measure them. In particular, it has been shown [25] that subleading divergences in the area of the causal surface generally differ from those of extremal surface: while the entanglement divergences can be written as the integral of local geometric quantities on ∂A, subleading divergences of the causal surface generally cannot. However, [25] conjectured that the leading-order divergences agree for $d > 2$. We investigate the analogous issues below for marginally trapped surfaces σ anchored to ∂A, showing first that leading area-divergence of σ does in fact agree with that of $m(A)$, and then demonstrating that subleading divergences generally differ.

2.4.1 Leading Order Divergences

It is useful to begin with the Fefferman-Graham expansion of the metric [29]. In $d \geq 2$ dimensions, this takes the form

$$ds^2 = g_{ab}dx^a dx^b = \frac{l^2}{z^2}(dz^2 + \tilde{\gamma}_{ij}(x, z)dx^i dx^j), \tag{2.9}$$

where l is the AdS length scale, x ranges over the boundary coordinates, and[8]

$$\tilde{\gamma}_{ij}(x,z) = \tilde{\gamma}^{(0)}_{ij}(x) + z^2\tilde{\gamma}^{(2)}_{ij}(x) + ...z^d\left(\tilde{\gamma}^{(d)}_{ij}(x) + \bar{\tilde{\gamma}}^{(d)}_{ij}(x)\log(z^2)\right). \tag{2.10}$$

Here, $\tilde{\gamma}^{(0)}_{ij}$ is the metric on the boundary, and the logarithmic term only appears for even d. Note that $ds^2 = \frac{l^2}{z^2}(dz^2 + \tilde{\gamma}^{(0)}_{ij}(x)dx^i dx^j) + O(z^0)$. In particular, the unphysical conformally-rescaled metric

$$\widetilde{ds}^2 = \tilde{g}_{ab}dx^a dx^b = \frac{z^2}{l^2}ds^2 \tag{2.11}$$

is finite as $z \to 0$ and gives the bulk the structure of a manifold $\tilde{M}$ with boundary.

Consider any marginally-trapped surface σ whose derivatives that are C^1 in $\tilde{M}$. Then tangent vectors to σ are well-defined both on $\tilde{M}$ and on the AlAdS boundary, and the geodesic equation on σ is also well-defined. We expect this condition to hold for surfaces constructed as in Section 3.3.

Near the boundary, we can use (generalized) Riemann normal coordinates $\{\hat{x}^\alpha\} = \{\hat{x}^i, z\}$ on σ defined by using the unphysical metric (2.11) to construct a congruence of geodesics orthogonal to the AlAdS boundary. Here we have generalized the notion of Riemann normal coordinates slightly by not requiring z to be proper distance. The $\hat{x}^i$ are constant along the geodesics and agree with x^i on the AlAdS boundary; however, they do not generally agree with the Fefferman-Graham x^i in the interior.

In terms of the coordinates $\hat{x}^\alpha$ on σ, the tangents to the above geodesics are $\tau^\alpha\partial_\alpha = \partial_z|_{\hat{x}^i}$. As a result, the metric induced by (2.11) takes the form

$$\tilde{h}_{\alpha\beta}dx^\alpha dx^\beta = \tilde{q}_{ij}(z)d\hat{x}^i d\hat{x}^j + \widetilde{|\tau|}^2 dz^2, \tag{2.12}$$

[8]At least when there are no operators or non-metric sources with conformal dimension $d \geq \Delta \geq 0$

with $\tilde{q}_{ij}(z) = \tilde{q}^{(0)}_{ij} + O(z)$ for $\tilde{q}^{(0)j}_{i}$ the projector onto the anchor set ∂A and where the error term allows for ∂A to have non-vanishing extrinsic curvature in σ (as computed with respect to (2.11)) even though the extrinsic curvature of the full AlAdS boundary vanishes with respect to this metric. We remind the reader that we use $\tilde{\gamma}^{(0)}_{ij}$ to raise and lower i, j indices on the boundary. In (2.12), $\widetilde{|\tau|}^2$ is the norm of τ^α in the rescaled metric (2.11). Note that while σ is spacelike in the bulk, a priori the norm $\widetilde{|\tau|^2}$ might vanish as $z \to 0$.

Since σ is marginally trapped, it has $\theta_k = 0$. We are free to choose k to have Fefferman-Graham components k^a that vanish like z as $z \to 0$ so that $\tilde{k}^a := k^a/z$ remains finite. We also define a rescaled extrinsic curvature tensor $\tilde{K}_{abc}$ such that for any null vector field v^a orthogonal to σ we have

$$v^a \tilde{K}_{abc} := z v^a K_{abc} = \frac{1}{2} z \pounds_v \left(\frac{l^2}{z^2} \tilde{h}_{bc} \right), \tag{2.13}$$

where $\pounds_v$ denotes the Lie derivative along v and h^c_b is the projector onto σ. Then the condition $\theta_k = 0$ is then equivalent to $\tilde{k}^a \tilde{K}_{abc} \frac{l^2}{z^2} \tilde{h}^{bc} = 0$, where $\tilde{h}^{bc}$ is obtained from $\tilde{h}_{bc}$ by raising indices with $\tilde{g}^{ab}$. Note that converting (2.12) to Fefferman-Graham coordinates $\{x^a\} = \{x^i, z\}$ gives

$$\tilde{h}_{ab} = \tilde{q}_{ab} + \frac{\tilde{\tau}_a \tilde{\tau}_b dx^a dx^b}{\widetilde{|\tau|}^2}, \tag{2.14}$$

where $\tilde{\tau}_a = \tilde{g}_{ab} \tau^b$ and $\tilde{q}_{ab} = \tilde{g}_{ac} \tilde{q}_b{}^c$, where $\tilde{q}_b{}^c$ is the projection onto the space tangent to σ. We may therefore compute as follows:

$$\begin{aligned} 2\tilde{k}^a \tilde{K}_{abc} &= z \pounds_{\tilde{k}} \left(\frac{l^2}{z^2} \tilde{h}_{bc} \right) && (2.15) \\ &= \frac{l^2}{z} \pounds_{\tilde{k}} \tilde{q}_{bc} - 2l^2 \frac{\pounds_{\tilde{k}} z}{z^2} \tilde{q}_{bc} - l^2 z^{-1} \left(\pounds_{\tilde{k}} \ln \widetilde{|\tau|}^2 \right) \frac{\tilde{\tau}_a \tilde{\tau}_b}{\widetilde{|\tau|}^2} + \frac{l^2}{z \widetilde{|\tau|}^2} \left(\tilde{\tau}_a \pounds_{\tilde{k}} \tilde{\tau}_b + \tilde{\tau}_b \pounds_{\tilde{k}} \tilde{\tau}_a \right) && (2.16) \end{aligned}$$

Since τ^a is annihilated by $\tilde{q}_{ab}$, we can derive the useful relation

$$\tau^b \tau^c \pounds_{\tilde{k}} \tilde{q}_{bc} = \tau^b \pounds_{\tilde{k}} (\tau^c \tilde{q}_{bc}) - \tau^b \tilde{q}_{bc} \pounds_{\tilde{k}} \tau^c = 0. \tag{2.17}$$

Contracting (2.15) with $\frac{l^2}{z^2}\tilde{h}^{bc}$ thus yields

$$\begin{aligned} 0 = 2\frac{l^2}{z^2}\tilde{h}^{bc}\tilde{k}^a \tilde{K}_{abc} &= z\pounds_{\tilde{k}} \left(\frac{l^2}{z^2} \tilde{h}_{bc} \right) && (2.18) \\ &= O(z) - 2(d-1)\left(\pounds_{\tilde{k}} z\right) - z\left(\pounds_{\tilde{k}} \ln \widetilde{|\tau|}^2\right) + \frac{2z}{\widetilde{|\tau|}^2} \tau^b \pounds_{\tilde{k}} \tilde{\tau}_b. && (2.19) \end{aligned}$$

But we also find

$$\begin{aligned} \tau^a \pounds_{\tilde{k}} \tilde{\tau}_a &= \tau^a \pounds_{\tilde{k}} (\tilde{g}_{ab} \tau^a) = \frac{1}{2} \pounds_{\tilde{k}} \widetilde{|\tau|}^2 - \frac{1}{2} \tau^a \tau^b \pounds_{\tilde{k}} \tilde{g}_{ab} && (2.20) \\ &= \frac{1}{2} \pounds_{\tilde{k}} \widetilde{|\tau|}^2 - \tau^a \tau^b \tilde{\nabla}_a \tilde{k}_b = \frac{1}{2} \pounds_{\tilde{k}} \widetilde{|\tau|}^2 - \tau^a \tilde{\nabla}_a (\tau^b \tilde{k}_b) = \frac{1}{2} \pounds_{\tilde{k}} \widetilde{|\tau|}^2, && (2.21) \end{aligned}$$

where $\tilde{\nabla}_a$ is the covariant derivative for $\tilde{g}_{ab}$ and the steps on the last line follow from the (non-affinely parametrized) geodesic equation $\tau^b \tilde{\nabla}_b \tau^a \propto \tau^a$ and the orthogonality of τ_a and $\tilde{k}^a$. As a result, (2.18) yields

$$0 = \frac{l^2}{z^2} \tilde{h}^{bc} \tilde{k}^a \tilde{K}_{abc} = -2(d-1)\left(\pounds_{\tilde{k}} z\right) + O(z) = -2(d-1)\tilde{k}^z + O(z). \tag{2.22}$$

I.e., to this order $\tilde{k}$ is tangent to the AlAdS boundary and is thus a null normal to ∂A with respect to the boundary metric $\tilde{\gamma}^{(0)}_{ij}$.

On the other hand, since $\tilde{k}$ is orthogonal to σ we have $\frac{\tilde{k}_a \tau^a}{|\tau|^2} = 0$, so τ_a lies in the null plane defined by $\tilde{k}_a$. And since τ^a is by definition orthogonal to ∂A, we may use the C^1 nature of τ, the fact that $\tau^\alpha \partial_\alpha = \partial_z|_{\hat{x}^i}$, and the equality of the z-component of τ in $\{\hat{x}^\alpha\}$ coordinates with that in Fefferman-Graham coordinates to write $\tau^a = \tau^k \tilde{k}_a + \partial_z x^a + O(z)$

for some finite coefficient τ^k and where the $O(z)$ term is again orthogonal to $\tilde{k}$. Since $\tilde{k}^a$ is both null and (to order z) orthogonal to ∂_z, we find $\widetilde{|\tau^2|} = 1 + O(z)$; in particular, τ^a remains spacelike at $z = 0$.

We are now ready to calculate the leading area-divergence of σ. This is simplest in the coordinates $x^\alpha = \{\hat{x}^i, z\}$ where $\tau^\alpha \partial_\alpha = \tau^z \partial_z|_{\hat{x}^i}$ and the metric induced by $\tilde{g}_{ab}$ is (2.12). It is clear that the physical area of σ takes the form

$$\text{Area}[\sigma] = \int_{\partial A} d^{d-2}x \int dz \frac{l^{d-1}\sqrt{q^{(0)}}}{z^{d-1}} + O(z^{-(d-1)}), \tag{2.23}$$

where the leading term agrees with the leading area-divergence for an extremal surface anchored to ∂A (as it must, since an extremal surface is also marginally-trapped and we have shown this term to be the same for all marginally-trapped surfaces).

Though we leave the details for future work, since we found $\widetilde{|\tau^2|} = 1 + O(z)$ but used only $\lim_{z\to 0} \widetilde{|\tau^2|} = 1$ it seems clear that this result also extends to marginally-trapped surfaces which are more singular at the boundary. This plausibly includes all cases where the constraints F, G of Section 3.3 admit expansions in fractional powers of z.

2.4.2 Subleading Divergences

While the are of σ agrees with that of an extremal surface to leading order, the subleading divergences do not generally match. We can show this by example. Consider the $d + 1 = 5$ dimensional bulk metric,

$$ds^2 = \frac{1}{z^2}(-dt^2 + dz^2 + dy^2 + X(x, y, u)dx^2 + du^2), \tag{2.24}$$

where $X(x, y, u)$ is an arbitrary function. We will take our boundary region to be a strip with $y \in [-f_0, f_0]$ and $t = g_0$ and take the constraints to be $t - G(z) = 0$ and $y - F(z) = 0$.

We can take both the constraints and the metric to be expandable in power series:

$$F(z) = f_0 + f_1 z + f_2 z^2 + f_3 z^3 + ..., \tag{2.25}$$

$$G(z) = g_0 + g_1 z + g_2 z^2 + g_3 z^3 + ..., \tag{2.26}$$

$$X(x,y,u) = X_0(x,u) + F(z)X_1(x,u) + F^2(z)X_2(x,u) + F^3(z)X_3(x,u) + ... \tag{2.27}$$

for some functions X_i and constants f_i, g_i. A calculation shows that for any F and G the two σ-orthogonal null congruences have

$$\theta_\pm = \pm \frac{3z\left(f_1 g_1^2 - f_1^3 - f_1 \pm g_1\sqrt{f_1^2 - g_1^2 + 1}\right)}{(f_1^2+1)\sqrt{f_1^2 - g_1^2 + 1}} + O(z^2). \tag{2.28}$$

$$\tag{2.29}$$

Choosing $\theta_+ = 0$ would then impose $f_1 = g_1$, while $\theta_- = 0$ would impose $f_1 = -g_1$. We can similarly solve $\theta_+ = 0$ or $\theta_- = 0$ to second order, and we find

$$f_2 = \frac{f_0^2 X_2(y,u) + 2f_0 X_1(y,u) + 3X_0(y,u)}{8f_0\left(f_0^3 X_3(y,u) + f_0^2 X_2(y,u) + f_0 X_1(y,u) + X_0(y,u)\right)} \pm g_2 - \frac{3}{8f_0}. \tag{2.30}$$

Now, the area of the marginally trapped surface will be given by

$$A = \int \mathrm{d}z\mathrm{d}u\mathrm{d}x \frac{1}{z^3}\sqrt{1 + F'(z)^2 - G'(z)^2}\sqrt{X(x,y,u)}. \tag{2.31}$$

Evaluating (2.31) on our solutions for f_1 and f_2, yields

$$\begin{aligned} A = &\int \mathrm{d}z\mathrm{d}u\mathrm{d}x \frac{1}{z^3}\left(\sqrt{X_0(x,u) + f_0 X_1(x,u) + f_0^2 X_2(x,u) + f_0^3 X_3(x,u)}\right) \\ &+ \int \mathrm{d}z\mathrm{d}u\mathrm{d}x \frac{1}{z^2}\left(\frac{g_1 X_1(x,u) + 2f_0 g_1 X_2(x,u) + 3f_0^2 g_1 X_3(x,u)}{4\sqrt{X_0(x,u) + f_0 X_1(x,u) + f_0^2 X_2(x,u) + f_0^3 X_3(x,u)}}\right) + O(\ln z). \end{aligned} \tag{2.32}$$

As expected, the leading divergence is fixed by boundary conditions only, as seen by the fact that it depends only on f_0. The subleading divergence, however, depends on g_1 as well. This g_1 is the asymptotic slope of the slice determined by $G(z)$, and thus will generally differ from that of the the extremal surface.

Since the divergence depends on the slope of the slice, we expect it to have some relation to the tangent plane to the marginally trapped surface. Consider the unique tangent vector

$$\tau^a = (t, x, y, u, z) = \frac{\partial}{\partial z}(G(z), x, F(z), u, z). \tag{2.33}$$

that is orthogonal to the boundary of σ. We expect the divergence to be in part determined by τ^a, though it must be contracted with some one index object that contains information about the boundary region A. A natural candidate is the trace of the extrinsic curvature of ∂A,

$$K^{(b),i}{}_i = \nabla^i n^{(A)}{}_i, \tag{2.34}$$

where the i index runs over the boundary indices, the b index runs over the 2 vectors orthogonal to our boundary subregion (and contained in the boundary), and n is the normal to ∂A that points outwardly away from A. The only nonzero component is

$$K^{(y),i}{}_i = \frac{X_1(x,u) + 2X_2(x,u)y + 3X_3(x,u)y^2 + ...}{2\left(X_0(x,u) + X_1(X,u)y + X_2(x,u)y^2 + 3X_3(x,u)y^3 + ...\right)}. \tag{2.35}$$

Define $\tau_\parallel$ to be the projection of τ^a into the AdS boundary. We can then contract with $K = (K^t, 0, K^y, 0) = (0, K^y, 0)$. This gives

$$K \cdot \tau_\parallel = \frac{\left(X_1(x,u) + 2X_2(x,u)y + 3y^2X_3(x,u) + ...\right) f_1}{2\left(X_0(x,u) + X_1(x,u)x + X_2(x,u)y^2 + X_3(x,u)y^3 + ...\right)}. \tag{2.36}$$

Integrating (2.36) over ∂A and using $y = f_0$ gives

$$\begin{aligned}&\int_{\partial A} \mathrm{d}u\mathrm{d}x \sqrt{X(x,y,u)} K \cdot \tau_{\|} \\ &= \int \mathrm{d}u\mathrm{d}x \frac{g_1 \left(X_1(x,u) + 2f_0 X_2(x,u) + 3f_0^2 X_3(x,u) + ...\right)}{2\sqrt{X_0(x,u) + f_0 X_1(x,u) + f_0^2 X_2(x,u) + f_0^3 X_3(x,u) + ...}},\end{aligned} \tag{2.37}$$

so that

$$\begin{aligned}A &= \int \mathrm{d}z \frac{1}{z^3} \int_{\partial A} \mathrm{d}u\mathrm{d}x \sqrt{X(x,y,u)} K \cdot \tau_{\|} \\ &= \int_A \sqrt{h_A} \left(-\frac{1}{2z^2} - \frac{1}{z} K \cdot \tau_{\|} \right).\end{aligned} \tag{2.38}$$

for h_A the induced metric on A from the boundary metric. Thus, the subleading divergence is given by the integral of the trace of the extrinsic curvature of ∂A contracted with the tangent vector orthogonal to the boundary of the marginally trapped surface.

2.5 Thermodynamics

It has been previously shown that, when they are compact, the areas of leaves of holographic screens monotonically increase [8, 7]. In this section, we generalize this proof to the case of non-compact leaves. The main difficulty in the original proof is constraining the ways in which holographic screens can change from spacelike to timelike. If, for instance, we knew that flowing along our screen moved a given leaf only toward the past and/or toward the boundary, we could quickly conclude that the area increased. If it was toward the past, we could first flow infinitesimally to the past along the k-congruence (i.e., in the negative k direction), and then to the past along the ℓ-congruence (i.e., in the negative k direction). Along the k-congruence, the area remains constant to first order as one moves away from any leaf. Since the expansion is non-negative in the negative ℓ direction, to first order the area cannot decrease. The net change is then non-negative, and the area of the leaves will not decrease. Likewise, if the nearby leaf was spacelike

and towards the boundary, we could first flow along the future $\theta_k = 0$ direction, then along the past $\theta_\ell > 0$ direction, leading again to non-decreasing area. Reversing these arguments, if the nearby leaf were to the future or spacelike away from the boundary, the area would decrease. We therefore would like to rule out transitions – like moving towards the past and then away from the boundary – that would lead to a non-monotonic area change.

Before we rule out out the problematic flow directions, we will review the assumptions of [7], and those made here.

Definition: We can define a set of leaf-orthogonal curves γ such that every point p in our holographic screen H lies on one curve. We can further choose a parameter r that is constant along each leaf σ but increases monotonically along each curve γ.

Since γ is taken to be orthogonal to each leaf, its tangent vector h^μ can be written as a linear combination of the null congruences,

$$h^\mu = \alpha \ell^\mu + \beta k^\mu. \tag{2.39}$$

where h is normalized such that r increases at unit length along h. Note that α and β cannot be both zero, though they may approach zero at the AlAdS boundary.

We will then use the following assumptions about the spacetime, following [7]. As above, we assume the null curvature condition, $R_{ab} = k^a k^b \geq 0$. We also assume two generic conditions. One, that $R_{ab}k^a k^b + \xi_{ab}\xi^{ab} > 0$ at every point on our holographic screen for the k-directed congruence. Two, if we denote by H_0, H_+, and H_- the sets where respectively $\alpha = 0, \alpha > 0$, and $\alpha < 0$ on H, then $H_0 = \partial H_- = \partial H_+$. Further, we assume that every inextendible portion of our holographic screen is either entirely timelike, or contains a complete leaf. Finally, we assume that every leaf σ on our screen splits a Cauchy surface Σ into two disjoint components. The extent to which such assumptions

are reasonable for compact leaves is discussed in [7]; similar comments apply here. From these assumptions, it follows that at least one leaf will have definite sign of α. We can take $r = 0$ on this leaf, and orient r such that $\alpha < 0$. It suffices to consider each connected component of H separately, so we may take H to be connected for the rest of the argument.

We make one additional assumption beyond those of [7], namely that H can be deformed continuously into a sequence of screens H_a by deforming the anchor sets of each leaf $\sigma_a(r_i)$ in a spacelike direction such that $A(\sigma_a(r_i)) \supset A(\sigma_a(r_j))$ for $r_i < r_j$, and $A(\sigma_a(r_i)) \subset A(\sigma_b(r_i))$ for $a < b$, with $H_0 = H$.

We can now quickly reduce our setting to (almost) the one considered in [7]. We proceed by first recalling that, as discussed above, the essence of the argument is really a theorem about certain changes of sign as one moves along the holographic screen. Those signs are conformally invariant, as they do not depend on the metric. So it suffices to prove the 'restricted changes of sign' version of the theorem for our screen as embedded in the unphysical conformally-rescaled spacetime associated with the metric $\widetilde{ds}^2$ of (2.11). The area increase theorem then follows for the original screen in the physical spacetime by using the conditions $\theta_k = 0, \theta_\ell \leq 0$ that hold there.

In this unphysical spacetime the leaves are now compact, but they have boundaries at the AlAdS boundary. To reduce this to the no-boundary case considered in [7], we now consider two copies of the unphysical conformally rescaled spacetime and identify them along their AlAdS boundaries. The resulting $\mathbb{Z}_2$-symmetric spacetime is compact, globally-hyperbolic (in the usual non-AdS sense), and has no boundary. This procedure also glues together the two copies of H_a and H to make holographic screens with compact leaves.

The only remaining difference from the setting of [7] is that, in the doubled spacetime, the leaves are generally only continuous and may not be smooth. However, the proof of [7]

proceeds by firing null congruences from various leaves and studying their intersections (or, at least the intersection of the associated boundaries of future and/or past sets) with the screen. Having shown that these intersections lie entirely on one side of the $r = 0$ leaf, continuity and compactness guarantee the intersection to have a minimum (or maximum) r. Smoothness is then used to argue that the intersection it tangent to the leaf at this minimum (maximum) r, and to find a contradiction with our Corrollary 2.3. In our case, taking H_a to be small deformations of H satisfying the above conditions guarantees that there can be no intersection on the AlAdS boundary, and so in particular the minimum (maximum) r does not occur there. Since the doubled screen is smooth away from the AlAdS boundary, the rest of the argument then proceeds as in [7] to yield:

Theorem 5.1 Let H be a future holographic screen satisfying the above assumptions, with a leaf orthogonal tangent vector field $h^a = \alpha \ell^a + \beta k^a$. Then $\alpha \leq 0$ on all of H.

The desired result then follows immediately.

Theorem 5.2 The area of the leaves of H increases monotonically as measured by the physical bulk metric ds^2.

2.6 Discussion

We have shown that boundary-anchored holographic screens anchored in AlAdS spacetimes have several interesting properties. First, for a boundary "spatial region" (partial Cauchy surface) A with no extremal surface barriers between the screen and the compliment of A in the boundary Cauchy surface, any screen anchored to ∂A lies above the future horizon of $D_{bndy}(A)$ but inside of the entanglement wedge of A. We further showed that the area of the holographic screen is bound below by the area of the extremal surface, and in certain cases, bounded above by the quantity we called future causal holographic information (fCHI) defined by the area of a cut of the causal horizon.

We also studied the divergences in area of the holographic screens. While the leading divergence of a holographic screen matches that of the extremal surface, the first subleading divergence generally differs from that of extremal surfaces. Finally, we have shown that, under a continuous choice of flow along leaves, there is a monotonic change in area, generalizing the results of [7] to the case of non-compact leaves.

A technical complication in our work is the large set of assumptions (matching those of [7]) used to prove the 2nd law in Section 2.5. Most of these are clearly true in the generic case, but this is far from clear for the assumption that every inextendible portion of the screen is either entirely timelike or contains a complete leaf. Another complication is that the various bounds on the area of boundary-anchored marginally-trapped surfaces are generally useful only for surfaces already known to coincide with extremal surfaces up to corrections vanishing faster than z^{d-2} – the order required to make the area only finitely different from that of an HRT surface. It would be much more natural to find a simple construction of marginally-trapped surfaces for which these assumptions were guaranteed to be satisfied, or which forced the desired results to apply more generally. It would also be interesting to (perhaps numerically) explore whether the inextendible portion assumption holds in general, either in our boundary-anchored setting or in the original compact context of [7]. However, we leave such explorations for future work.

Since the holographic screen lies inside the entanglement wedge, it should describe some property of any dual field theory in $D_{bndy}(A)$. Interestingly, this differs substantially from the original conjecture of [30] regarding the holographic properties of such screens which took the screen to describe degrees of freedom on what we would call the 'inside' (i.e., the ℓ-congruence side) of the screen. In contrast, our result suggests the screen to describe properties of $D_{bndy}(A)$ and the associated part of the entanglement wedge 'outside' the screen (i.e., on the k-congruence side). As described in Section 2.3, the above-mentioned bounds on the area of any leaf suggest such areas to measure a coarse-

grained entropy for the dual CFT (though one that is finer-grained than that associated with fCHI).

Indeed, while this work was in preparation, ref. [14] appeared which studied a closely related issue. Their work shows that the area of a black hole's apparent horizon measures a coarse-grained entropy, where the coarse-graining is over all solutions in the interior, keeping the geometry of the exterior fixed. In particular, they show that the apparent horizon area agrees with that of the largest HRT surface consistent with the above constraints. Although [14] does not study boundary anchored surfaces, we anticipate it to admit an extension to boundary anchored leaves whose divergences match those of extremal surfaces. In contrast, however, the analogous result is clearly forbidden when the divergences of the leaf fail to match all state-independent divergences of the extremal surface.

Now, as in [8], the area-increase result of Section 2.5 suggests a thermodynamic interpretation for the area. Here we find that the area increases toward the boundary, in the sense that one moves in the direction along the holographic screen that is most closely associated with the k-congruence, when the screen moves in a spacelike direction. Interestingly, on a timelike part of the screen this corresponds to moving the leaf toward the past [8]. There is also the somewhat uncomfortable property that the area-increase theorem requires comparing entire leaves; deforming a cut of the screen locally toward the future (so that it no longer coincides with a leaf) is not generally guaranteed to increase the area.

Recall, however, that Section 2.3 noted that the area of a leaf is also bounded above by the area of a cut Y of the future horizon when the leaf is constructed by requiring it to lie in the boundary of the future $\dot{I}^+(S)$ of some set S in the AlAdS boundary satisfying $\partial S = \partial A$. This Y is the intersection of the future horizon with $\dot{I}^+(S)$ introduced in [26], and its $A/4G$ is naturally called future causal holographic information. Here we

again emphasize the difference in perspective from constructions of marginally-trapped surfaces from light cones in [30], as the light cones of [30] were generated at σ by the k-congruence while our $\dot{I}^+(S)$ is generated at σ by the l-congruence.

Since deformations of S toward the future now move $\dot{I}^+(S)$ outward when the screen is spacelike, in such cases our second law makes the associated areas of marginally-trapped surfaces monotonically non-decreasing under any such flow. This reinterpretation of the results of Section 2.5 would then remove the discomforts mentioned above. In particular, when the screen is spacelike we now find non-increase toward what is clearly the future and, in addition, the system may be pushed forward in time independently at each point. We therefore hope to investigate this construction further in the future, as always with an eye toward better understanding the interpretation in the dual CFT.

Finally, as always in such discussions, one would like to progress beyond leading order in the bulk semi-classical expansion. This would presumably involve replacing the area of each leaf with the generalized entropy as in [31, 20, 32, 33]. However, it is unclear just how the bulk entanglement term should be defined for bulk gravitons. While the arguments of [32] and [33] can be used to define this entanglement across an HRT surface, at least at present there is no general understanding of how to define such entanglement across a general bulk surface – or even a general one that is marginally trapped. The issue is a classic one associated with the failure of the linearized graviton action to be gauge invariant on off-shell backgrounds such as those that would naturally be used in attempting to define this entanglement using the replica trick. Nevertheless, it would still be natural to explore the effects of entanglement terms associated with other bulk fields while awaiting a better understanding of graviton entanglement.

Chapter 3

Radial Cutoffs and Holographic Entanglement

3.1 Introduction

3.2 Introduction

There is a great deal of interest in generalizing the AdS/CFT correspondence so as to rely less on the presence of an asymptotically AdS boundary. An ultimate goal would be understand a notion of gravitational duality relevant to cosmology, and in particular to our own apparently-inflating spacetime.

A possible first step toward this goal is start with a standard asymptotically-AdS holographic set up, and then to remove the AdS boundary by introducing a finite radial cutoff. This was idea behind the work of [34] and its generalizations (e.g. [35, 36]; see also [37]), which posited that the introduction of such cutoffs was related to irrelevant deformations of the dual CFT. Such radial cutoffs are naturally taken to define codimension 1 boundaries at finite distance from the bulk, though we will emphasize the study

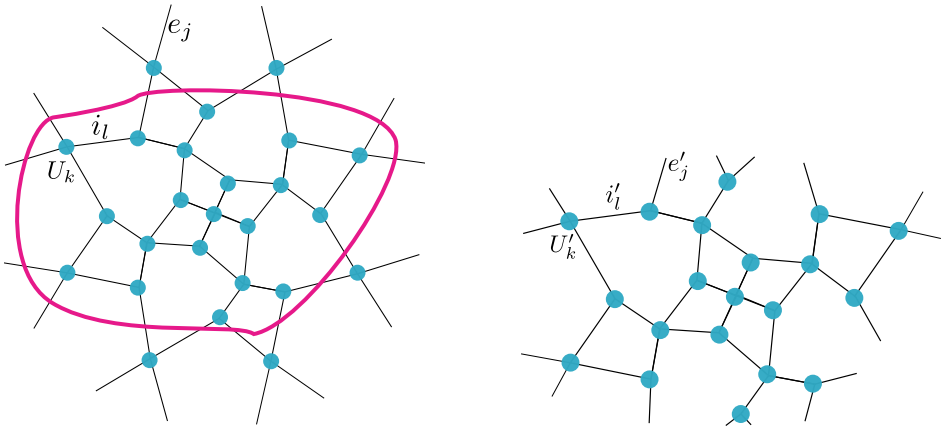

Figure 3.1: A tensor network is a graphical depiction of a quantum state in a multipartite Hilbert space. It also represents a circuit that prepares the state, consisting of tensors U_k contracted over internal indices i_l. Left: A tensor network representing a state $|\psi\rangle \in \mathcal{H}_{e_1} \otimes ... \otimes \mathcal{H}_{e_n}$ and a magenta curve along which this network will be cut off. We use e_j to denote the links at the boundary of the network, though only one is labelled explicitly in the figure. Right: Cutting off the tensor network at left defines a new tensor network which constructs a different state $|\psi'\rangle \in \mathcal{H}_{e'_1} \otimes ... \otimes \mathcal{H}_{e'_m}$ in a different Hilbert space associated with the new boundary links e'_j (again with only one labelled explicitly in the figure).

of codimension 2 boundaries in sections 3.3-6.4.

More generally, the idea that some notion of holography should persist in the presence of a radial cutoff is strongly motivated by tensor network models; see e.g.[38, 39, 40, 41, 42, 43, 44, 45]. In any tensor network, an arbitrary cut through the interior (perhaps defined by a cutoff surface) will define a state living on that cut; see figure 3.1. Furthermore, in many cases where the original tensor network defines an isometric embedding of a bulk Hilbert space into a boundary dual, the same will be true of the cutoff network. Such ideas are closely related to the surface/state correspondence suggested in [46], the entanglement of purification conjecture [47, 48], and the construction of tensor networks on sub-AdS scales described in [49, 50]. See also [51, 52].

However, there remains the question of how to access the supposed quantum state on the cutoff surface using bulk techniques, and in particular how to compute quantities related to quantum information. In the time symmetric context, it would appear that the

Ryu-Takayanagi (RT) formula [53, 9] continues to give consistent results for entanglement entropy in the presence of such cutoffs. In particular, in addition to the explicit checks performed in [54], it is easy to see that the original proof of strong subadditivity (SSA) [10] for contexts without cutoffs in fact continues to hold when one is present. Indeed, the argument of [10] relies only on the fact that RT surfaces are minimal subsurfaces on a common time slice, without regard to the nature of the geometry on that slice.

In dynamical contexts, however Hubeny-Rangamani-Takayanagi (HRT) surfaces anchored to a finite boundary may fail to be minimal subsurfaces of a common achronal surface, even when their boundary anchor sets are spacelike separated with respect to the bulk. In this context, SSA may simply fail to hold.

We discuss several examples of such SSA violations in sections 3.3.1 and 3.3.1 below. Other cases violating HRT-SSA with a radial cutoff were recently studied in [55], where it was found that entanglement wedge nesting failed as well. See also [56] for discussions of SSA failures in de Sitter space. The examples of [55] were associated with a discrepancy between bulk and boundary causality, as regions of the cutoff surface were spacelike separated with respect to the induced metric on the cutoff surface but were nevertheless causally related through the bulk. One might thus think that the SSA issue could be resolved by restricting to boundary regions that are also spacelike separated through the bulk. However, the examples of 3.3.1 below will show explicitly that SSA violations can occur even in contexts that respect bulk causality in this way.

Instead, the key feature of all violations turns out to be the failure of the relevant extremal surfaces to be contained in a single domain of dependence within the cutoff bulk. In the terminology of [46], this is called a failure of convexity. This means that entanglement wedge nesting also fails again. But with regard to SSA, the domain of dependence issue in particular implies that there cannot be a bulk achronal slice containing both the relevant slice of the cutoff boundary and all of the extremal surfaces. As

a result, and consistent with the explicit violation in our examples, one cannot readily use the same proof strategy of [10] as in the RT case. In particular, the HRT-SSA proof given for the cutoff free case in [13] does not apply.

Improving the situation appears to require a new proposal for holographic entropy in the presence of a radial cutoff. The above comparison with [13] immediately suggests that we consider instead a maximin based construction, which in simple cutoff free cases provides an alternate definition of holographic entanglement that turns out to be equivalent to HRT. The maximin approach can also be used to establish SSA in the the case of a convex cutoff surface [23]; see also [57, 58]. Now, as shown by the example in section 3.3.1, the original maximin construction of [13] does not suffice. But realizing that we do not currently understand what notion of causality might govern the propagation of information and excitations in a (likely nonlocal) dual description on the cutoff surface, we will take one further step and consider instead the *restricted* maximin procedure of [59] associated with a codimension 2 cutoff surface γ rather than a codimension 1 radial cutoff. Restricted maximin surfaces are confined by construction to the domain of dependence of an achronal surface that ends on γ, so any extremal surface outside this domain must differ from the associated restricted maximin surface. We will show below that the areas of our restricted maximin surfaces *do* satisfy SSA, suggesting that these surfaces give a better definition of holographic entanglement in settings with a radial cutoff. Indeed, we will see that in time-symmetric settings this prescription reproduces the successful RT prescription much better than does naive application of HRT. Entanglement wedge nesting and monogamy of mutual information [60] will follow as well.

In fact, we will work below with a very general notion of "cutoff." We consider any smooth codimension 2 surface in any spacetime satisfying basic positive energy properties (to be detailed below). In particular, we make no assumption that our spacetime with boundary be constructed from an asymptotically AdS spacetime, or that its dynamics

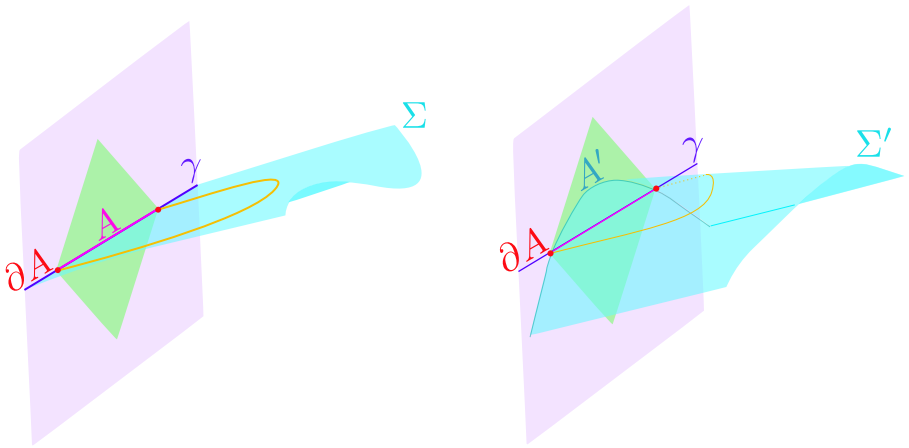

Figure 3.2: Left: A restricted maximin surface is defined by a maximin construction on Cauchy slices which are constrained to contain a codimension 2 surface γ. Right: For an (unrestricted) maximin surface, Σ' need not contain γ or A, but may instead meet γ only on the subset ∂A.

involve a negative cosmological constant.

Before proceeding, we pause to give a very brief summary of the restricted maximin approach from [59]. The construction begins by choosing a slice γ of the cutoff boundary, so that γ is a codimension 2 surface with respect to the bulk. It then constructs a bulk entangling surface for $A \subset \gamma$ using a two step procedure that first minimizes the area of surfaces homologous to A on each bulk achronal surface with boundary γ. We call these achronal surfaces 'Cauchy surfaces' as we are interested only in the corresponding domain of dependence. The second step then maximizes the above minima over all such Cauchy surfaces. We use $\mathrm{Mm}_\gamma(A)$ to denote the resulting restricted maximin surface. Here the term 'restricted' refers to the fact that in the second step, the boundary of the Cauchy surfaces is held fixed, whereas the original (unrestricted) maximin procedure considered all bulk Cauchy surfaces that include the much smaller set ∂A. In the contexts originally studied in [13], unrestricted and restricted maximin surfaces turn out to coincide [59].

Interestingly, the recent works [61, 62, 63, 64, 65, 66, 67, 68, 69, 70] on recovering the Page curve from quantum extremal surfaces suggest a rather different motivation

for fixing a codimension 2 surface γ. In those works it was noted that codimension 2 boundaries are natural when the bulk is not an isolated system. Time evolution then generally changes the entropies being studied, so one must fix a slice of the codimension 1 boundary (and thus effectively a codimension 2 boundary) to obtain a well-defined answer. Fixing a codimension 2 boundary is thus natural if the bulk inside the supposed cutoff surface continues to interact with the exterior; i.e., it is natural if one regards the codimension 1 "cutoff" as merely a slice through a larger bulk system as opposed to a true cutoff on the dynamics.

The remainder of the paper is organized as follows. We begin in section 3.3 by reviewing known violations of strong subadditivity for HRT areas in the presence of a radial cutoffs. This section also states various definitions and reviews certain useful results from prior works. The proofs of restricted maximin strong subadditivity, entanglement wedge nesting, and monogamy of mutual information for an arbitrary codimension 2 boundary γ are given in section 3.4. Section 6.4 concludes with a brief discussion. An appendix contains some additional results (not required for the main argument) showing that up to sets of measure zero our restricted maximin surfaces either coincide with γ or are spacelike separated from γ; i.e., null separations from γ are rare.

3.3 Preliminaries

We begin by reviewing known violations of strong subadditivity (SSA) for HRT areas in the presence of a finite radius cutoff. In each case, we will see that SSA is nevertheless satisfied by restricted maximin areas. We then establish notation for the remainder of the paper, formally define our restricted maximin surfaces, and review useful results from [13] regarding null congruences that touch at a point.

3.3.1 Violations of HRT Strong Subadditivity

We now review several examples of strong subadditivity violations for HRT areas from [23] and [71]. In each example, we will see that the restricted maximin areas in fact satisfy SSA.

Violations of Subadditivity Deep in the Bulk

Our first class of examples was described in [23]. In these situations, the HRT areas violate not only strong subadditivity but also the weaker subadditivity inequality $S_A + S_B \geq S_{AB}$. For simplicity, we consider the case of $d + 1 = 3$ bulk dimensions so that the codimension 2 cutoff surface γ is a curve. Specifically, we consider a case where γ contains two null geodesic segments A and B, whose past ends coincide at some point p, and where A and B are small enough that we may approximate the spacetime near them as flat Minkowski space; see figure 3.3. In particular, A and B will then lie in a common timelike plane. In the approximation that the spacetime is flat, the extremal surface $x(A)$ associated with subregion A coincides with A. Similarly, $x(B)$ then coincides with B. However, the extremal surface $x(AB)$ will be a spacelike curve with $S(AB) = |x(AB)| > 0$, where $|a|$ denotes the proper length of the surface a. But A and B are null, so $S(A) = |x(A)|$ and $S(B) = |x(B)|$ both vanish, violating subadditivity.

Suppose that we instead wish to use a standard maximin construction as in [13]. This would require the specification of a codimension 1 cutoff surface. If we take this cutoff to include the entire timelike plane containing A and B, then the maximin surfaces will again be given by the extremal surfaces $x(A) = A$, $x(B) = B$, and $x(AB)$ given above. So the same violation would remain.

In contrast, the restricted maximin surfaces $\mathrm{Mm}_\gamma(A)$, $\mathrm{Mm}_\gamma(B)$, and $\mathrm{Mm}_\gamma(AB)$ of A, B, and AB are $\mathrm{Mm}_\gamma(A) = A$, $\mathrm{Mm}_\gamma(B) = B$, and $\mathrm{Mm}_\gamma(AB) = AB$. This is clear from

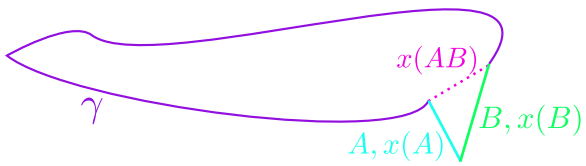

Figure 3.3: An example violating HRT subadditivity with a cutoff in an approximately flat (2+1) dimensional bulk. On a codimension 2 cutoff γ (solid curve), we choose two subregions, A (blue) and B (green). The cutoff γ is constructed so that A and B are null segments intersecting in a timelike plane. The extremal surfaces $x(A)$ and $x(B)$ associated with A and B respectively coincide with A and B. However, the extremal surface $x(AB)$ (dotted pink) associated with AB is a spacelike curve whose non-zero area violates subadditivity.

the fact that their areas all vanish, so they must be minimal on each allowed Cauchy surface. Maximizing zero over all Cauchy surfaces gives zero, so they are restricted maximin surfaces as claimed. Note that their vanishing areas satisfy both SA and SSA.

Violations of Strong Subadditivity Near the Boundary

A second violation of HRT-SSA arises when one imposes a simple radial cutoff on empty global AdS_3 [71]. Here we think of the cutoff as defined by a codimension 1 cylinder near the boundary (see figure 3.4). The construction of the example proceeds in stages. One first finds a situation saturating strong subadditivity. This may be done by starting with a null plane in the bulk, and considering two spacelike boundary intervals A_0 and C_0 formed by the intersection of this null plane and the cutoff cylinder. One also chooses another spacelike segment B_0 that connects A_0 and C_0 as in figure 3.4. In the limit where the cutoff surface becomes the original AdS boundary, A and C become null and the setup resembles both that of [72] and [55].

Since the bulk spacetime is just empty AdS_3, the HRT surfaces are known exactly. In particular, the familiar statement that entanglement wedges and causal wedges coincide in empty AdS_3 means that the HRT surfaces associated with any combination of the

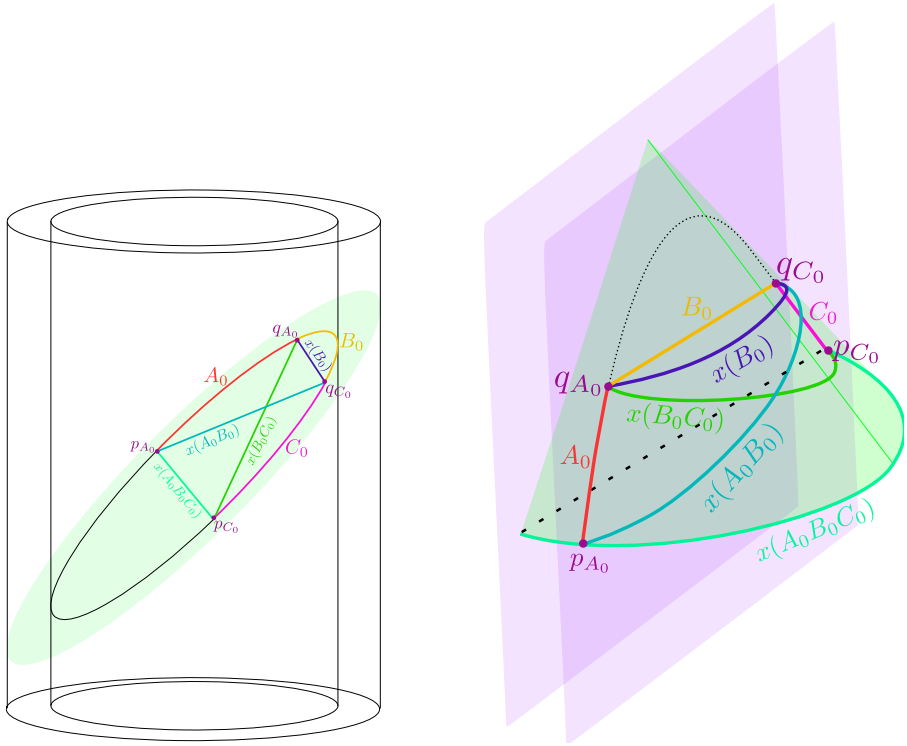

Figure 3.4: An example where HRT areas saturate strong subadditivity on a cutoff surface. Left: A null plane (green) in vacuum AdS_3 with a cylindrical cutoff, marked intervals A_0, B_0, C_0, and the corresponding extremal surfaces $x(A_0), x(B_0), x(C_0)$. Right: A rough sketch of the same setting in Poincaré coordinates centered on B_0. The sketch becomes an exact representation of the conformal structure in the limit where the spacelike intervals A_0, B_0, and C_0 are small in the sense that they are contained in a small neighborhood near the top of the ellipse in the left panel.

regions A_0, B_0, C_0 must lie in the above null plane for any value of the cutoff. And since the expansion of the null congruence generating this null plane vanishes, curves in the plane can be deformed along the plane without changing their length so long as the endpoints of the curves are held fixed. One thus finds

$$\begin{aligned} |x(A_0B_0C_0)| + |x(B_0)| &= |x(A_0)| + 2|x(B_0)| + |x(C_0)| \\ &= |x(A_0B_0)| + |x(B_0C_0)| \end{aligned} \tag{3.1}$$

so that strong subadditivity is saturated.

The key point is then that this example can be perturbed by translating the future

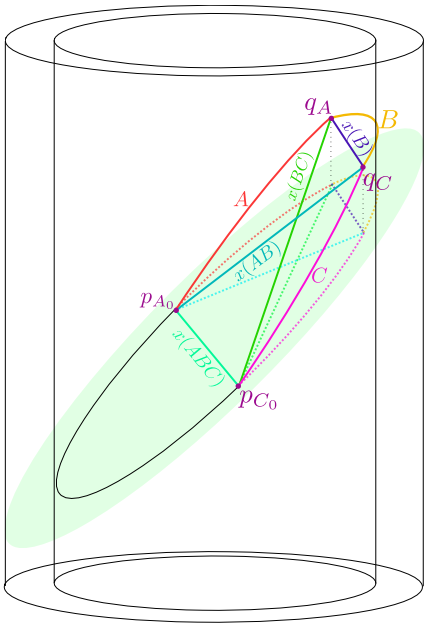

Figure 3.5: An example violating of strong subadditivity for HRT areas with a cutoff in vacuum AdS_3. The setting in figure 3.4 has been deformed by acting with a small time translation on the future endpoints q_{A_0} and q_{C_0} of A_0 and C_0 to define new future endpoints q_A, q_C, and new intervals A, B, and C.

endpoints q_{A_0} and q_{C_0} of A_0 and C_0 in a future timelike direction to define new future endpoints q_A and q_C (still spacelike separated from p_{A_0}, p_{C_0}) and new intervals A, B and C. Since the translation is an isometry, one finds $|x(B)| = |x(B_0)|$. Further, since the past endpoints p_{A_0}, p_{C_0} do not move, we have $x(ABC) = x(A_0B_0C_0)$ as shown in figure 3.4. But $x(AB)$ and $x(BC)$ become closer to being null, so their lengths decrease. As a result, the HRT areas now violate SSA.

Note that since the new endpoints lie to the future of the original null slice, the extremal surfaces and intervals can no longer be placed in a common Cauchy slice. In particular, though ABC remains achronal, $x(ABC)$ is now in the past of B. Thus, $x(ABC)$ cannot be a restricted maximin surface. The actual restricted maximin surfaces are harder to identify, but must satisfy SSA by Corollary 3 in section 3.4 below.

3.3.2 Definitions and Lemmas

We now state the notation and conventions that will be used in the remainder of the paper.

Throughout this work we will take the bulk spacetime to be classical, smooth. The spacetime is also assumed to satisfy 1) the Null Curvature Condition (NCC), $R_{ab}k^a k^b \geq 0$, for any null vector k^a and 2) a so-called generic condition such that there is nonzero null curvature $R_{ab}k^a k^b$ or shear $\sigma_{ab}\sigma^{ab}$ along any segment of any null curve. Note, however, that strong subadditivity is a closed inequality (e.g. saturation is allowed) and that the generic condition allows the above curvature or shear to be arbitrarily small. As a result, a proof of strong subadditivity using the generic condition immediately implies that strong subadditivity continues to hold even when the generic condition is not enforced. To see this, one need only approximate the spacetime in which the generic condition fails (but all other assumptions hold) by a sequence of generic spacetimes and take an appropriate limit.

In principle, we would like to allow the cutoff surface γ to be any closed codimension 2 achronal submanifold of the bulk spacetime. We emphasize that achronality is defined by the bulk causal structure. Indeed, we introduce no notion of a codimension 1 boundary. In fact, we could weaken the above condition to also allow portions of γ to lie along any asymptotically locally anti-de Sitter (AlAdS) boundary (and so, in particular, we do not require γ to be compact).

While the examples considered above include cutoff surfaces γ with sharp corners or null components, we will take γ to be smooth and spacelike for the purposes of making the arguments below. But again, because strong subadditivity is a closed inequality, a proof for smooth spacelike γ immediately implies that strong subadditivity holds for e.g. all piecewise smooth, achronal γ, as such a γ can be approximated by the appropriate

limit of a sequence of smooth spacelike curves.

The fact that we treat γ as a cutoff means that our bulk spacetime is the domain of dependence $D(\gamma)$ of an anchronal surface Σ with boundary $\partial\Sigma = \gamma$, so that we effectively work in a the globally hyperbolic spacetime $D(\gamma)$. We thus use the term Cauchy surface to refer to Σ or any other achronal Σ' with the same domain of dependence. We use $\mathcal{C}_\gamma$ to denote the set of all such Cauchy surfaces for $D(\gamma)$.

There are various possible subtleties associated with the fact that general Cauchy surfaces need not be smooth. It is not clear that all such subtleties were explicitly addressed in the original maximin paper [13], and we will not attempt to do so here. We will instead assume below that all relevant Cauchy surfaces Σ are at least piecewise smooth and leave treatment of the more general case for future work. Note that the piecewise smooth case allows points p on Σ where the space of tangent vectors at p depends on the direction from which p is approached. We expect this generalization of the smooth case to be important, as our maximin procedure may give rise to surfaces Σ that partially coincide with the boundary $\partial D(\gamma)$. Failures of smoothness will certainly occur at caustics of the null congruences along this boundary, and they may also arise when p lies at the boundary of $\Sigma \cup \partial D(\gamma)$. We will similarly assume below that any maximin surface is piecewise smooth.

As one may expect, we will make significant use of the ingoing and outgoing future pointing null congruences orthogonal to γ. We denote their affinely parametrized tangent vectors respectively by k^a and l^a respectively, with θ_k and θ_l the corresponding null expansions.

Having established this notation and the above conventions, we now define our restricted maximin surfaces in two steps.

Definition 3.3.1. For any subregion $A \subset \gamma$, and for each element $\Sigma \in C_\gamma$, let $\min(A, \Sigma)$ be the codimension 2 surface in Σ which is anchored to ∂A, homologous to A within Σ,

and has minimal area consistent with the above constraints. If there are multiple such surfaces, $\min(A, \Sigma)$ can refer to any of them.

Definition 3.3.2. The *restricted maximin surface* $\mathrm{Mm}_\gamma(A)$ is then the minimal surface $\min(A, \Sigma)$ whose area is maximal with respect to variations over surfaces $\Sigma \in C_\gamma$. By contrast, $x(A)$ will by used to denote the smallest extremal surface anchored to ∂A.

We also mention the following two lemmas that will be used in the next section.

Lemma 1. The boundary of $D(\gamma)$ is $\partial D(\gamma) = L^+ \cup L^- \cup \gamma$ where L^+ is the set of points $p \notin \gamma$ that are reached by null geodesics along the vector field k which start at γ and which have not arrived at any conjugate point or nonlocal geodesic intersection before reaching p. L^- is defined similarly with k replaced by $-l$. Note that $L^\pm$ includes points on caustics.

This lemma is precisely Theorem 1 of [73] restated in our particular context using the above notation. As a result, it follows immediately from their argument.

Lemma 2. Suppose N_1 and N_2 are two smooth null congruences that are tangent at some point p on a Cauchy surface Σ. If N_2 is nowhere to the (chronological) past of N_1, then in any sufficiently small neighborhood of p, either i) N_1 and N_2 coincide, or ii) there exists a point y at which $\theta_{N_2} > \theta_{N_1}$. Here we may use any smooth map between N_1 and N_2 to compare points on the two surfaces.

This lemma is Theorem 4 of [13]. Because we will often wish to study congruences which are not obviously smooth, we pause to state the following immediate corollary, which we number zero for later convenience.

Corollary 0. Note that both cases (i) and (ii) of Lemma 2 require $\theta_{N_2}(x) \geq \theta_{N_1}(x)$. Indeed, equality is manifest in case (i), and otherwise $\theta_{N_2}(y) > \theta_{N_1}(y)$ in sufficiently small neighborhoods of x. Since the inequality $\theta_{N_2}(x) \geq \theta_{N_1}(x)$ is closed, it must also hold whenever N_1, N_2 can be approximated by pairs of smooth congruences that are tangent

at x, even if N_1, N_2 are not smooth themselves. When $\theta_{N_2}(x)$ or $\theta_{N_1}(x)$ is ill-defined, we understand the inequality to hold for all smooth approximating congruences[1]. This allows one to deal with the case where N_1, N_2 have caustics or non-local intersections at x. And this in turn means that we can apply the result to congruences launched orthogonally from codimension 2 surfaces that are only piecewise smooth, and perhaps in worse cases as well.

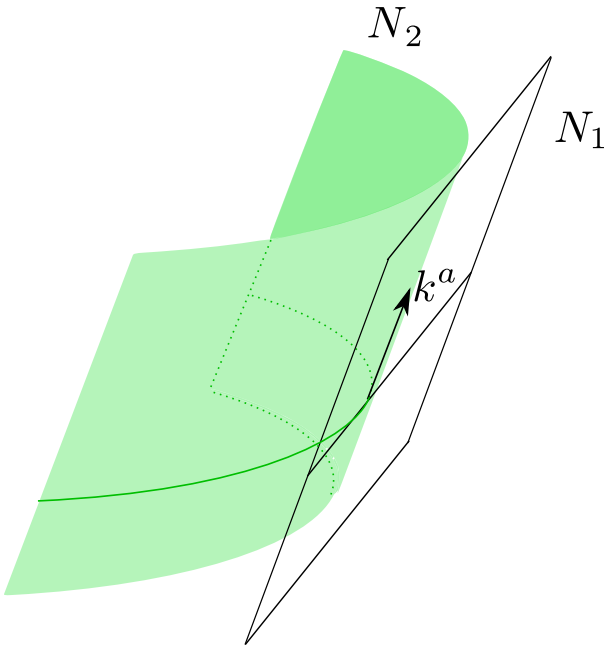

Figure 3.6: The lines depict spacelike cuts of null congruences N_1 and N_2, tangent at a point. N_2 is nowhere to the past of N_1 and is thus expanding faster by Lemma 2

As a final preliminary remark, we recall that [13] suggested that one may always choose a maximin surface that is stable in the following sense: when a Cauchy surface Σ on which $\mathrm{Mm}_\gamma(A)$ is minimal is deformed to a nearby Cauchy surface Σ_ϵ, the minimal surface on Σ_ϵ should remain close to $\mathrm{Mm}_\gamma(A)$. Indeed, it was suggested that when $\mathrm{Mm}_\gamma(A)$ is unique it is always stable and, when it is not, that at least one of the allowed

[1] Alternatively, one may treat the corresponding null expansions as having delta-function-like terms at places where piece-wise smooth codimension 2 surfaces from which they are orthogonally launched fail to be C^1.

choices will be stable (and one should make such a choice). When $\mathrm{Mm}_\gamma(A)$ is both spacelike and smooth, this follows by the technical argument in section 3.5 of [13]. But more generally the proof is incomplete. Below, we follow both [13] and [59] in simply assuming this property to hold and studying its implications.

3.4 Main Results

In deriving the desired results, we will follow the same basic proof strategy as in [13]. The first ingredient in this strategy is the realization that the expansions of null congruences orthogonal to maximin surfaces $\mathrm{Mm}_\gamma(A)$ are significantly constrained. In particular, Claim 2 below will establish that at any point $p \in \mathrm{Mm}_\gamma(A)$ with $p \notin \gamma$, null congruences orthogonal to $\mathrm{Mm}_\gamma(A)$ that do not immediately leave $D(\gamma)$ have non-positive expansion. For example, if $p \in L^+$, then it can have positive expansion θ_l, but the expansions $\theta_k, \theta_{-k}, \theta_{-l}$ must be non-positive. In particular, $\theta_k = -\theta_{-k}$ will vanish.

The second ingredient is the notion of joint (restricted-) maximin surfaces. Such surfaces are defined by choosing arbitrary $c, d > 0$ and considering the quantity $Z = c\mathrm{Area}(X_A) + d\mathrm{Area}(X_B)$. In particular, for each $\Sigma' \in C_\gamma$, we define the surfaces $\min(Z, \Sigma')_A$ and $\min(Z, \Sigma')_B$ to be the surfaces that minimize Z, subject to the constraint that X_A and X_B are codimension 2 surfaces in Σ' anchored respectively to ∂A and ∂B, and satisfying associated homology constraints on Σ'. Note that since $c, d > 0$, the surfaces $\min(Z, \Sigma')_A$ and $\min(Z, \Sigma')_B$ must each be separately minimal on Σ'. So for all such c, d, we have $\min(Z, \Sigma')_A = \min(A, \Sigma')$ and $\min(Z, \Sigma')_B = \min(B, \Sigma')$. The joint restricted-maximin surfaces Y_A and Y_B are then defined by maximizing Z with respect to variations of Σ'. We assume that Y_A and Y_B are stable in parallel with our assumption regarding $\mathrm{Mm}_\gamma(A)$.

By construction, the joint restricted-maximin surfaces are both minimal on the same

slice Σ. As a result, for such surfaces we can use the minimal surface argument of [10] to establish SSA. Indeed, while SSA involves three regions of γ, and thus three surfaces in the bulk, it turns out to be enough to work with pairs A, B of regions of γ that are nested in the sense that $A \subset B$. As a result, SSA for the original restricted maximin surfaces will follow if we can show that they agree with joint restricted-maximin surfaces for nested pairs $B \supset A$.

An important component of doing so is to show that, at least when $B \supset A$, the expansions of null congruences orthogonal to Y_A, Y_B obey precisely the same constraints as those described above for null congruences orthogonal to $\mathrm{Mm}_\gamma(A)$ and $\mathrm{Mm}_\gamma(B)$. For clarity, we state such results for Y_A, Y_B below as corollaries to the corresponding claims for $\mathrm{Mm}_\gamma(A), \mathrm{Mm}_\gamma(B)$, explaining any additional relevant details.

With the above-mentioned results about null expansions in hand, at least when $B \supset A$, one can indeed establish that $Y_A = \mathrm{Mm}_\gamma(A)$ and $Y_B = \mathrm{Mm}_\gamma(B)$. The main idea is to use the above results for null expansions to show that failure to coincide is inconsistent with $\mathrm{Mm}_\gamma(A)$ or $\mathrm{Mm}_\gamma(B)$ being minimal on any Cauchy slice Σ. A key tool in such comparisons is the notion introduced in [13] of the representative $\tilde{y}(\Sigma)$ on a Cauchy slice Σ of a codimension 2 achronal surface y. The precise definition we use largely follows the presentation in [59], but fixes issues associated with the fact that Cauchy surfaces Σ become null:

Definition 3.4.1. We begin with a spacetime-codimension 2 achronal surface y lying in a Cauchy slice Σ', and which is homologous within Σ' to some boundary region A. (Note that since Σ' is codimension 1 in the spacetime, y is codimension 1 with respect to Σ'.) Given another Cauchy surface Σ, representatives $\tilde{y}(\Sigma)$ are defined by observing that y splits the original slice Σ' into two pieces: Σ'_A (with boundary $y \cup A$) and $\Sigma'_{\bar{A}}$ (with boundary $y \cup \bar{A}$). Let the associated domains of dependence be $D(\Sigma'_A)$ and $D(\Sigma'_{\bar{A}})$ with boundaries $\partial D(\Sigma'_A)$ and $\partial D(\Sigma'_{\bar{A}})$. A representative $\tilde{y}(\Sigma)$ on Σ of y is a codimension 2

surface homologous to A within Σ that contains $y \cap \gamma$ and lies in both Σ and $\partial D(\Sigma'_A) \cup \partial D(\Sigma'_{\bar{A}})$. Note that at least one representative must exist on any Σ since both Σ and Σ' are Cauchy surfaces for D_γ and thus both contain γ itself. In particular, when Σ is spacelike, two possible choices of representative are $\Sigma \cap \partial D(\Sigma'_A)$ and $\Sigma \cap \partial D(\Sigma'_{\bar{A}})$. One may sometimes wish to state which such representative one chooses, but in fact the choice of representative will not matter for our purposes below.

This definition becomes useful when combined with the above results about null expansions. Since $\tilde{y}(\Sigma) \subset \partial D(\Sigma'_A) \cup \partial D(\Sigma'_{\bar{A}})$, each point on $y(\Sigma)$ can be reached from a distinct point on y by following a generator of a null congruence orthogonal to y that remains in $D(\gamma)$, and where the generator is free of conjugate points or non-local self-intersections. If y is a connected component of a restricted maximin surface or a joint restricted-maximin surface then, and if y itself does not lie in Σ, the generic condition and the above-mentioned results from Claim 2 and Corollary 2 guarantee the area of $\tilde{y}(\Sigma)$ to be strictly smaller than that of y. Here it is important that $\tilde{y}(\Sigma)$ contains $y \cap \gamma$ so that, at such points (where the null expansions are not controlled), the null geodesic is followed only for vanishing affine-parameter distance.

One can now quickly conclude that $Y_A = \mathrm{Mm}_\gamma(A)$. Since both surfaces are of the form $\min(\Sigma', A)$, the maximization step of the maximin procedure implies $\mathrm{Area}(\mathrm{Mm}_\gamma(A)) \geq \mathrm{Area}(Y_A)$. But if Y_A does not coincide with $\mathrm{Mm}_\gamma(A)$, then we may choose the Cauchy surface Σ on which $\mathrm{Mm}_\gamma(A)$ is minimal so that at least part of Y_A does not lie on this surface[2]. The representative $\widetilde{Y_A}(\Sigma)$ on Σ of Y_A must then have smaller area than Y_A, contradicting minimality of $\mathrm{Mm}_\gamma(A)$ on Σ. The identical argument also proves that Y_B coincides with $\mathrm{Mm}_\gamma(B)$. Entanglement wedge nesting then follows from the fact that Y_A, Y_B are minimal on the same slice Σ and thus cannot cross. Strong Subadditivity and

[2]The stability condition implies that if $\mathrm{Mm}_\gamma(A)$ is minimal on some Σ_0, then it is also minimal on all nearby slices Σ_ϵ that coincide with Σ_0 on some open set around $\mathrm{Mm}_\gamma(A)$. So since maximality forbids $Y_A \subset \mathrm{Mm}_\gamma(A)$ with $Y_A \neq \mathrm{Mm}_\gamma(A)$, for $Y_A \neq \mathrm{Mm}_\gamma(A)$ the condition will hold for some Σ_ϵ.

Monogamy of mutual information follow as well.

This completes our summary of the overall proof strategy. As in [59], the full proofs below repeatedly use the fact that portions of $\mathrm{Mm}_\gamma(A)$ lying entirely in the interior of $D(\gamma)$ will behave much like the maximin surfaces of [13]. As a result, we typically proceed by studying various cases, depending on whether relevant points lie in the interior, on L^+ or L^-, or on γ. When dealing with $L^\pm$, we will focus on studying L^+ with the understanding that analogous results immediately follow for L^-. Furthermore, even in dealing with issues associated with the boundary of $D(\gamma)$, the arguments below largely follow the structure of the derivations in [13].

Before proceeding, we remind the reader that we will treat every relevant Cauchy surface and every restricted maximin surface as being piecewise smooth. Proving this to be the case, or showing that the results hold more generally is an important open issue that is beyond the scope of this work.

3.4.1 Details of the argument

We now fill in the details of the argument sketched above, breaking the derivation into three separate claims regarding $\mathrm{Mm}_\gamma(A)$, together with two corollaries for joint restricted-maximin surfaces. The third claim establishes entanglement wedge nesting, and the other main results of SSA and Monogamy of Mutual Information are then an additional corollary.

Claim 1. Suppose $p, q \in \mathrm{Mm}_\gamma(A)$, with $p \neq q$ and neither p nor q in γ. Then p, q are spacelike separated.

Proof:

Since $p, q \in \mathrm{Mm}_\gamma(A)$, the points lie in a common Cauchy surface. This means that they cannot be connected by any timelike curve. So to establish the desired result, we

need only exclude the possibility that they might be connected by a null curve. The argument proceeds in two steps: (a) We first show that p, q cannot be connected by a null curve η lying in $\mathrm{Mm}_\gamma(A)$. (b) We then show that p, q cannot be connected by any null curve η.

(a) As argued in [13], (unrestricted) maximin surfaces cannot become null at any point y. This can be seen by realizing that, if they were null at some y, then the Cauchy slice containing the surface could be deformed slightly in a neighborhood of y to be everywhere spacelike. Stability of maximin surfaces then requires the minimal surface in the new Cauchy surface be nearby. The fact that a spacelike piece of the new surface is obtained by deforming a null and nearly null piece of the maximin surface means that its area is greater than that of the maximin surface at first order in the deformation. But this contradicts the fact that the maximin surface is maximal with respect to variations in the Cauchy slice. Thus there can be no point y at which the unrestricted maximin surface becomes null, and the surface can contain no null curves.

This argument depends only on variations in a neighborhood of y, and thus carries over unchanged to our restricted maximin construction if any portion of the null curve $\eta \in \mathrm{Mm}_\gamma(A)$ lies in the interior of $D(\gamma)$. But in fact the argument also holds when the case where η lies in $\partial D(\gamma)$, as the Cauchy surface can still be deformed to a spacelike slice using a diffeomorphism generated by a vector field that points into the interior on $\partial D(\gamma)$.

(b) We now extend this result to null curves η that are not contained in $\mathrm{Mm}_\gamma(A)$. We argue by contradiction, assuming that η exists and, without loss of generality, taking p to lie to the future of q. We consider in detail the case where p and q lie in L^+, so any null curve connecting them must be a null generator of L^+. Other cases follow similarly, or by arguments that are even more nearly identical to those of Thm 14 of [13]. As in [13], the proof is unchanged if we take p and q to be contained in distinct members of a

pair of joint restricted-maximin surfaces Y_A, Y_B. The latter case (which we list a separate corollary below) will be critical in the proof of Claim 3 below. To make it clear that the argument also applies in that context, in the remainder of this proof we will write $q \in Y_B$ and $p \in Y_A$, where Y_A and Y_B can be either different joint restricted-maximin surfaces or just different subsets of $\mathrm{Mm}_\gamma(A)$.

Since $p \in L^+$, it lies on some null generator of L^+. Because Σ is an achronal surface containing p and γ, Σ must also contain the part of that null generator lying to the past of p. As in figure 3.7, we can compare the future-directed ingoing null congruence N_B orthogonal to Y_B with the future-directed ingoing null congruence orthogonal to Y_A. Note that N_B must contain p since $N_B \subset D(\gamma)$ and the only such future-directed null geodesic at $q \in L^+$ which remains in $D(\gamma)$ is the generator of L^+ that connects q with p.

Now, since Y_A and Y_B lie on the same achronal slice, Y_B cannot enter the chronological past of Y_A. Similarly, the part of N_B to the future of Y_B cannot enter the chronological past of Y_A, and must in fact be nowhere to the past of N_A near p. We may thus apply Corollary 0 from Section 3.3, so that $\theta_k(B, p) \geq \theta_k(A, p)$. The generic condition then implies that either $\theta_k(B, q) > 0$ or $\theta_k(A, p) < 0$.

To proceed, we introduce the extrinsic curvature one-form $\mathbf{tr}(\mathbf{K^B}) \equiv K^B_i dx^i$ of Y_B. Since Σ contains the entire null generator of L^+ to the past of p (down to, but not including γ), it must be smooth along k at q. Using the fact that Y_B is minimal on Σ then yields $K^B_i k^i = 0$ at q, and thus $\theta_k(B, q) = 0$.

Our dichotomy above then requires $\theta_k(A, p) < 0$, and thus that $\theta_{-k}(A, p) > 0$. The latter refers to the past-directed null congruence. We may also say that $-k$ points outward (towards Y_B) along Σ from Y_A. But Y_A will also have an inward pointing normal in Σ, which we denote v. (If Σ is only piecewise smooth then v can differ from k.) Since Y_A is minimal on Σ, we have $K^A_i v^i \geq 0$. Note the the codimension 2 extrinsic curvature

K_i^A of $\mathrm{Mm}_\gamma(A)$ is well-defined[3] even if Σ fails to be smooth at $\mathrm{Mm}_\gamma(A)$. Since the above null expansion requires $-K_i^A k^i > 0$, the vectors $-k^i$ and v^i cannot be diametrically opposed so, to remain tangent to the achronal surface Σ, v^i must point in a spacelike or null past-inward direction; see again figure 3.7.

We can now consider deforming Σ to the past infinitesimally at p. Since the area of Y_A (or a positively weighted sum involving the area of Y_A) is maximal with respect to variations of Σ, there must be some vector u^i at p that is orthogonal to Y_A, points to the past of Σ, and which has $K_i^A u^i \leq 0$. But since Y_A has spacetime codimension two, this u^i must be a linear combination of v^i and $-k^i$. Furthermore, since u^i points to the past of Σ, it must be a *positive* linear combination of these vectors (see again figure 3.7). But this implies $K_i^A u^i > 0$, contradicting the conclusion above.

By contrast, note that if $q \in \gamma$ then $\theta_k(B, q)$ need not be strictly zero (as minimality on Σ only requires $\theta_k(B, q) \geq 0$). And if $\theta_k(B, q) > 0$, then $\theta_k(A, p)$ may also be positive. Thus, we cannot rule out possible null separations between p and q if $q \in \gamma$ (as consistent with the statement of the claim).

Corollary 1. Consider the joint restricted-maximin surfaces Y_A, Y_B defined by choosing $c, d > 0$ and performing restricted maximin using quantity $Z = c\mathrm{Area}(X_A) + d\mathrm{Area}(X_B)$. Here we require that X_A, X_B are codimension 2 surfaces anchored respectively to ∂A and ∂B and satisfying associated homology constraints on each Cauchy slice. As described above, this results in a pair of surfaces Y_A, Y_B that are minimal on the same slice Σ. Let $p \in Y_A$ and $q \in Y_B$. If neither p nor q are in γ, then either $p = q$ or p, q are spacelike separated.

The argument is identical to that for Claim 1. This corollary will be useful below in much the same way as in [13].

[3] If $\mathrm{Mm}_\gamma(A)$ is only piece-wise smooth, one may consider a family of smooth approximating surfaces.

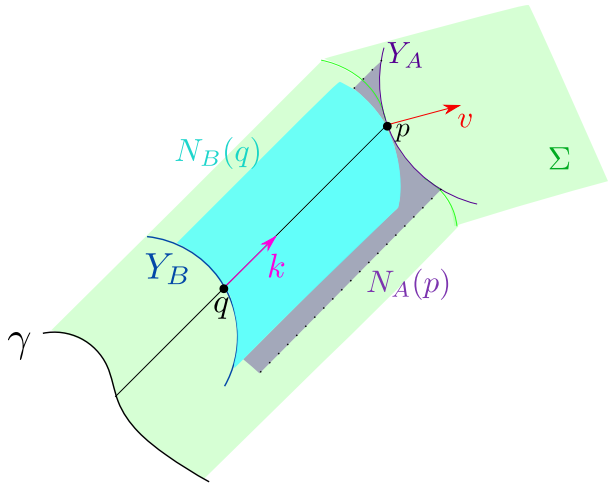

Figure 3.7: Consider two surfaces Y_A and Y_B as in Claim 1 which are constructed on the same slice Σ. Points q on Y_B and p on Y_A cannot have null separated points. $N_B(q)$ is the null congruence orthogonal to Y_B at q and $N_A(p)$ is the null congruence orthogonal to Y_A at p. This null congruence must bend towards the orthogonal vector v, because Y_A must stay contained in Σ (and so remain spacelike separated to Y_B). This places constraints of the relative signs of the expansions of the null congruences, which can in turn be used to contradict the maximality of the areas Y_A and Y_B along Σ.

Claim 2. Suppose $p \in \mathrm{Mm}_\gamma(A)$ with $p \notin \partial D(\gamma)$. Then, $\mathrm{Mm}_\gamma(A)$ is extremal at p. If $p \in L^\pm$, then $\theta(p) \leq 0$ for any null congruence orthogonal to $\mathrm{Mm}_\gamma(A)$ that is directed into the interior of $D(\gamma)$. Furthermore, $\theta_k = 0$ for $p \in L^+$ and $\theta_l = 0$ for $p \in L^-$. As a result, at any point $p \in \mathrm{Mm}_\gamma(A)$ with $p \notin \gamma$, null congruences orthogonal to $\mathrm{Mm}_\gamma(A)$ that do not immediately leave $D(\gamma)$ have non-positive expansion.

Proof: The analogous result for unrestricted maximin surfaces was proven in [13]. Since the arguments are local at p, they also establish Claim 2 for $p \notin \partial D(\gamma)$. By similar reasoning, even if $p \in L^+$ minimality of $\mathrm{Mm}_\gamma(A)$ on Σ implies that $\mathrm{Mm}_\gamma(A)$ is extremal along directions within Σ.

Note that the arguments of Claim 1 above show that Σ must be smooth at p. Otherwise, minimality along the two tangent vectors of Σ, $-k$ and v, would imply that the area of $\mathrm{Mm}_\gamma(A)$ could be increased by varying Σ to the past at p, contradicting maximality

of $\mathrm{Mm}_\gamma(A)$.

Since Σ is smooth at p, it must be tangent to the k direction at p. Minimality of $\mathrm{Mm}_\gamma(A)$ on Σ then gives $K_i^A k^i = 0$, and hence $\theta_k = 0$.

We can now consider the null expansion in the l direction. In the maximization step of the maximin procedure, Σ can be freely varied in the l direction into the interior of $\partial D(\gamma)$ at points near p. Maximality over these variations implies $K_i^A l^i \leq 0$, which in turn implies $\theta_l \leq 0$. Of course, similar arguments hold for $p \in L^-$.

Again, the argument generalizes to yield analogous results for the joint restricted-maximin surfaces Y_A, Y_B defined as in Corollary 1 by performing a restricted maximin procedure on $Z = c\mathrm{Area}(X_A) + d\mathrm{Area}(X_B)$. However, this time the generalization requires a bit more work as explained below:

Corollary 2. Let Y_A, Y_B be defined as in Corollary 1 for nested regions $B \supset A$, and consider $p \in Y_A \cup Y_B$ with $p \notin \partial D(\gamma)$. Then, $Y_A \cup Y_B$ is locally an extremal surface at p. In particular, if Y_A and Y_B coincide at p then they must do so in a neighborhood of p. Furthermore, if $p \in L^\pm$, then $\theta(p) \leq 0$ for any null congruence emanating from $Y_A \cup Y_B$ that is directed into the interior of $D(\gamma)$. We also have $\theta_k = 0$ for $p \in L^+$ and $\theta_l = 0$ for $p \in L^-$. As a result, at any point $p \in \mathrm{Mm}_\gamma(A)$ with $p \notin \gamma$, null congruences orthogonal to Y_A or Y_B that do not immediately leave $D(\gamma)$ have non-positive expansion.

Proof: For $p \notin \partial D_\gamma$, the key fact is that minimal surfaces on the same slice Σ' cannot touch, cross, or coincide, except in the case where an entire connected component of $\min(A, \Sigma')$ coincides with an entire connected component of $\min(B, \Sigma')$. At a point p where the surfaces coincide, maximizing one area under local variations of the Cauchy surface also clearly maximizes the other[4]. So extremality of Y_A and Y_B at such points follows from the same argument as for $\mathrm{Mm}_\gamma(A)$. Furthermore, Corollary 1 states that

[4]The fact that variations of Σ may cause Y_A, Y_B to separate from each other can affect the areas only at second order since both surfaces are minimal on the original Cauchy slice, and since we now consider only interior points where such minimal surfaces must be smooth.

(except on full connected components where Y_A, Y_B coincide), points on Y_A are spacelike separated from points on Y_B. On portions where they do not coincide, the stability requirement implies that we may then freely vary the Cauchy slice in the neighborhood of one surface without affecting the area of the other. So again extremality of Y_A, Y_B follows in precisely the same way as for $\mathrm{Mm}_\gamma(A)$.

It remains only to consider $p \in L^\pm$. We focus on the case $p \in L^+$, with the understanding that the time-reversed remarks hold for L^-. There are three cases to consider below.

Case 1: Suppose $p \in L^+$ lies in Y_A but not in Y_B. Recall that Corollary 1 states that no two points on these surfaces can be null separated if neither one is on γ. (They cannot be separated by a null ray that runs through the bulk, nor by a null generator contained in $\partial D(\gamma)$). Because minimal surfaces on the same slice cannot cross, if Y_A has a point on some generator k of L^+, then Y_B must have a point $q \in \gamma$ along the same generator. Since $q \in \gamma$, it lies in all Cauchy surfaces and changes in Z resulting from local variations of the Cauchy surface near the generator k receive no contributions from Y_B. Applying the arguments of Claim 2 to such variations then establish the desired results for Y_A (and the results for Y_B hold vacuously).

Case 2: Suppose $p \in L^+$ lies in Y_B but not in Y_A. Then we may again use Corollary 1 to show that if Y_B has a point in L^+ on some generator k then Y_A cannot intersect that generator at all. As a result, one is free to vary the Cauchy surface near k without affecting the area of Y_A. Applying the arguments of Claim 2 to such variations then proves the desired results for Y_B (and the results for Y_A hold vacuously).

Case 3: Finally, suppose that Y_A and Y_B coincide at $p \in L^+$. Below, we will show that Y_A and Y_B cannot just touch at such a point p, but must in fact must coincide on finite regions whose boundaries must lie in γ. Applying the arguments of Claim 2 then shows that a weighted sum of the A, B null expansions at p will satisfy the claim. But

since both surfaces define the same null congruences and null expansions near p, the same must be true for the expansions of the individual null congruences orthogonal to Y_A and Y_B.

The argument for coincidence of Y_A and Y_B on the above finite region will roughly follow the proof of Claim 1, though now p and q coincide. As above, we can compare the k directed null congruence $N_B(p)$ from Y_B at p to the k directed null congruence $N_A(p)$ from Y_A at p. As in Claim 1, because Y_A and Y_B lie on the same achronal slice, because minimal surfaces on the same slice cannot cross, and because $A \subset B$, we must have N_A nowhere to the past of N_B. Corollary 0 then requires $\theta_k(B,p) \geq \theta_k(A,p)$.

We further consider the extrinsic curvature $\mathbf{tr}(\mathbf{K^B}) \equiv K_i^B dx^i$ of Y_B and the analogous $\mathbf{tr}(\mathbf{K^A}) \equiv K_i^A dx^i$. Note that Σ must contain the full generator of L^+ to the past of p. Because Y_A and Y_B are minimal on Σ, we have $K_i^B(-k^i) \geq 0$ and $K_i^A(-k^i) \geq 0$, where $-k^i$ is the past-directed tangent vector to Σ which points along the generators of L^+ at p. Thus, $\theta_k(B,p) \leq 0$ and $\theta_k(A,p) \leq 0$.

Combining the two preceding paragraphs then requires either $\theta_k(A,p) = \theta_k(B,p) = 0$ or $\theta_k(A,p) < 0$. In the latter case, we can continue to follow the arguments of Claim 1. Σ will possess some other tangent vector normal to Y_A, which points to the interior. We call this vector v_i. Minimality on Σ implies $K_i^A v^i \leq 0$. However, because $\theta_k(A,p) < 0$, $K_i^A(-k)^i > 0$, Thus, v^i cannot point along the k direction, and v^i must point in a spacelike or null past direction into the interior of Y_A. We can now consider pushing Σ to the past infinitesimally at p. Since Y_A and Y_B have maximal area with respect to variations of Σ, pushing Σ to the past, along some vector u^i must decrease the area of Y_A and Y_B, such that $K_i u^i \leq 0$. But u^i must be a positive linear combination of v^i and $-k^i$, implying $K_i u^i > 0$ and contradicting the previous line. Thus, $\theta_k(A,p) = \theta_k(B,p) = 0$.

We now consider the set $\mathcal{C}$ on which the surfaces coincide, and in particular the connected component $\mathcal{C}_0 \subset \mathcal{C}$ that contains p. Since the surfaces are continuous, $\mathcal{C}_0$ must

be closed. Thus any point q in the boundary of $\mathcal{C}_0$ must also lie in $\mathcal{C}$. But if q lies in the interior of $D(\gamma)$, then we have $\theta_k(A) = \theta_k(B) = 0$ at all points near q (as these also lie in the interior). Lemma 2 then requires our surfaces to coincide on a larger set, contradicting the fact that q lies at the boundary of $\mathcal{C}_0$.

Similarly, if $q \in L^+$, then all nearby points are in L^+ or the interior. So by the arguments of the above cases θ_k for each surface must vanish on a larger set. Thus Lemma 2 again requires the surfaces to coincide on a larger set and yields a contradiction. The case $q \in L^-$ is similarly forbidden by the time-reversed argument. The only remaining possibility is that $\partial\mathcal{C}_0 \subset \gamma$ as claimed. This completes the proof of Corollary 2.

As described in the introduction to this section, the above results are sufficient to guarantee that for $A \subset B$ the joint restricted-maximin surfaces Y_A, Y_B agree with $\mathrm{Mm}_\gamma(A)$ and $\mathrm{Mm}_\gamma(B)$. It then follows that $\mathrm{Mm}_\gamma(A)$ and $\mathrm{Mm}_\gamma(B)$ lie on a common Cauchy surface Σ_0, on which they are both minimal. Nesting of the associated entanglement wedges then follows from the fact that minimal surfaces on Σ_0 cannot cross. We use the notation $EW(A)$ to denote the entanglement wedge of A and thus write $EW(A) \subset EW(B)$. As usual, we use bulk causality to covariantly define $EW(A)$. Thus we have:

Claim 3. If A and B are regions with $A \subset B$, $\mathrm{Mm}_\gamma(A)$ and $\mathrm{Mm}_\gamma(B)$ are minimal on a common Cauchy slice $\Sigma \in C_\gamma$. This also implies $\mathrm{EW}(A) \subset \mathrm{EW}(B)$.

Proof: The full proof was given in the introduction to this section. Note that as opposed to the original maximin surfaces of [13], for boundary regions $A \subset B$ the intersection $\mathrm{Mm}_\gamma(A) \cap \mathrm{Mm}_\gamma(B)$ can be very general. But as in the proof of Corollary 2, except when $\mathrm{Mm}_\gamma(A)$ and $\mathrm{Mm}_\gamma(B)$ coincide on finite regions, non-trivial intersections of $\mathrm{Mm}_\gamma(A)$ with $\mathrm{Mm}_\gamma(B)$ are confined to the boundary γ and thus lie in all Cauchy slices.

Having established that the maximin surfaces of nested subregions are minimal on a common Cauchy slice, SSA and monogamy of mutual information follow quickly by

adapting the original SSA argument of [10] and the monogamy argument of [60]. This discussion is identical to that of [13], but we repeat it for completeness below.

Corollary 3. Our restricted maximin construction satisfies strong subadditivity and negativity of tripartite mutual information (aka monogamy of mutual information).

Proof: Let A, B and C be non-overlapping regions in γ. Since $B \subset A \cup B \cup C$, we know that there exists a single surface $\Sigma \in \mathcal{C}_\gamma$ with $\mathrm{Mm}_\gamma(B)$ and $\mathrm{Mm}_\gamma(A \cup B \cup C)$ both minimal on Σ. As shown in figure 3.8, the same surgery argument as in [10, 13] requires

$$\mathrm{Area}(\mathrm{Mm}_\gamma(B)) + \mathrm{Area}(\mathrm{Mm}_\gamma(A \cup B \cup C)) \leq \mathrm{Area}(\min(A \cup B, \Sigma)) + \mathrm{Area}(\min(B \cup C, \Sigma))$$

. But $\mathrm{Area}(\min(A \cup B, \Sigma)) < \mathrm{Area}(\mathrm{Mm}_\gamma(A \cup B))$ and $\mathrm{Area}(\min(B \cup C, \Sigma)) < \mathrm{Area}(\mathrm{Mm}_\gamma(B \cup C))$ by the definition of Mm_γ.

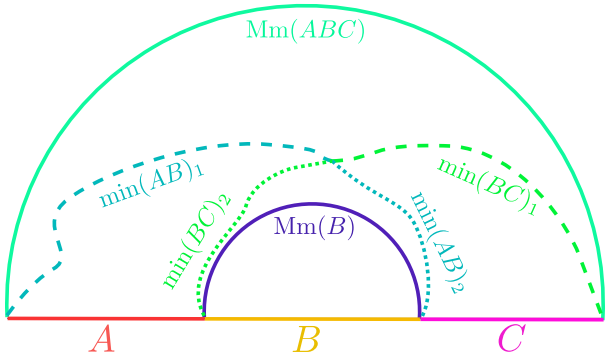

Figure 3.8: The argument for strong subadditivity, with boundary subregions A, B, and C. By Claim 3, the surfaces $\mathrm{Mm}_\gamma(ABC)$ and $\mathrm{Mm}_\gamma(B)$ are minimal on a common Cauchy slice Σ. Note that we can also form a curve anchored to $\partial(ABC)$ by following dashed lines along $\min(AB)_1$ and $\min(BC)_1$. A curve anchored to ∂B can likewise be found by following the dotted lines along $\min(AB)_2$ and $\min(BC)_2$. However, minimality on Σ means that $\mathrm{Area}[\mathrm{Mm}_\gamma(ABC)] \leq \mathrm{Area}[\min(AB)_1 \cup \min(AB)_1]$ and $\mathrm{Area}[\mathrm{Mm}_\gamma(B)] \leq \mathrm{Area}[\min(AB)_2 \cup \min(AB)_2]$. Furthermore, $\mathrm{Area}[\min(AB)] \leq \mathrm{Area}[\mathrm{Mm}_\gamma(AB)]$ and $\mathrm{Area}[\min(BC)] \leq \mathrm{Area}[\mathrm{Mm}_\gamma(BC)]$ by the maximization step of restricted maximin. Thus $\mathrm{Area}[\mathrm{Mm}_\gamma(ABC)] + \mathrm{Area}[\mathrm{Mm}_\gamma(B)] \leq \mathrm{Area}[(\min(AB)_1)] + \mathrm{Area}[(\min(AB)_2)] + \mathrm{Area}[\min(BC)_1] + \mathrm{Area}[\min(BC)_2] \leq \mathrm{Area}[\mathrm{Mm}_\gamma(AB)] + \mathrm{Area}[\mathrm{Mm}_\gamma(BC)]$ and strong subadditivity holds. A similar argument holds in cases where regions A, B, C do not meet at their boundaries.

Monogamy of mutual information is handled similarly. We take Σ such that $\mathrm{Mm}_\gamma(A)$, $\mathrm{Mm}_\gamma(B)$, $\mathrm{Mm}_\gamma(C)$ and $\mathrm{Mm}_\gamma(A \cup B \cup C)$ are all simultaneously minimized on Σ. then, the surgery argument implies that

$$\begin{aligned}&\mathrm{Area}(\mathrm{Mm}_\gamma(A)) + \mathrm{Area}(\mathrm{Mm}_\gamma(B)) + \mathrm{Area}(\mathrm{Mm}_\gamma(C)) + \mathrm{Area}(\mathrm{Mm}_\gamma(A \cup B \cup C)) \\ \leq &\mathrm{Area}(\min(A \cup B, \Sigma)) + \mathrm{Area}(\min(A \cup C, \Sigma)) + \mathrm{Area}(\min(B \cup C, \Sigma))\end{aligned}$$

from which the inequality follows. □

3.5 Discussion

Our work above studied possible definitions of holographic entropy in bulk spacetimes with a radial cutoff. In particular, we focused on globally hyperbolic bulk regions that one may think of as domains of dependence for some achronal surface Σ with boundary $\partial\Sigma = \gamma$. We think of the surface γ as defining the cutoff, even though it is codimension 2 in the full spacetime. It may also be useful to think of γ as an achronal slice of some codimension 1 timelike surface, whether the latter is a strict cutoff or just a partition of the bulk into two parts. While the areas of HRT surfaces anchored to γ can generally violate strong subadditivity (SSA), or even just subadditivity, we argued that the areas of similarly anchored restricted maximin surfaces will satisfy both SSA and monogamy of mutual information. Any other maximin-provable holographic entropy inequality [74] will of course follow as well.

The above qualifier 'restricted' means that the maximization is only with respect to achronal surfaces Σ with boundary $\partial\Sigma = \gamma$. This restriction is important, as the example of section 3.3.1 shows that SSA can fail for the areas of unrestricted maximin surfaces in precisely the same manner as for HRT areas. Appendix **??** establishes further

properties of our restricted maximin surfaces not required for the main argument, but which may be useful in the future. In particular, up to sets of measure zero it shows that our restricted maximin surfaces either coincide with γ or are spacelike separated from γ; i.e., null separations from γ are rare.

As in the previous works [13, 59] we have neglected certain technical issues associated with proving that our restricted maximin surfaces can be chosen to be stable, and also with the fact that general Cauchy surfaces are not piece-wise smooth. We hope that such points will be addressed in the near future, though we note that almost 30 years past before similar issues were fully resolved by [75] in the context of the Hawking area theorem [76].

An interesting feature of our construction is that restricted maximin surfaces often have regions that coincide exactly with portions of γ. This would not occur for an HRT surface except on portions of γ that happen to be extremal. However, it is clear that the same phenomenon *does* often occur for RT surfaces defined by minimizing areas over subsurfaces of some time-symmetric slice Σ. For example, in flat space it occurs whenever Σ fails to be convex; see figure 3.9. Our restricted maximin procedure is thus more similar to the RT prescription in the presence of a cutoff than is naive application of HRT.

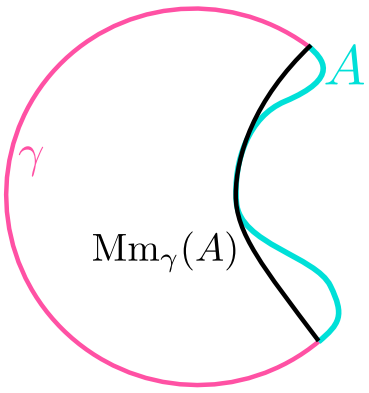

Figure 3.9: A time-symmetric example where γ fails to be convex, and consequently $\mathrm{Mm}_\gamma(A)$ (and the RT surface associated with A) would coincide with γ along some portion.

In retrospect, the reason that HRT surfaces behave so differently is simple to state. It is well known that extrema of a function can occur either at stationary points, or at the edge of the allowed domain. In the absence of a cutoff and with natural boundary conditions, the latter can be ruled out. But finite cutoffs provide an edge where extrema can arise, so an HRT-like prescription that involves solving differential equations for stationary points of the area functional can give very different results from applying a minimization procedure, or indeed from restricted maximin.

One would like to derive our prescription from an appropriate path integral in parallel with the cutoff-free arguments of [11] and [77]. One class of obstacles to doing so are uncertainties regarding physics of the cutoff surface. If we momentarily ignore these issues we may proceed as in [54]; see also [78, 79]. While those references focused on convex spacetimes, in more general cases one would expect end-point effects similar to those described above to naturally arise in studying the path integral. For example, if we study replica geometries by preserving the original boundary conditions but introducing codimension 2 cosmic branes which source conical singularities, the path integral over cosmic brane locations will again often receive important contributions from configurations in which the brane partially coincides with the boundary of the spacetime. This is particularly clear in the Euclidean context where the dominant contribution comes from the configuration with minimum action. As above, this minimum may well arise on the boundary of the space of allowed cosmic brane solutions, and in particular where the cosmic brane itself partially coincides with the boundary of spacetime[5].

The fact that our restricted maximin procedure succeeds may be taken as evidence supporting the utility of cutoff holography. However, it remains to better understand what further structures might be implied. For example, the success of our procedure may also suggest that when a slice γ of the cutoff surface is achronal with respect to the

[5]We thank Xi Dong and Henry Maxfield for discussions of this point.

bulk causal structre, distinct points on γ correspond to independent degrees of freedom for any bulk dual. This is also natural from the bulk point of view. But this viewpoint would in turn imply that the entropy of a boundary region A should depend only on the appropriate notion of a domain of dependence of A, perhaps as determined by the causal structure of the bulk rather than the causal structure of the boundary. And this statement is precisely what fails in the example of section 3.3.1, where the area of the restricted maximin surface for AB depends in detail on the choice of codimension 2 surface γ. It would thus be interesting to investigate such issues further, perhaps by studying $T\bar{T}$ deformations or their analogues in higher dimensions.

Part II

Traversable Wormholes

Chapter 4

A Perturbative Perspective on Self-Supporting Wormholes

4.1 Introduction

Wormholes have long been of interest to both scientists (see e.g. [80, 81, 82]) and the general public, especially in the context of their possible use for rapid transit or communication over long distances. While the topological censorship theorems [83, 84] forbid traversable wormholes in Einstein-Hilbert gravity coupled to matter satisfying the null energy condition (NEC) $T_{ab}k^a k^b \geq 0$, the fact that quantum fields can violate the NEC (and that higher-derivative corrections can alter the dynamics away from Einstein-Hilbert) has led to speculation (e.g. [82]) that traversable wormholes might nevertheless be constructed by sufficiently advanced civilizations.

Indeed, an Einstein-Hilbert traversable wormhole supported by quantum fields was recently constructed in [15]. Their wormhole connects two asymptotically 2+1-dimensional anti-de Sitter (AdS) regions that are otherwise disconnected in the bulk spacetime. However, the model contains an explicit non-geometric time-dependent coupling of quantum

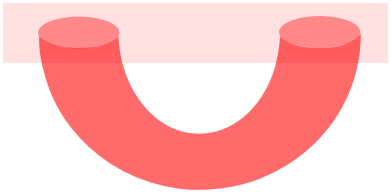

Figure 4.1: A moment of time in a spacetime with a wormhole (shaded region) formed by adding a handle to a space with a single asymptotic region.

field degrees of freedom near one AdS boundary to similar degrees of freedom near the other. Turning on this coupling briefly near $t = 0$ allows causal curves that begin at one AdS boundary in the far past to traverse the wormhole and reach the other boundary in some finite time. Though the wormhole collapses and becomes non-traversable at later times, the negative energy induced by the boundary coupling supports a transient traversable wormhole. The extension to the rotating case was performed in [85].

Here and below, we define the term "traversable wormhole" to mean a violation of the topological censorship results of [83, 84]; i.e., it represents causal curves that cannot be deformed (while remaining causal) to lie entirely in the boundary of the given spacetime. Note that there exist interesting solutions of Einstein-Hilbert gravity involving thin necks connecting large regions (e.g. [86]) which are not wormholes in this sense. In addition, an analogue of the effect in [15] without wormholes was recently discussed in [87].

From the perspective of the bulk spacetime, boundary interactions like those used in [15] are both non-local and acausal. However, it is expected that similar boundary couplings can be induced by starting with local causal dynamics on a spacetime of the form described by figure 5.1, in which the ends of the wormhole interact causally through the ambient spacetime. Integrating out the unshaded region in figure 5.1 clearly leads to an interaction between opposite ends of the wormhole (shaded region). Though not precisely of the form studied in [15], the details of the boundary coupling do not appear to be critical to the construction.

Indeed, during the final preparation of this manuscript, a traversable wormhole was constructed [88] using only local and causal bulk dynamics. In addition, the wormhole of [89] is stable and remains open forever. We refer to such wormholes as self-supporting. This construction was inspired by [89], which showed that adding time-independent boundary interactions to AdS_2 in some cases leads to static (eternal) traversable wormholes that in particular are traversable at any time. In [89], the eternal wormholes arise as ground states and, as the authors of [89] point out, more generally the time-translation invariance of a ground state leads one to expect that a geometric description must have either a static traversable wormhole or no wormhole at all[1].

The wormholes constructed in [89] are extremely fragile, yet in some sense their construction was easier than had long been assumed. It is therefore useful to find a clean and simple perspective explaining why self-supporting wormholes should exist. We provide such an explanation below using first-order perturbation theory about classical solutions. Indeed, we will find perturbative indications that self-supporting wormholes can indeed exist even when the number of propagating quantum fields is small. Our examples resemble the $\Delta < 1/2$ case studied in [89] in that the back-reaction grows in the IR limit. While by definition there can be no traverseable wormholes of our sort in closed cosmologies, there can nevertheless be related effects. For example, one can use these techniques to build a Schwarzschild-de Sitter-like solution in which causal curves from I^- to I^+ can pass through the associated Einstein-Rosen-like bridge.

At least for the purpose of establishing transient traversability for some choice of boundary conditions, the important properties of our backgrounds are that they are smooth, globally hyperbolic $\mathbb{Z}_2$ quotients of spacetimes with bifurcate Killing horizons

[1]Recall that familiar non-traversable wormholes like Reissner-Nordström, Kerr, or BTZ degenerate and disconnect in the limit of zero temperature. The full argument is best given in Euclidean signature so as to exclude non-traversable static wormholes of the form discussed in [90]. This is appropriate for a ground state defined by a Euclidean path integral.

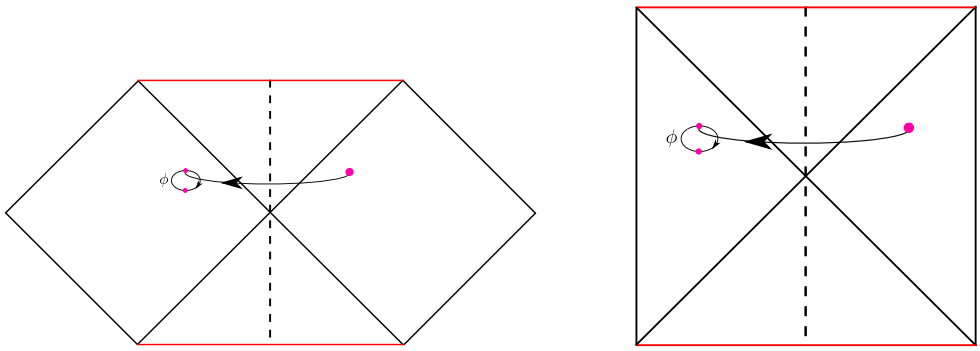

Figure 4.2: The asymptotically flat $\mathbb{RP}^3$ geon and the AdS $\mathbb{RP}^2$ geon are respectively $\mathbb{Z}_2$ quotients of Kruskal's extension (left) of the Schwarzschild solution and BTZ (right). The quotients act on the above conformal diagrams by reflection across the dashed lines, and simultaneously act as the antipodal map (see insets) on the suppressed S^2 or S^1. Due to this combined action, the resulting spacetimes are smooth. However, since this action maps the Killing field ξ^a to $-\xi^a$, the geon quotients lack globally-defined time-translation Killing fields. In particular, the dashed lines are orthogonal to preferred spacelike surfaces of vanishing extrinsic curvature that one may call $t = 0$. Our Kaluza-Klein end-of-the-world brane is a quotient of BTZ $\times S^1$ by a related isometry that acts trivially on the BTZ ϕ-circle but acts on the internal S^1 via the antipodal map.

and well-defined Hartle-Hawking states under an isometry that exchanges the left- and right-moving horizons. Such spacetimes may be said to generalize the $\mathbb{RP}^3$ geon described in [91, 83] (and in [92] at the level of time-symmetric initial data); see figure 4.2 (left). However, as discussed in section 6.4, they may also take the more familiar form shown in figure 5.1.

Much like the Bañados-Teitelboim-Zanelli (BTZ) case studied in [15], the bifurcate horizon in the covering space makes the wormholes nearly traversable, so that they might be rendered traversable by the perturbatively small backreaction sources of a quantum field. On the other hand, linear quantum fields in backgrounds with global Killing symmetries satisfy the averaged null energy condition (ANEC), meaning that the integral of $T_{ab}k^ak^b$ over complete null generators is non-negative[2]. Thus, a bifurcate Killing horizon

[2]This follows for both free and super-renormalizeable field theories from e.g. combining the results of [93] with those of [94], or from the free-field quantum null energy condition (QNEC) derived in [95]. This result should also hold for quantum field theories that approach a non-trivial UV conformal fixed

will not become traversable under first-order back-reaction from quantum fields in any quantum state and the above-mentioned $\mathbb{Z}_2$-quotient operation plays a key role in our analysis below.

After describing the general framework for such constructions and the relation to [15] and [89] in section 4.2, we study simple examples of transient such traversable wormholes in section 4.3, and a more complicated example in 4.4 that admits an extremal limit in which the wormhole appears to remain open forever. We consider only scalar quantum fields in the work below, though similar effects should be expected from higher spin fields. It would be particularly interesting to study effects from linearized gravitons.

For simplicity, section 4.3 considers backgrounds defined by the AdS $\mathbb{RP}^2$ geon [99] and simple Kaluza-Klein end-of-the-world branes[3] (KKEOW branes) that are respectively quotients of AdS_3 and $AdS_3 \times S^1$. In particular, the former are $\mathbb{Z}_2$ quotients of BTZ spacetimes, and the latter are quotients of BTZ $\times S^1$; see figure 4.2. In each case, as explained in section 4.2, we take the bulk quantum fields to be in the associated Hartle-Hawking state defined by the method of images using the above $\mathbb{Z}_2$ quotient, or equivalently defined via a path integral over the Euclidean section of the background geometry. Both backgrounds define wormholes with $\mathbb{Z}_2$ homotopy[4] fully hidden by a single black hole horizon. They are also non-orientable, though with additional Kaluza-Klein dimensions they admit orientable cousins as in [99]. Outside the horizons, the spacetimes are precisely BTZ or BTZ $\times S^1$, and even inside the horizon these quotients preserve exact

point as one expects that the arguments of [96, 97] generalize (at least in the static case where analytic continuation is straightforward) directly to Killing horizons in curved spacetimes. For such more general theories, one could alternately use the QNEC connection of [95] and generalize the results of [98] to appropriate Killing horizons.

[3] Such spacetimes (for AdS_d with $d \geq 4$) were studied in [100] where they were called higher-dimensional geons. We use the term KKEOW brane here as we emphasize the AdS_3 perspective, and in particular because it provides a smooth top-down model of the end-of-the-world brane spacetime of [101, 87].

[4] It is useful to define the wormhole homotopy group to be the quotient $\pi_1^w M := \pi_1(M)/\pi_1(\partial M)$ of the bulk homotopy group $\pi_1(M)$ by the boundary homotopy group $\pi_1(\partial M)$. If there is no boundary ($\partial M = \emptyset$), we define $\pi_1(\emptyset)$ to be trivial. The examples described here have $\pi_1^w(M) = \mathbb{Z}_2$.

rotational symmetry.

Unfortunately, the examples of section 4.3 do not admit smooth zero-temperature limits. We thus turn in section 4.4 to a slightly more complicated $\mathbb{Z}_2$ quotient of BTZ $\times S^1$ that breaks rotational symmetry but nevertheless supports the addition of angular momentum. The four-dimensional spacetime is smooth, though after Kaluza-Klein reduction on the S^1, the resulting three-dimensional spacetime has two conical singularities with π deficit angles. We therefore refer to this example as describing Kaluza-Klein zero-brane orbifolds (KKZBOs). This construction admits a smooth extremal limit and (as it turns out) yields an orientable spacetime. In our first-order perturbative analysis, back-reaction renders the KKZBO wormhole traversable until a time t_f that becomes later and later as extremality is approached. This suggests that a complete non-perturbative analysis would find a self-supporting eternal traversable wormhole. The large effect near extremality is associated with a divergence of the relevant Green's function in the extremal limit. It would be interesting to better understand the relationship of this divergence to other known instabilities of extreme black holes.

We end with some discussion in section 6.4, focusing on back-reaction in the extremal limit, showing that the general class of wormholes described in section 4.2 includes wormholes of the familiar form depicted in figure 5.1. In particular, assuming that perturbations of Reissner-Nordström black holes display an instability similar to the one noted above for extreme BTZ, our mechanism also appears to explain the existence of the self-supporting wormholes constructed in [88]. An appendix also describes a slight generalization of the framework from section 4.2.

4.2 $\mathbb{Z}_2$-quotient wormholes and their Hartle-Hawking states

As stated above, at least for the purpose of establishing transient traversability, the important properties of our backgrounds M are that they are smooth globally hyperbolic $\mathbb{Z}_2$ quotients of spacetimes $\tilde{M}$ with bifurcate Killing horizons and well-defined Hartle-Hawking states $|0_{HH,\tilde{M}}\rangle$ under a discrete $\mathbb{Z}_2$ isometry J (i.e., with $J^2 = \mathbb{1}$) that exchanges the left- and right-moving horizons. Here, by a Hartle-Hawking state we mean a state of the quantum fields that is smooth on the full bifurcate horizon and invariant under the Killing symmetry. Such spacetimes M are then generalizations of the (Schwarzschild) $\mathbb{RP}^3$ geon described in [91, 83] and the $\mathbb{RP}^2$ AdS geon of [99]; see figure 4.2. For later purposes, note that the homotopy group $\pi_1(\tilde{M})$ is a normal subgroup of $\pi_1(M)$ with $\pi_1(M)/\pi_1(\tilde{M}) = \mathbb{Z}_2$. In order to describe the additional topology introduced by the $\mathbb{Z}_2$ quotient, it will be useful to choose some associated $\gamma \in \pi(M)$ which projects to the non-trivial element of $\pi_1(M)/\pi_1(\tilde{M}) = \mathbb{Z}_2$ and for which $\gamma^2 = \mathbb{1}$.

To set the stage for detailed calculations in section 4.3, we give a simple argument in section 4.2.1 below that – for either periodic or anti-periodic boundary conditions around γ – this setting generically leads to traversability in the presence of free quantum fields. In order to provide a useful perspective and explore connections with both recent work [89] by Maldacena and Qi and the original traversable wormhole [15] of Gao, Jafferis, and Wall, section 4.2.2 then describes an alternate construction via path integrals that generalizes this construction to interacting fields.

4.2.1 The free field case

Our explicit work in sections 4.3 and 4.4 below involves free quantum fields. We may therefore follow [102, 99] and define a state on the quotient M of $\tilde{M}$ using the method of images. For reasons explained below, we refer to this state as the Hartle-Hawking state $|0_{HH,M}\rangle$ on M. In fact, since free fields ϕ on M admit a $\mathbb{Z}_2$ symmetry $\phi \to -\phi$, we may in principle consider two such states $|0_{HH,M}\rangle_\pm$ defined using either periodic or anti-periodic boundary conditions around the new homotopy cycle γ in M. Since we will concentrate on the periodic case $|0_{HH,M}\rangle_+$ below, we will also denote this state by $|0_{HH,M}\rangle$ with no subscript.

Since M is globally hyperbolic, it contains no closed causal curves. Thus the image $J\tilde{x}$ of any $\tilde{x} \in \tilde{M}$ never lies in either the causal future or past of $\tilde{x}$. And since M is smooth, $\tilde{x}$ and $J\tilde{x}$ cannot coincide. Thus $\tilde{x}$ and $J\tilde{x}$ are spacelike related and quantum fields at $\tilde{x}$ commute with those at $J\tilde{x}$. As a result, in linear quantum field theory, one may define quantum fields $\phi_\pm$ on M in terms of quantum fields $\tilde{\phi}$ on $\tilde{M}$ via the relations

$$\phi(x)_\pm = \frac{1}{\sqrt{2}} \left[\tilde{\phi}(\tilde{x}) \pm \tilde{\phi}(J\tilde{x}) \right], \tag{4.1}$$

where $(\tilde{x}, J\tilde{x})$ are the two points in $\tilde{M}$ that project to $x \in M$. Of course, in the antiperiodic $(-)$ case, the overall sign of ϕ is not well-defined. This case is best thought of as making ϕ charged under a $\mathbb{Z}_2$ gauge field with non-trivial holonomy around the $\mathbb{Z}_2$ cycle γ of M. Note that in either case $\phi(x)$ satisfies canonical commutation relations on a Cauchy slice of M and so does indeed define a quantum field as claimed.

Any quantum state $\tilde{\phi}$ on $\tilde{M}$ then induces an associated quantum state $\phi_\pm$ on M. In particular, this is true of the Hartle-Hawking state $|0_{HH,\tilde{M}}\rangle$, and we call the induced state $|0_{HH,M}\rangle_\pm$. We will be interested in the expectation value in such states of the stress tensor operator $T_{ab\pm}(x)$ (where the $\pm$ again refer to the choice of $\pm$ boundary conditions),

and in particular the associated back-reaction on the spacetime M. This back-reaction is most simply discussed by defining a new stress tensor $T_{ab\pm}(\tilde{x})$ on $\tilde{M}$ as the pull-back of $T_{ab\pm}(x)$ under the natural projection $\tilde{M} \to M$. In particular, for our Hartle-Hawking states we have

$$ {}_{\pm}\langle 0_{HH,M}|T_{ab\pm}(x)|0_{HH,M}\rangle_{\pm} = \langle 0_{HH,\tilde{M}}|T_{ab\pm}(\tilde{x})|0_{HH,\tilde{M}}\rangle. \tag{4.2}$$

for any $\tilde{x}$ that projects to x. The difference between $T_{ab}(\tilde{x})$ and the stress tensor $\tilde{T}_{ab}(\tilde{x})$ of the quantum field $\tilde{\phi}$ on $\tilde{M}$ will be made explicit below, but the important point is that the construction of the former involves the isometry J which fails to commute with the Killing symmetry of $\tilde{M}$; see figure 4.2. So while the expectation value of $\tilde{T}_{ab}(\tilde{x})$ in the Hartle-Hawking state $|0_{HH,\tilde{M}}\rangle$ is invariant under the Killing symmetry, this property does *not* hold for the pull-back $T_{ab}(\tilde{x})$ of $T_{ab}(x)$.

The point of pulling-back the stress tensor to $\tilde{M}$ is to reduce the analysis of back-reaction to calculations like that in [15]. Since the (Hartle-Hawking) expectation value of $T_{ab\pm}(\tilde{x})$ is invariant under the action of J, the back-reaction of $T_{ab\pm}(x)$ on M is just the $\mathbb{Z}_2$ quotient under J of the back-reaction of $T_{ab\pm}(\tilde{x})$ on $\tilde{M}$. Since $\tilde{M}$ has a bifurcate horizon, after back-reaction traversability of the associated wormhole is related to the integral of $T_{ab\pm}(\tilde{x})k^a k^b$ over the null generators of the horizon. In particular, with sufficient symmetry (as in section 4.3) the wormhole is traversable if and only if this value is negative along some generator. More generally, the wormhole can become traversable only if this integral is negative along some generator [83, 84] and, as we will discuss in section 4.4 below, in our contexts traversability will be guaranteed if the average of this integral over all generators is negative.

To allow explicit formulae, we now specialize to the case of scalar fields. The stress

tensor of a free scalar field of mass m takes the form

$$T_{ab\pm} = \partial_a \phi_\pm \partial_b \phi_\pm - \frac{1}{2} g_{ab} g^{cd} \partial_c \phi_\pm \partial_d \phi_\pm - \frac{1}{2} g_{ab} m^2 \phi_\pm^2. \tag{4.3}$$

In general, this diverges and requires careful definition via regularization (e.g., point-splitting) and renormalization. However, using (4.1), the symmetry under J of the actual stress energy $\tilde{T}_{ab}(\tilde{x})$ of the quantum field $\tilde{\phi}$ on $\tilde{M}$, and the fact that k^a is null we find

$${}_\pm\langle 0_{HH,M}|T_{ab\pm}k^a k^b(x)|0_{HH,M}\rangle_\pm = \langle 0_{HH,\tilde{M}}| \left[\tilde{T}_{ab}k^a k^b(\tilde{x}) \pm k^a k^b \partial_a \phi(\tilde{x}) \partial_b \phi(J\tilde{x})\right] |0_{HH,\tilde{M}}\rangle. \tag{4.4}$$

The second term on the right in (4.4) is manifestly finite since $\tilde{x}, J\tilde{x}$ are spacelike separated (and would be so even without contracting with $k^a k^b$). Renormalization of $T_{ab\pm}$ is thus equivalent to renormalization of the stress tensor $\tilde{T}_{ab}$ of the $\tilde{\phi}$ quantum field theory on the covering space $\tilde{M}$. However, when evaluated on the horizon and contracted with $k^a k^b$, any smooth symmetric tensor Q_{ab} on $\tilde{M}$ that is invariant under the Killing symmetry must vanish[5]. As a result, the divergent terms in $\tilde{T}_{ab}k^a k^b(\tilde{x})$ (which are each separately smooth geometric tensors with divergent coefficients) vanish on the horizon in all states, and invariance of the Hartle-Hawking state $|0_{HH,\tilde{M}}\rangle$ means that the finite part of $\tilde{T}_{ab}k^a k^b(\tilde{x})$ also gives no contribution to (4.4). Thus we have

$${}_\pm\langle 0_{HH,M}|T_{ab\pm}k^a k^b(x)|0_{HH,M}\rangle_\pm = \pm\langle 0_{HH,\tilde{M}}|k^a k^b \partial_a \phi(\tilde{x}) \partial_b \phi(J\tilde{x})|0_{HH,\tilde{M}}\rangle. \tag{4.5}$$

This result shows the key point. Unless the integral of the right-hand-side vanishes,

[5]This is most easily seen by the standard argument that if ξ^a is the Killing vector field then $Q_{ab}\xi^a\xi^b$ is smooth scalar invariant under the symmetry. It is thus constant along the entire bifurcate horizon, and so must vanish there since ξ^a vanishes on the bifurcation surface. But $Q_{ab}k^a k^b \propto Q_{ab}\xi^a\xi^b$ on the horizon away from the bifurcation surface, so it must vanish there as well. Smoothness then also requires $Q_{ab}\xi^a\xi^b$ to vanish on the bifurcation surface. This comment also justifies our use of Einstein-Hilbert gravity, as the first-order perturbative contributions from any higher derivative terms will vanish for the same reason.

it will be negative for some choice of boundary conditions ($\pm$). With that choice, back-reaction will then render the wormhole traversable. It thus remains only to study this integral in particular cases, both to show that it is non-zero and to quantify the degree to which the wormhole becomes traversable. We perform this computation for the AdS_3 $\mathbb{RP}^2$ geon and a simple Kaluza-Klein end-of-the-world brane in section 4.3, and for a related example involving Kaluza-Klein zero-brane orbifolds in section 4.4.

4.2.2 A path integral perspective

Before proceeding to explicit calculations, this section takes a brief moment to provide some useful perspective on the above construction, the relation to AdS/CFT, and in particular the connection to recent work [89] by Maldacena and Qi and the original traversable wormhole of Gao, Jafferis, and Wall [15]. Readers focused on the detailed computations relevant to our examples may wish to proceed directly to sections 4.3 and 4.4 and save this discussion for a later time.

For the purposes of this section we assume that the Hartle-Hawking state $|0_{HH,\tilde{M}}\rangle$ on the covering space $\tilde{M}$ is given by a path integral over (half of) an appropriate Euclidean (or complex) manifold $\tilde{M}_E$ defined by Wick rotation of the Killing direction in $\tilde{M}$. In rotating cases, this may also involve analytic continuation of the rotation parameter to imaginary values, or a suitable recipe for performing the path integral on a complex manifold[6]. We further assume that (as in figure 4.2) the isometry J maps the Killing field ξ^a to $-\xi^a$. Note that global hyperbolicity of M requires J to preserve the time-orientation of $\tilde{M}$ so that, since J exchanges the right- and left-moving horizons, it is not possible for J to leave ξ^a invariant.

Following [102], one can extend the isometry J to act on the complexification $\tilde{M}_{\mathbb{C}}$

[6]In the presence of super-radiance or instabilities this procedure gives a non-normalizeable state that is not appropriate for quantum field theory. In such cases one often says that the Hartle-Hawking state does not exist [103].

of $\tilde{M}$, and thus on the particular section $\tilde{M}_E$. The quotient $M_E = \tilde{M}_E/J$ and the desired Lorentzian spacetime $M = \tilde{M}/J$ are then associated with the complex quotient $M_{\mathbb{C}} = \tilde{M}_{\mathbb{C}}/J$. As a result, M_E is an analytic continuation of M.

Furthermore, for free fields the path integral over (half of) M_E defines a state that is related to $|0_{HH,\tilde{M}}\rangle$ via the method of images. This state is thus $|0_{HH,M}\rangle_+$, and we may instead obtain $|0_{HH,M}\rangle_-$ by coupling the bulk theory to a background $\mathbb{Z}_2$-valued gauge field with non-trivial holonomy around the $\mathbb{Z}_2$ cycle associated with taking the quotient by J. It is due to this direct Euclidean (or complex) path integral construction that we call $|0_{HH,M}\rangle_\pm$ Hartle-Hawking states. Taking this as the definition, such Hartle-Hawking states on M can also be introduced for interacting quantum fields.

Indeed, in the AdS/CFT context one can go even farther. Let us suppose that M_E is the dominant bulk saddle point of a gravitational path integral over asymptotically locally AdS (AlAdS) geometries with conformal boundary ∂M_E. Then following [104] the CFT state defined by cutting open the path integral on ∂M_E (perhaps again coupled to a $\mathbb{Z}_2$ gauge field having non-trivial holonomy) is dual to our Hartle-Hawking state $|0_{HH,M}\rangle_\pm$ on the bulk manifold M_E at all orders in the bulk semi-classical approximation.

The zero temperature limit

Let us in particular consider the limit in which the temperature T vanishes as defined by the Killing horizon in the bulk covering space $\tilde{M}$. The Euclidean (or complex) period of $\tilde{M}_E$ diverges in this limit, so that $\tilde{M}_E$ can be approximated by $\tilde{\Sigma}\times\mathbb{R}$ for some manifold $\tilde{\Sigma}$ and $\partial\tilde{M}_E \to \partial\tilde{\Sigma}\times\mathbb{R}$; see figure 4.3. Similarly, $M_E \to \Sigma\times\mathbb{R}$ and $\partial M_E \to \partial\Sigma\times\mathbb{R}$ for $\Sigma = \tilde{\Sigma}/J$. So in the AdS/CFT context, we are studying the ground state of the CFT on $\partial\Sigma\times\mathbb{R}$.

This setting is now in direct parallel with that recently studied by Maldacena and Qi [89], which considered two copies of the SYK theory [105, 106] coupled through

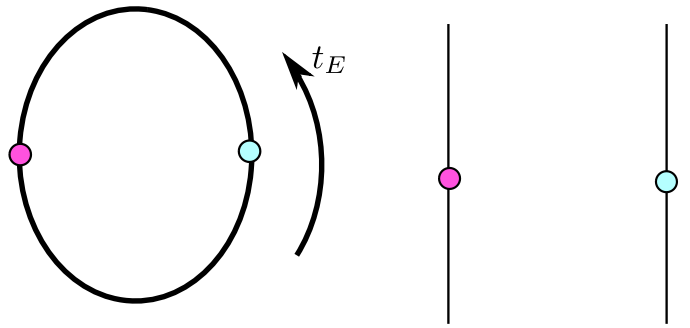

Figure 4.3: The boundary $\partial\tilde{M}_E$ of the non-extreme case (left) grows longer and longer to become $\partial\tilde{\Sigma} \times \mathbb{R}$ in the extreme limit (right).

some multi-trace interaction and the associated two-boundary AdS_2 bulk dual to the Schwarzian sector of the SYK theory [107]. From the CFT perspective, the multi-trace coupling is clearly critical to allow the two SYK models to interact. From the bulk perspective, this coupling is again critical in allowing traversability, as without it the system would be invariant under separate time-translations along each of the two boundaries (associated with separate time-translations in each of the two SYK models). Preserving this symmetry would then forbid any bulk solution in which the two boundaries are connected. In our setting, there is generally just a single time-translation symmetry of $\Sigma \times \mathbb{R}$ along $\mathbb{R}$.

The formulation in terms of ground states was useful in the non-perturbative SYK analysis of [89]. It also provides a useful perspective on our perturbative bulk analysis. In particular, since the bulk ground state will be invariant under Euclidean time-translations (see footnote 1), any zero temperature wormholes must either be traversable at all times or not at all. Now, noting that a trip through a traversable wormhole can be started at arbitrarily early times, but that (unless the wormhole is eternal) there is generally a latest time t_f at which such a trip may be begun, we can use t_f to quantify the extent to which a given wormhole is traversable[7]. So if the finite T wormholes become traversable,

[7]It is in fact more natural to use $t_f - t_i$, where t_i is the earliest time at which a *past*-directed causal curve can traverse the wormhole. But we implicitly assume some symmetry that includes time-reversal

and if perturbative calculations indicate that t_f increases as $T \to 0$, then we may take this as an indication that the wormhole is both traversable and static (eternal) in the actual bulk ground state. Consistent with [89], we will find indications in section 4.4 that this occurs in the presence of sufficiently many bulk fields.

As a final comment, even if one is most interested in $T = 0$, we see that the finite temperature setting is useful for performing perturbative computations. A corresponding finite-T version of [89] can be obtained by studying SYK on a thermal circle defined by periodic Euclidean time t_E, so that slicing the circle at both $t_E = 0$ and the antipodal point $t_E = 1/(2T)$ yields two-copies of SYK. Introducing a multi-trace interaction that is non-local in t_E, and which in particular couples $t_E = 0$ with $t_E = 1/(2T)$, then reproduces the ground state path integral of [89] in the limit $T \to 0$ so long as one focuses on Euclidean times t_E near both $t_E = 0$ and $t_E = 1/(2T)$ and takes the non-local coupling to become time-independent in these regions. For example, the coupling might take the form $g_T(Tt_E)\mathcal{O}(t_E)\mathcal{O}(\frac{1}{2T} - t_E)$ where g_T is symmetric under $Tt_E \to \frac{1}{2} - Tt_E$; see figure 4.4. In field-theoretic cases (as opposed to the 0+1 SYK context), one may also wish to require that g vanish at $t_E = \pm\frac{1}{4T}$ to prevent additional UV singularities. At finite temperature, the Euclidean time-translation invariance is then broken by this non-local coupling, just as it is broken in our setting by the $\mathbb{Z}_2$ quotient of $\tilde{M}_E$ by J. We also note that Wick rotation to Lorentz signature and appropriate choice of the resulting real-time coupling $g(t)$ then gives essentially the original traversable wormhole setting of [15], though with Feynman boundary conditions instead of the retarded boundary conditions used in [15].

(e.g., $(t, \phi) \to (-t, -\phi)$) in the main text.

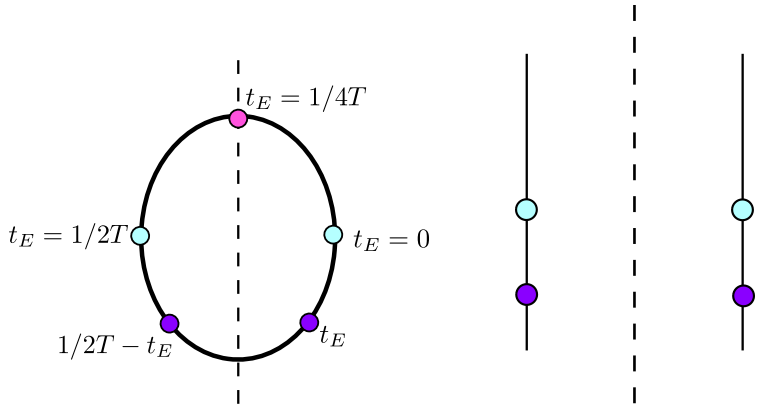

Figure 4.4: The ground states of Maldacena and Qi [89] can be obtained as limits of path integrals dominated by finite-temperature backgrounds in the bulk semi-classical limit. At finite T, these path integrals would yield thermo-field double states if not for the additional multi-trace interaction that is bi-local in the Euclidean time t_E, coupling points t_E and $\frac{1}{2T} - t_E$ related by reflection about the vertical dashed line.

4.3 Simple traversable AdS_3 wormholes from Hartle-Hawking states

The non-rotating AdS_3 $\mathbb{RP}^2$ geon and KKEOW brane that form our first examples were defined in figure 4.2 as simple $\mathbb{Z}_2$ quotients of BTZ and BTZ $\times S^1$ under appropriate isometries J. Since quantum fields on the latter can be Kaluza-Klein reduced to an infinite tower of quantum fields on BTZ, it is clear from section 4.2 that both cases may be studied by computing the right-hand-side of (4.5) as defined by the two-point function of a single scalar field in the BTZ Hartle-Hawking state.

4.3.1 BTZ and back-reaction

As is well known, BTZ is itself a quotient of AdS_3, and the BTZ Hartle-Hawking two-point function is induced[8] via the method of images with periodic boundary conditions from the corresponding two-point function in the AdS_3 vacuum $|0\rangle_{AdS_3}$. Since the latter

[8]Due to the fact that AdS_3 is an infinite cover of BTZ, this construction is slightly different than that discussed in section 4.2.1.

is available in closed form, this construction provides a useful starting point for detailed calculations.

At this stage it is useful to introduce Kruskal-like coordinates (U, V, ϕ) on (non-rotating) BTZ. We choose them so that the BTZ metric is

$$\mathrm{d}s^2 = g_{ab}\mathrm{d}x^a\mathrm{d}x^b = \frac{1}{(1+UV)^2}(-4\ell^2\mathrm{d}U\mathrm{d}V + r_+^2(1-UV)^2\mathrm{d}\phi^2) \tag{4.6}$$

where ϕ is periodic with period 2π. Such coordinates in particular allow us to write explicit expressions for the isometries J. For the AdS_3 $\mathbb{RP}^2$ geon, we take $J_{\mathrm{geon}}(U, V, \phi) = (V, U, \phi + \pi)$; i.e., it is given by reflecting the conformal diagram 4.2 (right) about the dashed vertical line and acting with the antipodal map on the BTZ ϕ-circle. For the KKEOW brane, there is an additional periodic angle $\theta \in [0, 2\pi)$ on the internal S^1 and we take $J_{\mathrm{eow}}(U, V, \phi, \theta) = (V, U, \phi, \theta + \pi)$; i.e., this action is similar to J_{geon} but with the antipodal map acting on the internal S^1 as opposed to the BTZ ϕ-circle.

As discussed in section 4.2, the integral $\int \mathrm{d}\lambda \langle T_{ab}\rangle k^a k^b$ along horizon generators will play a primary role in our analysis. Here λ is an affine parameter and k^a the associated tangent vector. In particular, since U is an affine parameter along the BTZ horizon $V = 0$, it will be useful to take $\lambda = U$ and $k^a\partial_a = \frac{\partial}{\partial U}$.

Let us begin with the observation that (as in [15]), at linear order the geodesic equation implies a null ray starting from the right boundary in the far past to have

$$V(U) = -(2g_{UV}(V=0))^{-1}\int_{-\infty}^{U}\mathrm{d}U h_{kk} \tag{4.7}$$

where h_{kk} is the norm of k^a after first-order back-reaction from the quantum stress tensor (since $g_{ab}k^a k^b = 0$) and we have used the fact that the background metric (4.6) has constant g_{UV} along the horizon ($V = 0$).

It thus remains to integrate h_{kk}. Since our $\mathbb{RP}^2$ geon and KKEOW brane both preserve rotational symmetry, this integral can be performed following [15]. Defining $T_{kk} := T_{ab}k^a k^b$, the linearized Einstein equations give

$$\frac{1}{2}\left[\ell^{-2}(h_{kk} + \partial_U(U h_{kk})) - r_+^{-2}\partial_U^2 h_{\phi\phi}\right] = 8\pi G_N \langle T_{kk}\rangle. \tag{4.8}$$

To find the shift ΔV at $U = +\infty$, one merely integrates this equation over all U to find

$$8\pi G_N \int \mathrm{d}U \langle T_{kk}\rangle = \frac{1}{2}\ell^{-2}\int \mathrm{d}U h_{kk}, \tag{4.9}$$

where we have used asymptotically AdS boundary conditions and the requirement that the boundary stress tensor be unchanged at this order to drop the additional boundary terms[9]. Thus,

$$\Delta V(+\infty) = -\frac{8\pi G_N \ell^2}{g_{UV}(0)}\int_{-\infty}^{\infty}\mathrm{d}U\langle T_{kk}\rangle = 4\pi G_N \int_{-\infty}^{\infty}\mathrm{d}U\langle T_{kk}\rangle. \tag{4.10}$$

Similarly, if we are interested in measuring the shift at the center of the wormhole ($U = V = 0$), we can integrate equation (4.8) from $U = -\infty$ to $U = 0$. The contribution from $\partial_U(U h_{kk})$ again vanishes, as $U h_{kk}|_{U=0} = 0$. We thus find

$$\Delta V(0) = -\frac{8\pi G_N \ell^2}{g_{UV}(0)}\int_{-\infty}^{0}\mathrm{d}U\langle T_{kk}\rangle = 2\pi G_N \int_{-\infty}^{\infty}\mathrm{d}U\langle T_{kk}\rangle = \frac{1}{2}\Delta V(+\infty), \tag{4.11}$$

where we have used the fact that in our examples $\langle T_{kk}\rangle$ is also symmetric about $t = 0$. This quantity gives a measure of the length of time that the wormhole remains open as

[9]In the presence of scalars with $\Delta < 1$ (see below), the metric can receive large corrections near the boundary. But in AdS_3 such corrections give only a conformal rescaling of the original metric and so cannot contribute to (4.7). The specification that the boundary stress tensor be unchanged determines the choice of boundary gravitons – or in other words the choice of linearized diffeomorphism along with the change in gravitational flux threading the wormhole – to be added along with the perturbation.

measured by an observer at the bifurcation surface. Since the result is simply related to the shift at the left boundary, it will be convenient below to define $\Delta V := \Delta V(+\infty)$ and to understand that all quantities of interest are simply related to this ΔV.

For example, we might also like to compute the minimum length of time it takes to travel through the wormhole. Note that at first order in perturbation theory, any null ray that traverses the wormhole (from right to left) will be perturbatively close to $V = 0$. As a result, at this order it will differ from (4.7) by at most a constant off-set; i.e.,

$$\Delta V(U) := V(U) - V(-\infty) = -\int_{-\infty}^{U} \mathrm{d}U \frac{h_{kk}}{2g_{UV}(V=0)}. \tag{4.12}$$

Choosing a conformal frame in which the boundary metric is $\mathrm{d}s^2_{\partial \mathrm{BTZ}} = -\mathrm{d}t^2 + \ell^2 \mathrm{d}\phi^2$, we find on the boundary $\mathrm{d}t^2 = \frac{\ell^4 \mathrm{d}V^2}{r_+^2 V^2}$, so we may choose $t = \pm \frac{\ell^2}{2r_+} \ln\left(\pm \frac{V}{\ell}\right)$, with the choice of signs $(\pm)$ being both $(+)$ on the right boundary and both $(-)$ on the left. Since the wormhole is traversable for $\Delta V < 0$, the shortest transit time t_* from the right to left boundary is realized by the geodesic that leaves the right boundary at $V = -\Delta V/2$ and arrives at the left boundary at $V = \Delta V/2$. We thus find

$$t_* = -\frac{\ell^2}{r_+} \ln\left(\frac{|\Delta V|}{2\ell}\right). \tag{4.13}$$

4.3.2 Ingredients for the stress tensor

The quotient of AdS_3 used to obtain BTZ is associated with the periodicity of ϕ. As a result, taking ϕ in (4.6) to range over $(-\infty, \infty)$ yields a metric on a region of empty global AdS_3.

Now, at spacelike separations (as appropriate for $\tilde{x}, J\tilde{x}$), the AdS_3 two-point function

for a free scalar field of mass m is determined by its so-called conformal weight

$$\Delta = 1 \pm \sqrt{1 + m^2 \ell^2}, \tag{4.14}$$

where the choice of $\pm$ is associated with a choice of boundary conditions, though for $m^2 \geq 0$ only the $(+)$ choice is free of ghosts [108]. The AdS_3 two-point function is then (see section 4.1 of reference [109])

$$G(x, x') = G_{AdS_3}(Z) = \frac{1}{4\pi}(Z^2 - 1)^{-1/2}(Z + (Z^2 - 1)^{1/2})^{1-\Delta} \tag{4.15}$$

where $Z = 1 + \sigma(x, x')$ and $\sigma(x, x')$ is half of the (squared) distance between x and x' in the four dimensional embedding space[10], and with all fractional powers of positive real numbers defined by using the positive real branch. The BTZ two-point function is

$$G_{BTZ}(\tilde{x}, \tilde{x}') = \frac{1}{4\pi} \sum_{n \in \mathbb{Z}} (Z_n^2 - 1)^{-1/2}(Z_n + (Z_n^2 - 1)^{1/2})^{1-\Delta}, \tag{4.16}$$

where $Z_n = 1 + \sigma(x, x'_n)$ where x is any point in AdS_3 that projects to $\tilde{x}$ in BTZ and x'_n are the inverse images in AdS_3 of $\tilde{x}'$ in BTZ. A standard calculation then gives

$$\begin{aligned} \sigma(x, x'_n) = & \frac{\ell^2}{(UV+1)(U'V'+1)} \left[(UV-1)(U'V'-1) \cosh\left(r_+ (\phi - \phi'_n)\right) \right. \\ & \left. -(UV+1)(U'V'+1) + 2(UV' + VU') \right] \end{aligned} \tag{4.17}$$

in terms of our Kruskal-like BTZ coordinates. Here we take $x = (U, V, \phi)$ (in either the geon/KKEOW brane or AdS_3) and $x'_n = (U', V', \phi'_n)$. As noted above, the x'_n are related by 2π shifts of the BTZ ϕ coordinate so that $\phi'_n := \phi(x'_n) = \phi' + 2\pi n$ for some ϕ'.

In computing (4.5), we will set $\tilde{x}' = J\tilde{x}$ and thus $U' = V, V' = U$. For the AdS_3 geon

[10] In reference [110], this distance was called the "chordal distance" in the embedding space. Here, $\sigma(x, x')$ is half of this chordal distance.

we also set $\phi' = \phi + \pi$, while $\phi' = \phi$ for our KKEOW brane. So for each n both cases involve computations of (4.5) that differ only by an overall shift of ϕ' by π.

In fact, one sees immediately from (4.17) that the integral of (4.5) depends only on $C \equiv \cosh\left(r_+(\phi - \phi'_n)\right)$. For the geon case, this is $-2\pi(n_{\rm geon} + \frac{1}{2})r_+^{\rm geon}$, while for the KKEOW brane it is $-2\pi n_{\rm eow} r_+^{\rm eow}$. So for $r_+^{\rm geon} = 2r_+^{\rm eow}$ and $n_{\rm eow} = 2n_{\rm geon} + 1$ (for odd $n_{\rm eow}$) or $r_+^{\rm geon} = 4r_+^{\rm eow}$ and $n_{\rm eow} = 4n_{\rm geon} + 2$ (for even $n_{\rm eow}$), the two computations involve precisely the same integral over generators of the BTZ horizon. Below, we briefly comment on this integral for general C and then use it to obtain the desired geon and KKEOW brane results. In particular, working on the horizon $V = 0$ we define

$$f(C, U; \Delta) := \langle 0_{HH,{\rm AdS}_3} | \partial_U \phi(x) \partial_U \phi(x') | 0_{HH,{\rm AdS}_3} \rangle |_{V=0} \tag{4.18}$$

for x, x' as above in AdS_3. Using (4.15) and (4.17) then gives

$$\begin{aligned} f(C, U; \Delta) =& \frac{\left(\sqrt{B^2-1} + B\right)^{-\Delta}}{2\pi \left(B^2-1\right)^{5/2}} \Big\{ \left(B^2-1\right)^2 (1-\Delta) \left(-\frac{2B^2U^2}{\left(B^2-1\right)^{3/2}} + \frac{2U^2+B}{\sqrt{B^2-1}} + 1 \right) \\ &+ \Big[\left(B^2-1\right) \left(2(\Delta^2 - \Delta - 1)U^2 - B \right) + 4B\sqrt{B^2-1}(\Delta-1)U^2 + 6B^2U^2 \Big] \\ &\times \left(\sqrt{B^2-1} + B \right) \Big\}, \end{aligned} \tag{4.19}$$

where $B(U) \equiv 2U^2 + C$. To give the reader a feel for this complicated-looking function, we plot f in figure 4.5 below for various values of C, Δ.

We can also consider simple, limiting cases of $f(C, U; \Delta)$. For instance, when $\Delta = 0, 1, 2$, this becomes

$$f(C, U; 0) = f(C, U; 2) = \frac{1 - C^2 + 2CU^2 + 8U^4}{2\pi \left[\left(C + 2U^2\right)^2 - 1 \right]^{5/2}}, \tag{4.20}$$

$$f(C, U; 1) = \frac{C - C^3 + 4U^2 - 2C^2U^2 + 4CU^4 + 8U^6}{2\pi \left[\left(C + 2U^2\right)^2 - 1 \right]^{5/2}}. \tag{4.21}$$

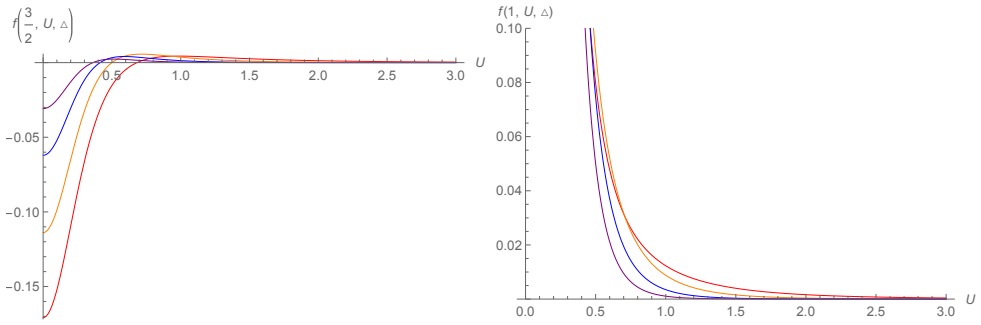

Figure 4.5: Some of the functions (4.19). **Left:** $C = 1.5$, for $\Delta = 1$ (red), $\Delta = 2$ (orange), $\Delta = 3$ (blue), and $\Delta = 4$ (purple). **Right:** $C = 1$, for $\Delta = 1$ (red), $\Delta = 2$ (orange), $\Delta = 3$ (blue), and $\Delta = 4$ (purple).

More generally, when $\Delta = 0, 1/2, 1, 3/2, 2 \ldots$, the integral $\int \mathrm{d}U f(C, U; \Delta)$ can be performed analytically. For example, we find

$$\int_0^\infty f(C,U;0)\mathrm{d}U = \int_0^\infty f(C,U;2)\mathrm{d}U = \frac{(C-1)\,K\left(\frac{2}{C+1}\right) - CE\left(\frac{2}{C+1}\right)}{8\sqrt{2}\pi\,(C-1)\,\sqrt{C+1}} < 0 \tag{4.22}$$

$$\int_0^\infty f(C,U;1)\mathrm{d}U = -\frac{E\left(\frac{2}{C+1}\right)}{8\sqrt{2}\pi\,(C-1)\,\sqrt{C+1}} < 0, \tag{4.23}$$

for $C > 1$ where $K(k)$ is the complete elliptic integral of the first kind and $E(k)$ is the complete elliptic integral of the second kind. Since both E and K are positive functions, the second inequality is manifest. The first inequality can be seen from figure 4.6 (left).

For other values of Δ and C, numerical integration suggests that the result continues to be negative as seen in figure 4.6:

$$\int_0^\infty f(C,U;\Delta)\mathrm{d}U < 0, \text{ for } \Delta \geq 0, C > 1. \tag{4.24}$$

For all $\Delta \geq 0$, when $C \to 1^+$, the integral $\int_0^\infty f(C,U;\Delta)\mathrm{d}U$ becomes divergent and goes to $-\infty$. In contrast, both f and its integral vanish for all Δ as $C \to \infty$. For later use,

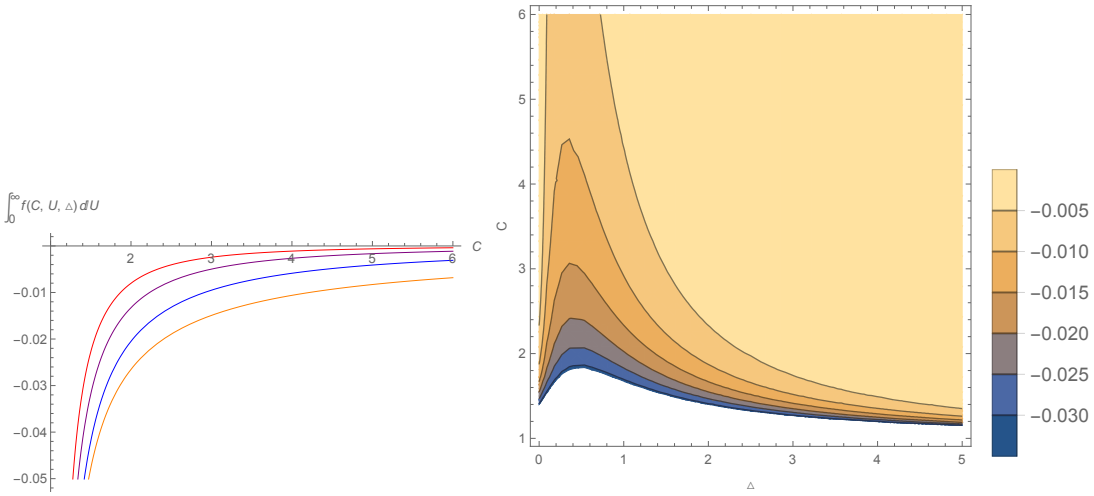

Figure 4.6: **Left:** $\int_0^\infty f(C,U;\Delta)\mathrm{d}U$ as a function of C for $\Delta = 0$ (red), $\Delta = 0.5$ (orange), $\Delta = 1$ (blue), $\Delta = 1.5$ (purple). **Right:** Further numerical results for $\int_0^\infty f(C,U;\Delta)\mathrm{d}U$ supporting (4.24). The white region is even more negative than those shown in color.

we note that expression (4.17) simplifies in the $r_+ \to 0$ limit, which gives

$$f(1,U;\Delta) = \frac{\left(U+\sqrt{1+U^2}\right)^{2-2\Delta}}{32\pi U^3(1+U^2)^{5/2}}\Big[1+2U\sqrt{1+U^2}\,(-1+\Delta)+8U^3\sqrt{1+U^2}\,(-1+\Delta) \\ +4U^4\left(2-2\Delta+\Delta^2\right)+U^2\left(6-8\Delta+4\Delta^2\right)\Big]\,. \tag{4.25}$$

Some of these functions are plotted in figure 4.5 (right).

4.3.3 Traversability of the AdS $\mathbb{RP}^2$ geon

We can now use the above ingredients to study the traversability of the $\mathbb{RP}^2$ geon with back-reaction from a periodic (+) scalar. Since the analysis involves only a single bulk quantum field, we have

$$\int \mathrm{d}U\langle T_{kk+}\rangle = \sum_{n\in\mathbb{Z}}\int \mathrm{d}U\, f(C_n,U;\Delta) \tag{4.26}$$

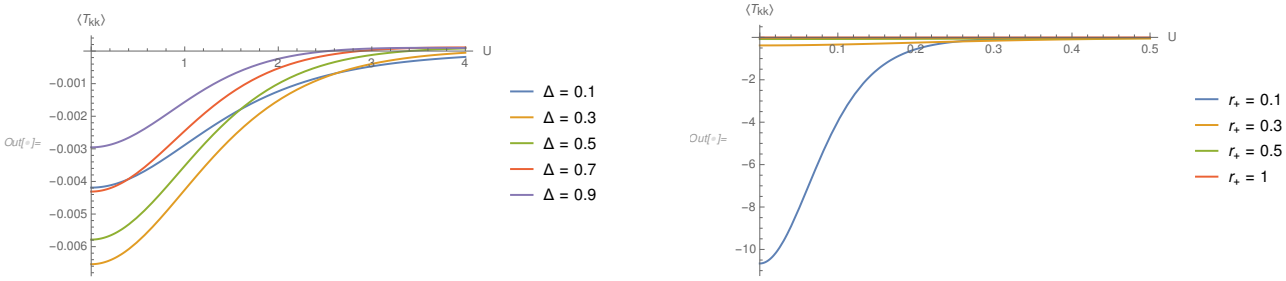

Figure 4.7: **Left:** $\langle T_{kk+}\rangle$ on the AdS_3 geon for various Δ with $r_+ = \ell$. **Right:** $\langle T_{kk+}\rangle$ on the AdS_3 geon for various r_+ (in units of ℓ) with $\Delta = 0.5$.

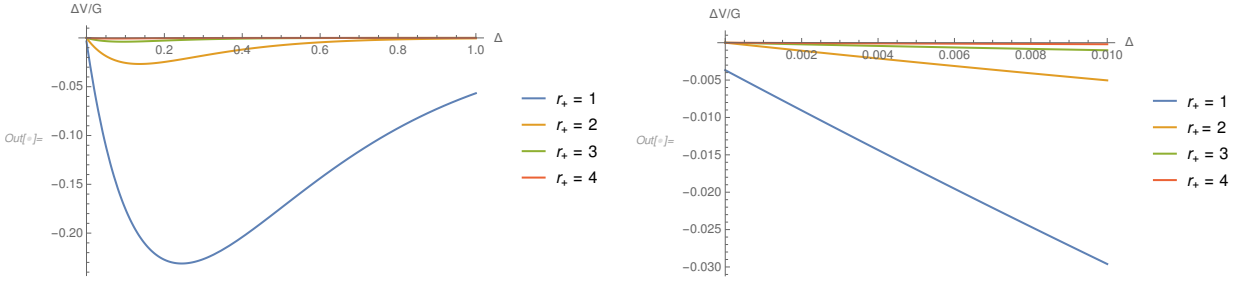

Figure 4.8: **Left:** The shift ΔV as measured on the left boundary. **Right:** ΔV remains negative at $\Delta = 0$.

for C_n defined by $\phi - \phi'_n = (2n+1)\pi$. From (4.24) we can already see that the associated first-order back-reaction will make the wormhole traversable. As pointed out in [15] and shown in figure 4.6 (right), $\Delta V \to -\infty$ as $r_+ \to 0$. But in contrast to [15], it follows from (4.22) that ΔV remains finite as $\Delta \to 0$ (though it is numerically small, see figure 4.8). Typical stress tensor profiles and horizon shifts ΔV are shown in figures 4.7 and 4.8, where we used Mathematica to numerically perform both the integral over U and the sum over n in (4.26). While the total stress energy is used in the figures, since f decreases rapidly at large C, for $r_+ > 1$ there is little difference between $\langle T_{kk+}(U)\rangle$ and the $n = 0$ term $f(C_0, U; \Delta)$ (except for a factor of 2 that arises because $C_0 = C_{-1}$ for the geon since these cases represent $\phi - \phi_n{}' = \pm\pi$). An interesting feature of the results is that the value $\Delta_{\max}$ of Δ that maximizes $|\Delta V|$ depends strongly on r_+ as shown in figure 4.9.

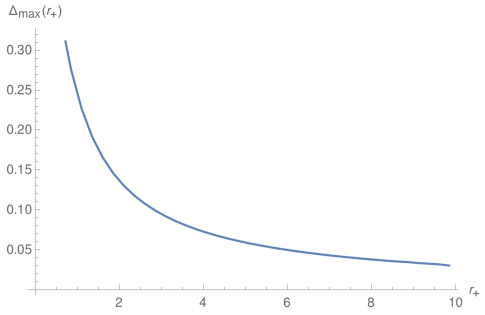

Figure 4.9: The Δ which maximizes $|\Delta V|$ for a given r_+.

4.3.4 Traversability and the KKEOW brane

Although it involves only a single scalar from the 4d perspective (say with 4d mass m), Kaluza-Klein reduction to $d = 3$ gives a tower of scalar fields with effective 3d masses $m_{\text{eff}}\ell = \sqrt{m^2\ell^2 + (\ell/R_{S^1})^2 p^2}$ is the radius of the Kaluza-Klein circle. For each p, the corresponding effective conformal dimension Δ is then

$$\Delta(k) = 1 \pm \sqrt{1 + m^2\ell^2 + \left(\frac{\ell}{R_{S^1}}\right)^2 p^2}. \tag{4.27}$$

The choice of sign ($\pm$) can be made independently for each p so long as one allows boundary conditions that are non-local on the internal S^1. But violating the CFT unitarity bound $\Delta > 0$ leads to ghosts [108], so the ($+$) sign is required at large p.

Because each p is associated with a wavefunction $e^{ip\theta}$ on the internal S^1, and since J maps $\theta \to \theta+\pi$, the contribution to (4.5) from each p is $(-1)^p$ times the result $\langle T_{kk}(U;\Delta)\rangle$ one would obtain from a single scalar of weight Δ on BTZ under the (singular) $\mathbb{Z}_2$ quotient by $(U, V, \phi) \to (V, U, \phi)$. As a result, and using the symmetry under $p \to -p$ we have

$$\langle T_{kk+}(U)\rangle = \sum_{n\in\mathbb{Z}} \hat{f}(C_n, U; \ell/R_{S^1}), \tag{4.28}$$

where

$$\hat{f}\left(C_n, U; \ell/R_{S^1}\right) = f\left(C_n, U; \Delta\left(0\right)\right) + 2\sum_{p=1}^{\infty}\left(-1\right)^p f\left(C_n, U; \Delta\left(p\right)\right) \tag{4.29}$$

with $\phi - \phi_n' = 2\pi n$.

As discussed near (4.25), the function $f\left(C_n, U; \Delta\right)$ has a non-integrable singularity at $U = 0$ for $n = 0$ at each Δ but is finite for $n \neq 0$. Yet since the full 4d spacetime is smooth, the 4d-stress tensor and the back-reacted metric must be smooth as well. This occurs because the alternating signs in (4.29) cause the $U = 0$ singularities to cancel when summed over p.

For $U \neq 0$ the sums over n and p converge rapidly. In particular, for each $n \neq 0$ the sum over p converges exponentially since $f(C_n, U; \Delta(p))$ evaluates the BTZ two-point function at some fixed spacelike separation on BTZ set by C_n for 3d fields that have large mass at large p. Indeed, for fixed $U \neq 0$ the same is true even when $n = 0$. And the sum over n is also exponentially convergent since $\sigma(\tilde{x}, J\tilde{x})$ grows exponentially with n. As a result, one approach to computing (4.28) is to numerically perform the sums away from $U = 0$ and then to recover the value at $U = 0$ by taking a limit, though care will be required as contributions from very large p will be important at small U.

We can improve the numerics at small U somewhat by employing a regularization procedure at small U. Though we will not rigorously justify this procedure, we will check numerically that it gives results consistent with the more awkward (but manifestly correct) procedure described in the previous paragraph. We begin by studying the leading terms in (4.25) near $U = 0$. For $U > 0$, Laurent expansion around $U = 0$ gives

$$f\left(1, U; \Delta\right) = \frac{1}{32\pi U^3} + \frac{3 - 8\Delta + 4\Delta^2}{64\pi U} + \frac{-2\Delta + 3\Delta^2 - \Delta^3}{6\pi} + O\left(U\right). \tag{4.30}$$

We know that the singular terms should cancel when summed over $p \in \mathbb{Z}$ with a factor

of $(-1)^p$. This is especially natural for the first term on the right-hand side of (4.30) which is independent of p. Choosing to perform this sum using Dirichlet eta function regularization does indeed give zero as $\sum_{p=1}^{\infty}(-1)^p = -\eta(0) = -\frac{1}{2}$.

Using (4.27), the second term on the right-hand side of (4.30) becomes

$$\frac{3-8\Delta+4\Delta^2}{64\pi U} = \frac{3+4m^2\ell^2+4\left(\frac{\ell}{R_{S^1}}\right)^2 p^2}{64\pi U}. \tag{4.31}$$

Thus, it gives a term independent of p and a term proportional to p^2. Again applying Dirichlet eta-function regularization and recalling that $\sum_{p=1}^{\infty}(-1)^p p^2 = -\eta(-2) = 0$, the $1/U$ term also cancels completely when summed over p.

Since we did not rigorously justify the use of eta-function regularization, there remains the possibility that we have missed some important finite piece that could remain after the above divergences cancel. But we now provide numerical evidence that this does not occur by computing $\hat{f}(1,0;\ell/R_{S^1})$ in two different ways. The first is to use (4.30) with Dirichlet regularization of the $1/U^3$ and $1/U$ terms and using Abel summation (i.e., replacing $(-1)^p$ by $(-1+\epsilon)^p$ and taking $\epsilon \to 0$) for the finite term. The second is to compute the result for fixed but small $U \neq 0$ by numerically summing over p up to $|p| = N$ for some large N, but taking care to include an even number of terms with opposite signs; i.e., for $|U| > \alpha$ we take

$$\hat{f}_{\text{hybrid}}(1,U;\ell/R_{S^1}) = f(1,U;\Delta(0)) + 2\sum_{p=1}^{N-1}(-1)^p f(1,U;\Delta(p)) + (-1)^N f(1,U;\Delta(N)) \tag{4.32}$$

for some fixed large N.

Sample results are shown in figure 4.10, where we plot f_{hybrid} defined by introducing a parameter $\alpha > 0$, performing the sums numerically for $|U| > \alpha$, and then taking f_{hybrid} to be constant for $|U| < \alpha$ with a value given by the above Abel summation. The

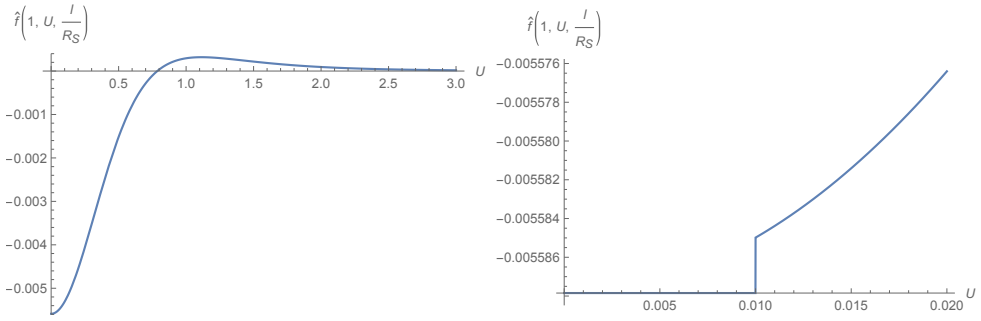

Figure 4.10: An example of $\hat{f}_{\text{hybrid}}\,(1, U; \ell/R_{S^1})$ calculated numerically for $\ell/R_{S_1} = 1$ and $\Delta\,(p) = 1 + \sqrt{1+p^2}$, $N = 5000$, $\epsilon = 10^{-6}$, and $\alpha = 0.01$. The numerical integral gives $\int_0^\infty \hat{f}\,(1, U; \ell/R_{S^1})\,\mathrm{d}U = -9.05\times10^{-4}$, which is negative. In comparison, the triangle defined in the rightmost plot by the horizontal line for $U < \alpha$ and the vertical line representing the discontinuity gives a measure of the numerical error in our computation of this integral and is of order 10^{-8}.

small discontinuity at $U = \alpha$ in the resulting $\hat{f}_{\text{hybrid}}$ supports the validity of the above regularization. We can then approximate $\int \mathrm{d}U \hat{f}(1, U; \ell/R_{S^1})$ by numerically integrating $\hat{f}_{\text{hybrid}}$.

It is interesting to compare the $\hat{f}$ in figure 4.10 with a graph of the first term $f(1, U, \Delta = 2)$ in its definition (4.29) (the orange curve on the right figure of figure 4.5). The first term is manifestly positive, while the intgeral of $\hat{f}$ is negative. This emphasizes the importance of the higher terms in the sum near $U = 0$. The dependence of $\hat{f}$ on $\Delta(p = 0)$ and ℓ/R_{S^1} is illustrated in figures 4.11 and 4.12.

In the limit of large r_+/ℓ, the contributions from $n \neq 0$ are suppressed and the $\langle T_{kk} \rangle$ exactly becomes $\hat{f}\,(1, U; \ell/R_{S^1})$. Moreover, numerical calculation shows that this is a good approximation even for $r_+/\ell \geq 1$; see figure 4.13. Up to the factor of $4\pi G$ in (4.10), ΔV becomes just $\int \mathrm{d}U \hat{f}(1, U; \ell/R_{S^1})$. Numerical results for this integral are shown in figure 4.14 with the signs $(\pm)$ in (4.27) chosen to be $(+)$ for $p \neq 0$. The integral is negative for all such cases we have explored. As one would expect, the magnitude of the integral becomes large for large ℓ/R_{S^1}. We again find a finite (negative) shift ΔV at

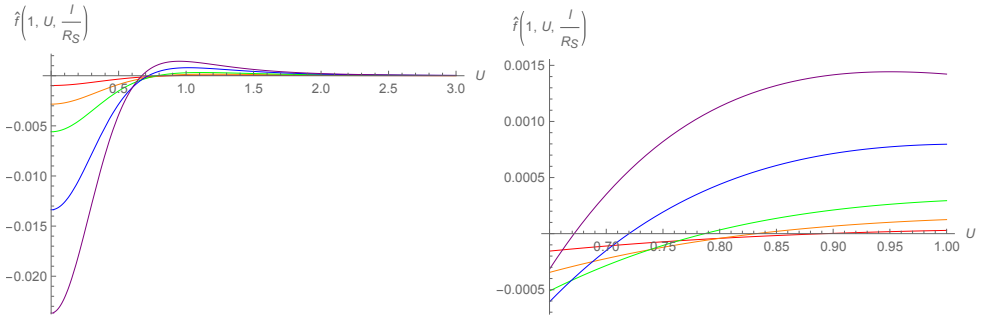

Figure 4.11: Profiles of $\hat{f}$ for fixed $m = 0$ and $(\ell/R_{S^1})^2 = 0.5$ (red), $(\ell/R_{S^1})^2 = 0.75$ (orange), $(\ell/R_{S^1})^2 = 1$ (green), $(\ell/R_{S^1})^2 = 1.5$ (blue), $(\ell/R_{S^1})^2 = 2$ (purple). For this figure, we have chosen all $(\pm)$ signs in (4.27) to be $(+)$ for all p. Note that the zero of $\hat{f}$ shifts to smaller U as ℓ/R_{S^1} increases.

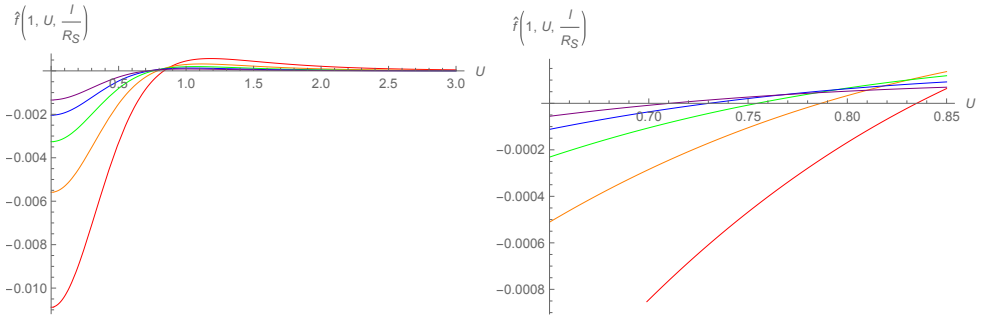

Figure 4.12: Profiles of $\hat{f}$ for fixed $\ell/R_{S^1} = 1$ and $m^2\ell^2 = -0.5$ (red), $m^2\ell^2 = 0$ (orange), $m^2\ell^2 = 0.5$ (green), $m^2\ell^2 = 1$ (blue), $m^2\ell^2 = 1.5$ (purple). For this figure, we have chosen all $(\pm)$ signs in (4.27) to be $(+)$ for all p. As m increases, the zero of $\hat{f}$ shifts to smaller U.

$r_+ = \infty$ for $\Delta(p = 0) = 0$, and ΔV vanishes in the limit of large mass m, though the maximum value of $|\Delta V|$ depends on ℓ/R_{S^1}.

However, it turns out that for some choices m and ℓ/R_{S^1}, we can choose the $(\pm)$ signs in (4.27) to be $(-)$ for $|p| = 1$ and to be $(+)$ for all other values of p (including $p = 0$). In at least some such cases $\int_0^\infty \hat{f}\,(1, U; \ell/R_{S^1})\,\mathrm{d}U$ is positive and the back-reacted wormhole remains non-traversable when our scalar satisfies periodic boundary conditions. One example is shown in figure 4.15.

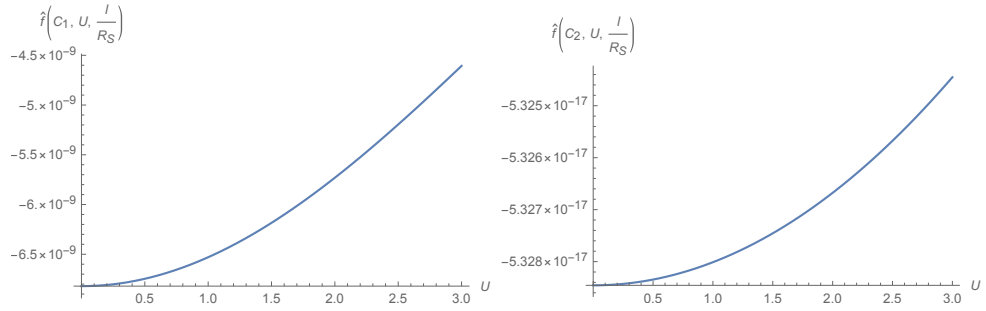

Figure 4.13: The $n = 1, 2$ contributions for the example in figure 4.10, where we have chosen $r_+/\ell = 1$. We find $\int_0^\infty \hat{f}\,(C_1, U; \ell/R_{S^1})\,\mathrm{d}U = -1.18 \times 10^{-8}$ (left) and $\int_0^\infty \hat{f}\,(C_2, U; \ell/R_{S^1})\,\mathrm{d}U = -2.10 \times 10^{-15}$ (right). Thus, for black holes with size $r_+/\ell \geq 1$, contributions from $n \neq 0$ terms are negligible.

4.4 Rotating traversable wormholes with Kaluza-Klein zero-brane orbifolds

We now turn to a slightly more complicated construction that allows rotation and thus admits a smooth extremal limit. We begin with the rotating BTZ metric

$$\mathrm{d}s^2 = \frac{1}{(1+UV)^2}\left\{-4\ell^2 \mathrm{d}U\mathrm{d}V + 4\ell r_-\left(U\mathrm{d}V - V\mathrm{d}U\right)\mathrm{d}\phi + \left[r_+^2\left(1-UV\right)^2 + 4UVr_-^2\right]\mathrm{d}\phi^2\right\}. \tag{4.33}$$

Note that the $\mathbb{Z}_2$ operations used earlier exchange $U \leftrightarrow V$ while preserving the sign of $\mathrm{d}\phi$. As a result, they change the sign of the $4r_-\left(U\mathrm{d}V - V\mathrm{d}U\right)\mathrm{d}\phi$ term in (4.33) and are not isometries for $r_- > 0$.

This can be remedied by simultaneously acting with $\phi \to -\phi$. To remove the would-be fixed-points at $\phi = 0, \pi$ for $U = V = 0$, as for the KKEOW brane, we consider a Kaluza-Klein setting involving BTZ $\times S^1$ and act on this circle with the antipodal map $\theta \to \theta + \pi$. Our full isometry is thus $J : (U, V, \phi, \theta) \to (V, U, -\phi, \theta + \pi)$. This quotient breaks rotational symmetry by singling out the points $\phi = 0, \pi$ as Klauza-Klein orbifolds (i.e., as points that become oribifold singularities with deficit angle π after Kaluza-Klein

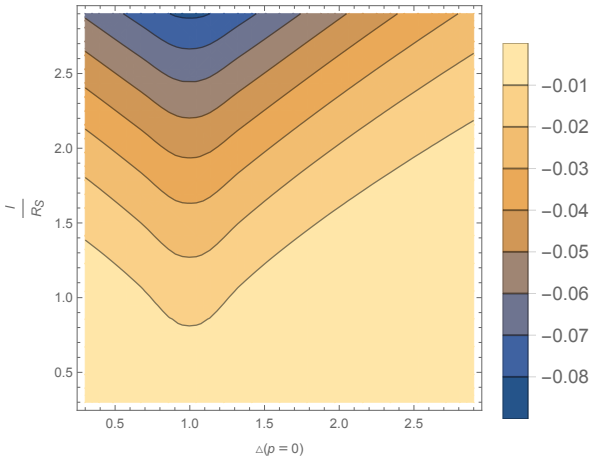

Figure 4.14: The quantity $\int_0^\infty \mathrm{d}U \hat{f}(1, U; \ell/R_{S^1})$ as a function of $\Delta(p=0)$ and ℓ/R_{S^1}. For all $p \neq 0$, we have chosen all $(\pm)$ signs in (4.27) to be $(+)$.

reduction along the internal S^1), but allows non-zero rotation and admits a smooth extremal limit. The computations then proceed much as before, though we review the main points below.

4.4.1 Geometry and back-reaction

At first order in the metric perturbation h_{ab}, the analysis of null geodesics traversing the wormhole turns out to be identical to that in the non-rotating case; i.e., equations (4.7) and (4.12) continue to hold without change. However, choosing a conformal frame in which the boundary metric is $\mathrm{d}s^2_{\partial BTZ} = -\mathrm{d}t^2 + \ell^2 \mathrm{d}\phi^2$ now yields

$$t = \pm \frac{\ell^2 r_+}{2(r_+^2 - r_-^2)} \ln\left(\pm \frac{V}{\ell}\right), \tag{4.34}$$

with the signs being both $(+)$ on the right boundary and both $(-)$ on the left.

Nevertheless, the critical change occurs in the linearized Einstein equation that de-

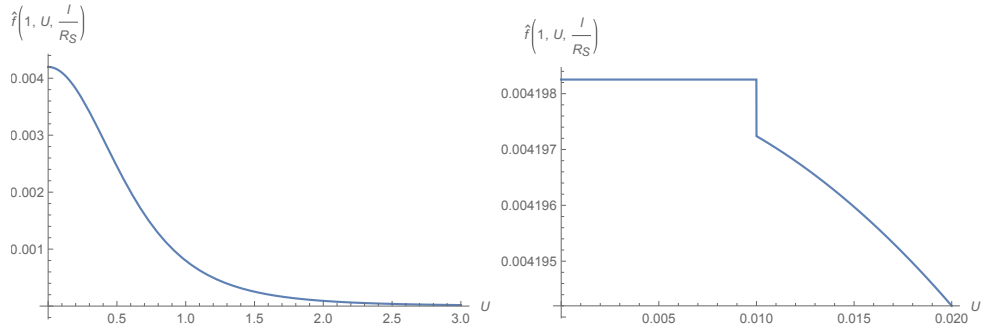

Figure 4.15: An example of $\hat{f}_{\text{hybrid}}\left(1, U; \ell/R_{S^1}\right)$ that is everywhere positive. Here $m^2\ell^2 = -0.12$, $\left(\ell/R_{S_1}\right)^2 = 0.1$, $N = 5000$, $\epsilon = 10^{-6}$, and $\alpha = 0.01$. Moreover, we have chosen the $(\pm)$ signs in (4.27) to be $(-)$ for $|p| = 1$ and to be $(+)$ for both $p = 0$ and $|p| > 1$. We find $\int_0^\infty \hat{f}\left(1, U; \ell/R_{S^1}\right) \mathrm{d}U = 1.44 \times 10^{-3} > 0$.

termines h_{ab}. We find

$$\begin{aligned} 8\pi G\langle T_{kk}\rangle = &-\frac{1}{2\ell^2 r_+^2}\left[\left(r_-^2 - r_+^2\right) h_{kk} + 2\ell r_- \partial_\phi h_{kk} + \ell^2 \partial_\phi^2 h_{kk}\right. \\ &\left. + \left(r_-^2 - r_+^2\right) \partial_U \left(U h_{kk}\right) - 2\ell^2 \partial_U \partial_\phi h_{k\phi} + \ell^2 \partial_U^2 h_{\phi\phi}\right], \end{aligned} \tag{4.35}$$

where G is the 3 dimensional Newton's constant. Integrating over U and applying asymptotically AdS boundary conditions gives

$$8\pi G \int \langle T_{kk}\rangle \mathrm{d}U = -\frac{1}{2\ell^2 r_+^2}\left[\left(r_-^2 - r_+^2\right) + 2\ell r_- \partial_\phi + \ell^2 \partial_\phi^2\right] \int h_{kk} \mathrm{d}U. \tag{4.36}$$

Equation (4.36) is easily solved for $\left(\int \mathrm{d}U h_{kk}\right)(\phi)$ using a Green's function H, so that

$$\left(\int \mathrm{d}U h_{kk}\right)(\phi) = 8\pi G \int \mathrm{d}\phi' H\left(\phi - \phi'\right) \int \mathrm{d}U \langle T_{kk}\rangle\left(\phi'\right), \tag{4.37}$$

with

$$H(\phi-\phi') = \begin{cases} \dfrac{e^{-(r_+-r_-)(\phi'-\phi)/\ell}}{2r_+/\ell\,[1-e^{-2\pi(r_+-r_-)/\ell}]} + \dfrac{e^{(r_-+r_+)(\phi'-\phi)/\ell}}{2r_+/\ell\,[e^{2\pi(r_-+r_+)/\ell}-1]} & \phi' \geq \phi \\ \dfrac{e^{(r_-+r_+)(2\pi-\phi+\phi')/\ell}}{2r_+/\ell\,[e^{2\pi(r_-+r_+)/\ell}-1]} + \dfrac{e^{-(r_+-r_-)(2\pi-\phi+\phi')/\ell}}{2r_+/\ell\,[1-e^{-2\pi(r_+-r_-)/\ell}]} & \phi' \leq \phi. \end{cases} \tag{4.38}$$

in position space where we take $\phi, \phi' \in [0, 2\pi)$. It is also useful to write H in Fourier space:

$$H\left(\phi-\phi'\right) = \sum_q e^{iq(\phi-\phi')} H_q, \quad H_q = \frac{1}{2\pi}\frac{2\ell^2 r_+^2}{r_+^2 - r_-^2 - 2iq\ell r_- + \ell^2 q^2}. \tag{4.39}$$

Note in particular that the zero-mode Green's function $H_{q=0} = \frac{\ell^2 r_+^2}{\pi(r_+^2 - r_-^2)}$ diverges in the extremal limit $r_- \to r_+$. This feature was also independently and simultaneously noted in [85], where the somewhat different form of their expression appears to be due to differences in the detailed definition of the Kruskal-like coordinates. While we have not explored the connection in detail, it is natural to expect this feature to be related to other known instabilities of extreme black holes [111, 112, 113, 114, 115, 116, 117] and in particular to the Aretakis instability for gravitational perturbations (see e.g. [117] for the Kerr case), though our present instability seems to occur only for the zero-mode while at least in Kerr the Aretkis instability is strongest at large angular momentum [118]. In our first-order perturbative analysis, this divergence implies that any non-vanishing zero-mode component $\int \mathrm{d}U \mathrm{d}\phi \langle T_{kk}\rangle$ of the averaged null stress tensor in the extremal limit leads to diverging ΔV. The perturbative analysis can then no longer be trusted in detail, though for $\int \mathrm{d}U \mathrm{d}\phi \langle T_{kk}\rangle < 0$ it certainly suggests that the wormhole remains traversable until very late times V_f. And so long as $V_f > \ell$, the extreme limit of (4.34) then implies that the wormhole remains traversable at arbitrarily late times t; i.e., it becomes an eternal static wormhole.

In contrast, the non-zero modes of H_q remain finite at extremality. So even though

the source $\int \mathrm{d}U\langle T_{kk}\rangle$ will break rotational symmetry, in the extreme limit the geometry approximately retains this invariance and it suffices to study only the zero mode. Recalling that the BTZ temperature is given by $T = \frac{r_+^2 - r_-^2}{2\pi r_+ \ell^2}$, we may write

$$\frac{T\pi}{r_+}\int h_{kk}\mathrm{d}U\mathrm{d}\phi = 8\pi G\int\langle T_{kk}\rangle\mathrm{d}U\mathrm{d}\phi, \tag{4.40}$$

so that (4.7) gives

$$T\Delta V_{\text{average}} = \frac{2Gr_+}{\pi\ell^2}\int_{-\infty}^{\infty}\int_{-\pi/2}^{\pi/2}\langle T_{kk}\rangle\mathrm{d}U\mathrm{d}\phi. \tag{4.41}$$

This is a convenient form for displaying results in the extreme limit, which will be the main focus of our calculations below. And more generally if $\Delta V_{\text{average}} < 0$ it follows that the wormhole must become traversable when entered from at least one direction. However, it is also interesting to consider the high temperature limit $r_+ \to \infty$ (say, for $r_- = 0$) in which the Green's function $H(\phi - \phi')$ becomes sharply peaked at $\phi - \phi' = 0$ and the $\int \mathrm{d}U h_{kk}$ at each ϕ can be thought of as locally determined by $\int \mathrm{d}U\langle T_{kk}\rangle$.

4.4.2 KKZBO results

We again compute the stress tensor using (4.5) and the BTZ Green's function (4.16), which remains valid so long as we use the correct expression for proper distance in the rotating BTZ metric

$$\begin{aligned}\sigma(x, x_n{}') =& \frac{1}{(UV+1)(U'V'+1)} 2\ell^2 \{(UV-1)(U'V'-1)\cosh\left[r_+(\phi-\phi_n')\right] \\ &+ 2\cosh\left[r_-(\phi-\phi_n')\right](UV' + VU') - 2UV'\sinh\left[r_-(\phi-\phi_n')\right] \\ &+ 2VU'\sinh\left[r_-(\phi-\phi_n')\right] - UU'VV' - UV - U'V' - 1\}\end{aligned} \tag{4.42}$$

As before, the basic elements of our computations are the functions

$$f(C_+, C_-, S_-, U; \Delta) := \langle 0_{HH,\mathrm{AdS}_3} | \partial_U \phi(x) \partial_U \phi(x') | 0_{HH,\mathrm{AdS}_3} \rangle |_{V=0} \tag{4.43}$$

defined by the vacuum on global AdS_3 where the dependence on angles appears only through $C_\pm = \cosh(r_\pm[\phi - \phi'])$ and $S_- = \sinh(r_-[\phi - \phi'])$. We find

$$\begin{aligned} f\left(C_-, C_+, S_-, U; \Delta\right) =& \frac{\left(\sqrt{Y^2-1}+Y\right)^{-\Delta}\left(S_- + C_-\right)}{2\pi(Y^2-1)^{5/2}}\Bigg[\left(1-Y^2\right)\Bigg(1+\Big(Y^2-1 \\ &+ Y\sqrt{Y^2-1}\Big)\Delta\Bigg) + 2(S_- + C_-)U^2\Bigg((2-\Delta)\Delta\sqrt{Y^2-1} \\ &+ \Delta(\Delta+1)Y^3 - \left(\Delta^2+\Delta-3\right)Y + \Delta(\Delta+1)\sqrt{Y^2-1}Y^2\Bigg)\Bigg], \end{aligned} \tag{4.44}$$

where $Y \equiv 2U^2\left(C_- + S_-\right) + C_+$. Much as in section 4.3.4 we write

$$\langle T_{kk}\left(U\right)\rangle = \sum_{n\in\mathbb{Z}} \hat{f}\left(C_{+n}, C_{-n}, S_{-n}, U; \ell/R_{S^1}\right) \tag{4.45}$$

where

$$\begin{aligned} \hat{f}\left(C_{+n}, C_{-n}, S_{-n}, U; \ell/R_{S^1}\right) =& f\left(C_{+n}, C_{-n}, S_{-n}, U; \Delta\left(0\right)\right) \\ &+ 2\sum_{p=1}^{\infty}(-1)^p f\left(C_{+n}, C_{-n}, S_{-n}, U; \Delta\left(p\right)\right) \end{aligned} \tag{4.46}$$

with $\phi'_n = 2\pi n - \phi$.

At general values $\phi \neq 0, \pi$ we have $C \neq 1$ and each term above is separately finite and smooth. The same is true at $\phi = 0, \pi$ for $n \neq 0$. But for $n = 0$ and $\phi = 0, \pi$, the contribution for each p diverges at $U = 0$. In fact, since $C_\pm = \cosh[r_\pm(\phi - \phi')] = 1$, $S_- = \sinh[r_-(\phi - \phi')] = 0$, at $n = 0$, $\phi = 0, \pi$ we find $\hat{f}\left(C_{+n}, C_{-n}, S_{-n}, U; \ell/R_{S^1}\right) = \hat{f}\left(1, U; \ell/R_{S^1}\right)$; i.e., in this case the computations reduce precisely to those for the $n = 0$

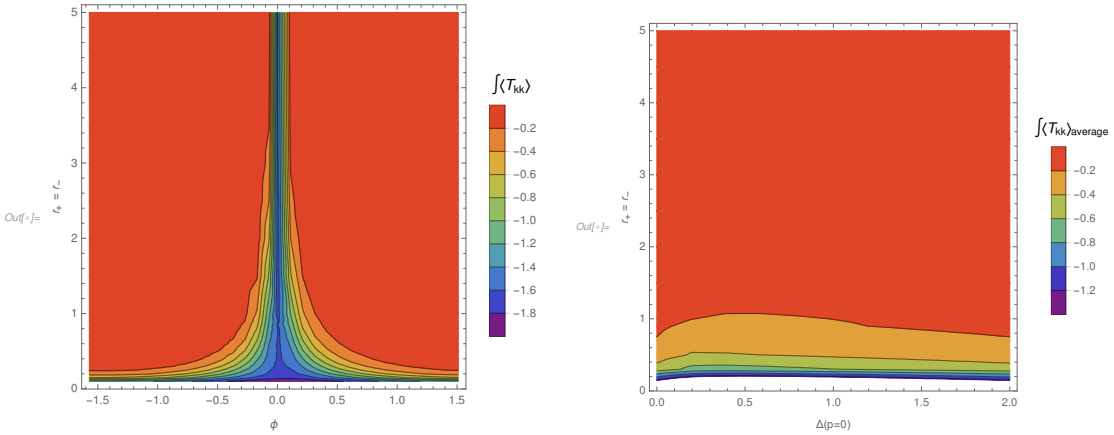

Figure 4.16: **Left:** The dependence of $\int\langle T_{kk+}\rangle \mathrm{d}U$ on ϕ and r_+ at extremality ($r_- = r_+$, in units of ℓ). **Right:** Dependence of the zero-mode $\int\langle T_{kk+}\rangle \mathrm{d}U r\mathrm{d}\phi$ on $\Delta(p=0)$ (with all $\pm$ signs in (4.27) chosen to be $+$ for $p \neq 0$) and $r_- = r_+$ in units of ℓ. For both figures, we have chosen $\ell/R_{S^1} = 10$ and $m = 0$.

term studied for the non-rotating KKEOW brane in section 4.3.4.

Numerical results computed using a function $\hat{f}_{\text{hybrid}}$ analogous to that in section 4.3.4 are displayed in figures 4.16 and 4.17. As for the EOW brane, the analysis simplifies in the limit of large r_+/ℓ where contributions from $n \neq 0$ can be ignored. In that limit, the stress tensor profile becomes sharply peaked near $\phi = 0, \pi$ on a scale set by the Kaluza-Klein scale and the mass of the scalar field (though in a manner that is not symmetric under $\phi \to -\phi$); see figure 4.16 (left). As shown in figure 4.16 (right), the integral of the stress tensor becomes large (and negative) at small values of R_{S^1}, corresponding to the fact that Kaluza-Klein reduction on the S^1 gives orbifold singularities at which the stress tensor would diverge. But the back-reaction (4.41) involves an extra factor of r_+ and, as shown in figure 4.17, our numerics for the quantity ΔVT suggest that this quantity may become independent of $r_+ = r_-$ in the extremal limit.

In general, one finds $\int \mathrm{d}U\langle T_{kk}\rangle$ to be negative for all ϕ. Positivity of the Green's function (4.39) then shows that ΔV is negative at each ϕ and the wormhole is traversable when entered from any direction. However, much as in section 4.3.4, one can engineer

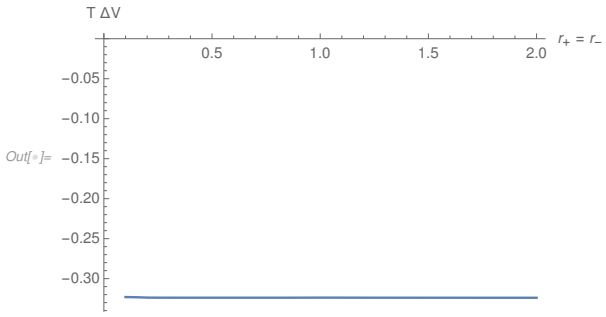

Figure 4.17: $\Delta V_{\text{average}} T$ at extremality as a function of $r_- = r_+$, with $\ell = G = 1$. For this figure, we have chosen $\Delta(p = 0) = 2$ and $\ell/R_{S^1} = 10$. Though we have not peformed a thorough analysis of numerical errors, our results appear consistent with this quantity perhaps being independent of $r_+ = r_-$.

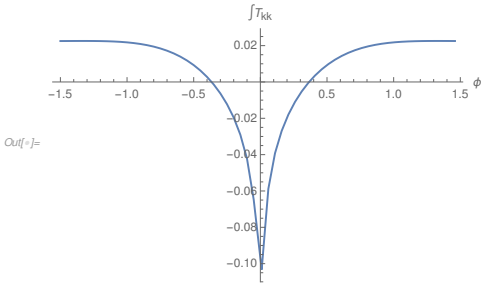

Figure 4.18: A ϕ profile of $\int \mathrm{d}U \langle T_{kk} \rangle$, which is negative for small $|\phi|$ and positive for larger $|\phi|$. $\Delta(p = 0) = 1$, the $(-)$ sign is chosen for $p = 1$, and the $(+)$ sign is chosen for all higher p. $m^2 = -0.2$, $\ell/R_{S^1} = 0.1$, $r_+ = 1$ and $r_- = 0$.

exceptions to this general rule by making use of the dependence of the integrals on Δ. In this way one can find examples where the sign of ΔV does in fact depend on ϕ and the wormhole is traversable only when entered from certain directions, see figure 4.18. The interesting feature of such examples is that they are then traversable with either periodic or anti-periodic boundary conditions, though the directions from which one must enter the wormhole to traverse it are complimentary in the two cases.

4.5 Discussion

The above work studied back-reaction from quantum scalar fields in Hartle-Hawking states on simple explicit examples of $\mathbb{Z}_2$ wormholes asymptotic to AdS_3 and $\mathrm{AdS}_3 \times S^1$.

These examples generally become traversable when the scalar satisfies periodic boundary conditions around the $\mathbb{Z}_2$ cycle, though as described in section 4.3.4 one may engineer examples where this fails and anti-periodic boundary conditions are required for traversability. The examples of section 4.4 break rotational symmetry and, while they generally become traversable everywhere with periodic boundary conditions around the $\mathbb{Z}_2$-cycle, with care they can be similarly engineered to become traversable only for observers entering the wormhole at certain values of the angular coordinate ϕ.

The most interesting result came from the rotating examples of section 4.4, where we found the back-reaction to diverge when the background spacetime became extremal. Though our analysis is perturbative, even when sourced by only a single scalar quantum field this suggests that a fully non-perturbative treatment would find a self-supporting eternal wormhole. Indeed, the growth of our effect at small temperatures T is directly analogous to the $\Delta > 1/2$ cases studied in [89] where the perturbation grows in the IR limit. Though the potential for diverging back-reaction at extremality was also simultaneously and independently found in [85], such a divergence did not in fact arise in their context.

The diverging back-reaction near extremality follows directly from the linearized Einstein equations. In our examples the extremal spacetimes are smooth and contain a non-contractible $\mathbb{Z}_2$ cycle of finite length. As a result, it is natural in our examples (but in contrast to the setting studied in [85]) that $\int \mathrm{d}U \langle T_{kk} \rangle$ remains non-zero and negative at extremality. But from (4.36) any finite such perturbation causes a divergence in the zero-mode of the metric perturbation h_{kk}. Thus the wormhole becomes traversable along each generator of the background horizon and – at least at first order in perturbation theory – the wormhole appears to remain open for arbitrarily long times as the extreme limit ($T = 0$) is approached. It would be useful to better understand the apparent lack of dependence on $r_+ = r_-$ in the resulting first-order $T\Delta V$ shown in figure 4.17.

If this conjecture is correct, the breaking of rotational symmetry appears to play a key role in the construction. In particular, we conjecture the existence of time-independent such wormholes with arbitrary size for the wormhole throat, and thus presumeably with arbitrary total mass. Now, the attentive reader will notice that we have worked in what are effectively co-rotating coordinates. So by 'time-independent,' we mean invariant under translations along a co-rotating Killing. And the lack of rotational symmetry means that our conjectured spacetimes should not be invariant under standard translations of the boundary time t. This is important for consistency with the conjecture about arbitrary mass as (in the absence of horizons) Hamilton's equations imply that the generator of time-translation symmetry should be constant along any one-parameter family of time-independent solutions. We thus expect that M varies but $M - J$ is constant along our family of wormholes, and that (as one would also expect from supersymmetry considerations) even with quantum corrections the condition for extremality remains $M - J = 0$.

While we have not performed a complete analysis of more general cases, and while the Aretakis instability is strongest for large angular momentum [118] and our instability appears to occur only for the zero mode while, it is nevertheless natural to expect our effect to be related to other known instabilities of extreme black holes [111, 112, 113, 114, 115, 116, 117] and thus to be generic in the extremal limit. This may make the construction of self-supporting wormholes more straightforward than might otherwise be expected.

Indeed, as described in section 4.2 our basic framework applies much to much more general cases than those studied explicitly here. Given any globally hyperbolic $\mathbb{Z}_2$ quotient of a spacetime with bifurcate Killing horizons and a well-defined Hartle-Hawking states under an isometry that exchanges the left-moving and right-moving horizons, at least one choice of boundary conditions (periodic or anti-periodic) for free scalar fields on

that spacetime must give a (transient) traversable wormhole. As described in appendix B, there may also be generalizations in which the covering space has no Killing symmetry and the horizon is merely stationary (i.e., both divergence-free and shear-free).

We have studied only scalar fields in detail, but the general arguments of section 6.4 apply equally well to higher spin fields. It would be especially interesting to study back-reaction from linearized gravitons, which are always present for spacetime dimension $d \geq 4$. Indeed, they are in principle relevant even to our AdS_3 constructions that involve Kaluza-Klein directions (so that the full spacetime has $d \geq 4$). Indeed, since in those examples the amount of negative energy is governed by the Kaluza-Klein scale, one expects contributions from gravitons to be similar to those of scalars despite the absence of 3-dimensional gravitons. And since changing the sign of the metric perturbation is not a symmetry of the full Einstein-Hilbert theory, only periodic boundary conditions will be physically relevant. One would generally expect gravitons to contribute with the same sign as other bosons, and in particular with the scalars studied above. We therefore expect inclusion of gravitons to make our wormholes even more traversable. Should this expectation turn out to be false, one could nevertheless ensure that the wormhole becomes traversable by adding an order one number of additional scalar fields.

While it is natural to think of the above quotients as geon-like (i.e., as generalizations of the $\mathbb{RP}^3$ geon described in [91, 83]), they can also describe more familiar wormholes of the form shown in figure 5.1 with wormhole homotopy group $\mathbb{Z}$. To see this, recall that static axisymmetric vacuum solutions to $d = 4$ Einstein-Hilbert gravity take a simple form [119] found by Weyl in 1917, and that particular examples [120] found by Bach and Weyl in 1922 can be understood [121] as describing a pair of Schwarzschild black holes separated along the z-axis. The black holes are prevented from coalescing by a strut (i.e., by a negative tension cosmic string) along the axis between them and/or by positive-tension cosmic strings stretching from each black hole to infinity along the z-axis

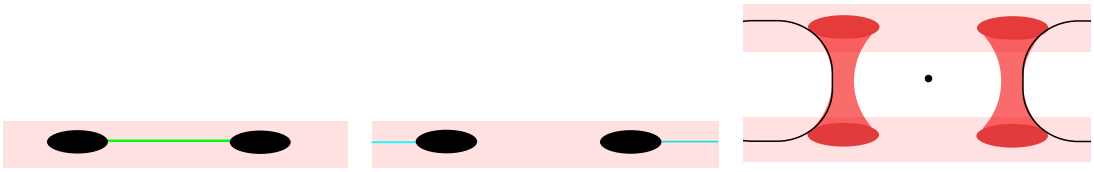

Figure 4.19: A moment of time in a spacetimes containing two black holes (black disks) held apart by a negative-tension strut (left) or by cosmic strings stretching to infinity (center and right) along the z-axis. The right-most figure shows both asymptotic regions and the wormholes that connect them. The $\mathbb{Z}_2$ quotient described in the text acts as a π rotation about the non-physical point indicated by the dot at the center of the right figure.

as shown in figure 5.3. Furthermore, as described in [121], a natural analytic extension of this solution beyond the horizons gives a geometry with two asymptotically flat regions and a bifurcate Killing horizon. The spacetime is thus similar to the standard Kruskal extension of the Schwarzschild black hole, except that this connection involves a pair of wormholes (threaded by cosmic strings); see figure 5.3 (right). This defines the $\mathbb{Z}_2$ cover $\tilde{M}$ of the desired spacetime M.

To construct M itself, we simply note that $\tilde{M}$ has a $\mathbb{Z}_2$ symmetry J that acts by simultaneously reflecting across the bifurcation surface and the surface $z = 0$; i.e., it simultaneously exchanges the two sheets shown in figure 5.3 (right) and also exchanges the two wormholes; i.e., it acts as a π rotation about the non-physical point marked at the center of figure 5.3 (right). This J has no fixed points, so $\tilde{M} = M/J$ is smooth up to cosmic strings and takes the familiar form described by figure 5.1.

In fact, at least in the positive-tension case, much as in section 4.4 it is straightforward to go one step farther and describe $\tilde{M}$ as the Kaluza-Klein reduction of a completely smooth spacetime. Here one simply chooses parameters so that the cosmic strings are associated with deficit angles $2\pi(1 - 1/n)$. We then consider a 5-dimensional spacetime $\tilde{M}_{KK}$ that is just $\tilde{M} \times S^1$ away from the strings. At the location of the 4-dimensional cosmic strings, we instead take M_{KK} to be locally what one might call the Kaluza-Klein

cosmic string defined by $M^{3,1} \times S^1/\mathbb{Z}_n$ with the $\mathbb{Z}_n$ isometry acting by simultaneous rotations by $2\pi/n$ along the S^1 and about the z-axis[11]. This M_{KK} is then a smooth $\mathbb{Z}_2$ quotient of a 5d spacetime $\tilde{M}_{KK}$ with bifurcate Killing horizon. Since the spacetime is static and smooth, it also supports a Hartle-Hawking state defined by the Euclidean path integral. Thus the analysis of section 4.2 applies and – barring a miraculous general cancellation – at least for generic values of parameters the wormhole must become traversable under first-order back-reaction from either periodic or anti-periodic scalar fields[12].

Although the form of the metric becomes more complicated, one may also add electric charge to the above solution as described in [124]. This would then provide an example of the standard wormhole form shown in figure 5.1 with a smooth extremal limit satisfying all requirements from section 4.2 and in particular admitting a well-defined Hartle-Hawking state. In contrast, even at extremality, the rotating version will spin down due to spontaneous emission of angular momentum via the super-radiant modes [125], though this effect will in practice be slow for large black hole.

It would be interesting to analyze such examples in more detail, especially in the extreme limit. Here the non-contractible cycles become long in the extreme limit, so that $\int \mathrm{d}U \langle T_{kk} \rangle$ may become vanishingly small. But the instability of extreme black holes raises the hope that even a vanishingly small perturbation could render the wormhole self-supporting and eternal at zero temperature. Indeed, a naive analysis ignoring the redshift and issues associated with normalizing the affine parameter along the horizon

[11]This 5-dimensional spacetime is usually Kaluza-Klein reduced along a different Killing field and then interpreted as a 4-dimensional spacetime sourced by a magnetic field [122, 123]. Since the energy of the solution is fixed by Noether's theorem independent of the reduction, the results of [122, 123] show that the reduction used here gives a 4d solution with positive tension (rescaled from [122, 123] by the relative length of their Kaluza-Klein circle relative to ours) but which in our case is 4d vacuum except at the string singularity on the z-axis.

[12]Indeed, since this example breaks rotational symmetry it may be that both cases become traversable, with traversability being achieved along different generators for each of the two boundary conditions.

would note that the length of a Reissner-Nordström throat grows like $T^{-1/2}$ so that an integrated Casmir-like energy would decay as $T^{1/2}$. An instability that grows like T^{-1} as in (4.36) would then suggest an eternal self-supporting wormhole. We will perform a more complete analysis using an effective 2-dimensional description for a model with conformal invariance in the near future. If a large back-reaction does result, it would provide a simple perspective explaining the existence of the self-supporting wormhole recently constructed in [88] – here with the wormhole mouths kept from coalescing by cosmic strings instead of the orbital angular momentum used in [88].

Chapter 5

Traversable, Asymptotically Flat Wormholes with Short Transit Times

5.1 Introduction

The study of wormholes in general relativity dates back many years (see e.g. [80, 81, 82]), with varying discussions of whether an observer might be able to pass through and perhaps find a shortcut to a distant region. In particular, it is now well understood that the existence of traversable wormholes is limited in two important ways. First, topological censorship theorems [83, 84] forbid wormholes from being traversable in globally hyperbolic solutions to Einstein-Hilbert gravity coupled to matter satisfying the null energy condition (NEC)[1], $T_{ab}k^a k^b \geq 0$. Second, even when the NEC is violated by quantum effects, general arguments expected to hold in quantum gravity forbid wormholes in

[1]Though traversable wormholes can be constructed if one drops the requirement of global hyperbolicty, e.g. by introducing NUT charge [126, 127].

globally hyperbolic spacetimes from providing the fastest causal curves between distant points [128, 15]. This condition also prohibits the further possible pathologies discussed in [82, 129, 130]. Recently, several examples of traversable wormholes supported by well-controlled quantum effects and respecting the above restrictions have been constructed [15, 131, 89, 88, 132, 85]. Instantons producing such wormholes by quantum tunneling were also discussed in [133]. While the second limitation significantly restricts the utility of any shortcut they might provide, such solutions remain of theoretical interest.

These various traversable wormholes solutions naturally fall into two classes. Wormholes in the first class (see e.g. [15, 131, 89, 85]) connect two separate asymptotic anti-de Sitter (AdS) regions and are supported by negative energy in the bulk that is generated by explicit couplings between the two dual boundary CFTs. While such couplings are non-local and acausal from the perspective of the bulk, they may be thought of as simple models for couplings that would be induced between wormhole mouths lying in the same asymptotic region and interacting causally through ambient space. Wormholes in this second, more natural class were constructed in [88, 132]. In particular, Maldacena, Milekhin, and Popov (MPP) [88] used a nearly-AdS_2 approximation to construct a static wormhole in asymptotically flat spacetime. This approach allowed [88] to address many non-perturbative issues.

In contrast, [132] used a perturbative framework to give a general method of constructing traversable wormholes with both mouths in the same asymptotic region, and in particular argued that a broad class of (almost traversable) classical wormhole backgrounds would become traversable after incorporating the back-reaction from standard local quantum fields in Hartle-Hawking states. By an almost traversable background, we mean one in which there is a null geodesic γ traversing the wormhole that lies in both the boundary of the past of future null infinity and the boundary of the future of past null infinity. As in e.g. [15], under these circumstances a negative value for the integrated null

stress tensor along γ will often lead back-reaction moving γ into both the past of future null infinity and the future of past null infinity; i.e., the wormhole becomes traversable. Note, however, that in contrast to the wormholes of [88], this perturbative approach generally yields wormholes with strong time-dependence, so that the back-reaction slows but does not stop the collapse of the wormhole interior. The result is that the wormhole is traversable only at sufficiently early times. This is the price to be paid for studying a more general class of constructions. Consistent with the results of [88], and as discussed in [132] and also reviewed below, perturbative calculations indicate that the wormholes described here and in [132] can in fact become time-independent in the limit where the background almost-traversable wormhole becomes extremal.

Here, we return to the perturbative framework of [132] in order to explore the above back-reaction in more detail for a simple class of classical wormholes (suggested in [132] and closely related to the setting of [88]) which have both mouths in the same asymptotically flat region of spacetime. Our classical backgrounds contain a pair of charged, Reissner-Nordström-like black holes held apart by the tension of a cosmic string that threads the wormhole and stretches to infinity. We also include a second cosmic string that wraps the non-contractable cycle through the wormhole; see figure 5.1. The classical wormholes are not traversable, but are almost so. Quantum fluctuations from this compact cosmic string generate the negative Casimir energy whose back-reaction renders the wormhole traversable. As in [132], the back-reacted wormhole will generally exhibit strong time-dependence and can be traversed by causal curves from past null infinity only if such curves depart at sufficiently early times.

Below, we review the general framework of [132] and apply it to the asymptotically flat wormholes of interest here. As in [132], we define traversable wormholes to be the set of curves that can witness non-trivial topology while escaping out to infinity – e.g. causal curves that cannot be deformed, while remaining causal, to lie in the boundary of

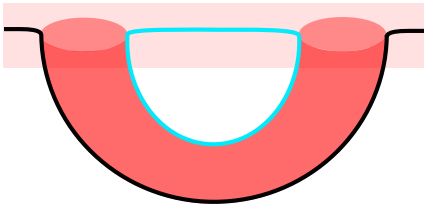

Figure 5.1: A moment of time in a spacetime with a wormhole (shaded region) formed by adding a handle to a space with a single asymptotic region. The wormhole is threaded by two cosmic strings, one stretching to infinity (black line) and the other compact (blue line). The string that stretches to infinity provides a tension that counteracts the gravitational (and, in our case, also electric) attraction of the two mouths, as well as the tension of the compact string, and thus prevents the black holes from coalescing. Quantum fluctuations from the compact cosmic string will render the wormhole traversable.

the spacetime. To construct our relevant classical geometry, we start with a spacetime $\tilde{M}$ with a bifurcate Killing horizon and one asymptotic region on each side of the horizon; $\tilde{M}$ can be thought of as an *almost* traversable wormhole with two asymptotic regions. If this spacetime admits a freely-acting $\mathbb{Z}_2$ isometry J exchanging the right and left asymptotic regions and preserving the time orientation, then the quotient $M = \tilde{M}/J$ describes an *almost* traversable wormhole with a single asymptotic region. While in principle, a small perturbation of either geometry could render the wormholes traversable, for $\tilde{M}$ the horizon generating Killing field forces the null stress-energy of any perturbation respecting this symmetry to be zero. In M, however, this Killing symmetry is broken by the quotient by J, which necessarily maps the horizon-generating Killing field ξ to $-\xi$, since it identifies the right and left regions while preserving the time-orientation of the spacetime. This allows small perturbations to render the wormhole in the quotient space traversable.

The simplest examples of such quotient wormholes are like the $\mathbb{RP}^3$ geon [92, 91, 83] shown in figure 5.2. Though the quotient M then contains only a single wormhole mouth, it nevertheless admits causal curves γ that are not deformable to the spacetime boundary. Similar spacetimes with asymptotically AdS_3 (or $AdS_3 \times X$) boundary conditions and

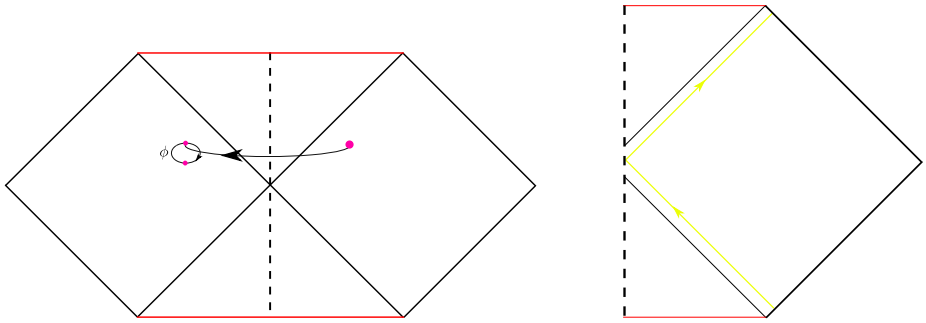

Figure 5.2: (Left) The $\mathbb{RP}^3$ geon is a $\mathbb{Z}_2$ quotient of the maximally-extended Schwarzschild black hole. The quotient acts on the above conformal diagram by reflection across the dashed line, and simultaneously acts as the antipodal map on the suppressed S^1. This action maps the Killing field ξ^a to $-\xi^a$, and so the geon quotient lacks a globally defined time translation Killing field. In particular, the dashed line is orthogonal to preferred spacelike surfaces of vanishing extrinsic curvature that one may call $t = 0$. (Right) A small perturbation of maximally-extended Schwarzschild renders the $\mathbb{Z}_2$ quotient wormhole traversable. This results in a causal curve running between past and future null infinity that is not deformable to the boundary.

their back-reaction from quantum scalar fields were explored in detail in [132], and similar back-reaction from bulk fermions will be explored in [134]. Here, we will instead study the more sophisticated case where the covering space $\tilde{M}$ contains a pair of maximally-extended black holes, as in figure 5.3, so that the quotient M takes the form depicted in figure 5.1. Since the particular solution M studied below involves two cosmic strings, one stretching to infinity and the other compact, we require three cosmic strings in the covering space $\tilde{M}$. The compact cosmic string in M lifts to a single longer compact cosmic string in $\tilde{M}$, while the string stretching to infinity in M lifts to a pair of disconnected strings in $\tilde{M}$.

Once we have formed our classical backgrounds, it remains to understand the back-reaction from quantum fields sitting on the spacetime. As explained in [132], if quantum fields on $\tilde{M}$ have a well-defined Hartle-Hawking state, there will be a corresponding Hartle-Hawking-like state on M. This state is defined by the path integral over the appropriate quotient of the Euclidean geometry of $\tilde{M}$. For linear fields this state can

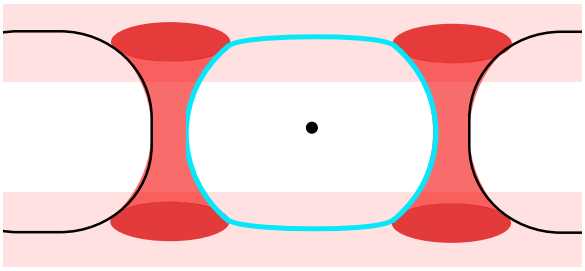

Figure 5.3: A moment of time symmetry in our covering space $\tilde{M}$. Each of the two asymptotic regions contains a pair of black holes held apart by cosmic strings that stretch to infinity. A pair of strings thread the two wormhole throats and return to infinity in the second asymptotic region. The $\mathbb{Z}_2$ isometry used to construct $M = \tilde{M}/\mathbb{Z}_2$ acts as a π rotation about the non-physical point indicated by the dot at the center of the right figure. As a result, a moment of time-symmetry for M takes the form shown in figure 5.1 and contains two wormhole mouths in a single asymptotic region.

also be constructed by applying the method of images to the Hartle-Hawking state on $\tilde{M}$. In particular, we can use the method of images to calculate expectation values of the stress tensor of quantum fields in their Hartle-Hawking state $\langle T_{kk} \rangle_M = \langle T_{ab} k^a k^b \rangle_M$ along affinely parameterized generators k^a of the background spacetime's horizon. Because the stress tensor is a quadratic composite operator, the method of images implies that $\langle T_{kk} \rangle_M$ in our $\mathbb{Z}_2$ quotient space can be written as 4 terms in our covering space. Two of these are just $\langle T_{kk} \rangle_{\tilde{M}}$ in the Hartle-Hawking state on $\tilde{M}$ which are forced to vanish by the Killing symmetry. The remaining terms involve two-point functions evaluated at some point x on one horizon in the covering space $\tilde{M}$ and the image point Jx under the isometry J, located on the other horizon. Since J acts freely and the quotient $\tilde{M}/J$ contains no closed causal curves, the points x and Jx are spacelike separated and this two-point function is finite. The spacelike separation of x and Jx also guarantees that the two cross-terms coincide.

As mentioned above, though the Killing symmetry of the covering space forces $\langle T_{kk} \rangle_{\tilde{M}} = 0$, breaking this symmetry by quotienting now allows non-zero $\langle T_{kk} \rangle_M$. More powerfully,

the actual expression for $\langle T_{kk} \rangle_M$ depends on whether the quantum field is periodic or anti-periodic around the non-contractible cycle created by the quotient, and the two choices differ only by an overall sign. Because the effect of back-reaction on traversability is governed by the integral $\int \langle T_{kk} \rangle_M d\lambda$ (with respect to an affine parameter λ over the generators of the horizon), barring surprising cancellations the above choice of sign allows us to tune the boundary conditions of our fields to render the wormhole traversable. For bosons, this sign tends to correspond to periodic boundary conditions in accord with the famous negative Casimir energy of periodic bosons on $S^1 \times \mathbb{R}^{d-1}$.

Returning to the asymptotically flat wormholes of interest here, we consider the stress-energy provided by the cosmic strings. Since the relevant null vectors k are tangent to the cosmic string worldsheets and the classical cosmic string stress tensor is proportional to the induced metric, classically the cosmic strings do not contribute to $\langle T_{kk} \rangle_M$. Quantum fluctuations in the location of the string will contribute, however. We will model such fluctuations as 1+1 dimensional massless free scalar fields. Since correlators of 1+1 quantum fields diverge only logarithmically at short distance, it is easy to find a regime where these fluctuations remain small when compared with any classical scale (at least when the fluctuations are averaged over any classical time or distance scale), and our free field approximation is valid in such regimes. For the string stretching to infinity in M, the points x, Jx in the covering space $\tilde{M}$ will lie on two distinct non-compact strings. Since fluctuations on two different strings are uncorrelated, the cross-terms in $\int \langle T_{kk} \rangle_M d\lambda$ will vanish. The contributions from quantum fluctuations of the compact string are non-zero, however, and studied below using a conformal transformation associated with the method-of-images construction described above.

At finite temperatures, we find that our wormholes become traversable for test signals and that, when the mouths are separated by a large distance d, well-timed signals require only the relatively short time $t_{\text{min transit}} = d + logs$ (in units with the speed of light c

set to 1) to traverse the wormhole, where *logs* denote terms logarithmic in d and in the black hole parameters. In particular, the transit time is shorter than for MPP wormholes by more than a factor of 2 and, as discussed in section 6.4, for $d \to \infty$ the higher-dimensional analogue of this result would approach the minimum transit time consistent with the above-mentioned prohibition against wormholes providing the fastest causal curves between distant points [128, 15]. However, in such cases traversability is exponentially fragile, and can be destroyed by exponentially small perturbations.

One should note that our background spacetime is unstable, as small perturbations will cause the black holes to either fall towards each other or fly apart. However, the time scale for the black holes to merge is $\sim d^{3/2}$, so the solutions are long lived compared to the transit time. Furthermore, one could engineer more complicated stable configurations using additional cosmic strings and anchoring to some stable structure at a finite distance (e.g., a large stable spherical shell surrounding both wormhole mouths) instead of running the strings off to infinity. It will be clear below that the results for such more complicated models will be essentially the same.

Additionally, as in [89, 88, 132], we take particular interest in studying the extremal limit of our classical backgrounds. In [85, 132] it was shown that this limit gives large back-reaction for rotating BTZ, and we see here that this limit also gives large back-reaction for $d = 4$ Reissner-Nordström black holes. On general grounds[2] this feature is related to the fact that far in the throat of a nearly extremal spherically-symmetric black hole, the size of the spheres is approximately constant, and thus one can approximately Kaluza-Klein reduce the dynamics to two-dimensional gravity. However, the Einstein-Hilbert action $\int \sqrt{g}R$ becomes a topological invariant in two dimensions, and does not contribute to the equations of motion, modeling the higher-dimensional case in the infinite coupling limit $G_N \to \infty$. Thus, in the extremal limit, the effective coupling diverges.

[2]We thank Zhenbin Yang for explaining this point.

Though our perturbation theory breaks down when the back reaction becomes large, we take the divergence as an indication that a full, non-perturbative calculation would reveal traversable wormholes that remain open for all time.

In Section 5.2, we compute $\int \langle T_{kk} \rangle_M d\lambda$ from the Hartle-Hawking state quantum fluctuations of the cosmic strings. We then compute the back-reaction on our geometry and the resulting degree of traversability in section 6.3, and conclude with some brief remarks in section 6.4. As a contrasting side-note and because it provides an exactly solvable model for scalar fields of arbitrary mass, we also compute effects for what one may call a cosmological wormhole $dS_d/\mathbb{Z}_2$ in appendix C where the back-reaction has the opposite sign so that negative energy from quantum fields in fact makes the wormhole harder to traverse.

5.2 Stress-energy on the horizon

The introduction outlined a simple background spacetime M with a wormhole whose mouths are held apart by cosmic strings. This wormhole is not traversable, but is almost so and will be rendered traversable by the back-reaction of quantum fields. As noted in [132], the 2-fold covering space $\tilde{M}$ of this background is a charged version of the analytic extension behind the horizon [121] of solutions found by Bach and Weyl in 1922 [120]. For our case where the black holes have identical mass and opposite charge, an explicit form for this solution was found in [135] based on the implicit solutions in [136]; see also [137, 138, 139, 140] for the simpler extreme case. Additionally, we wrap a compact cosmic string through both wormholes mouths, and our goal here is to understand any additional contributions to $\langle T_{kk} \rangle_M$ associated with its fluctuations. As discussed above, the contributions from any strings stretching to infinity will all vanish and we ignore contributions from bulk fields. We will not need the full details of the covering space

(which can be found in the above references), as we will instead focus on ranges of parameters where the analysis simplifies.

We will take the tension μ of the strings to be large compared with the length scale r_0 set by the black holes, $\mu r_0^2 \gg 1$, but we take Newton's constant G_N even smaller ($G_N \mu \ll 1$) so that the conical deficit associated with the strings can be neglected. The first condition allows us to linearize the fluctuations, while the second means that we can ignore local effects of the strings on the geometry[3]. Note that the tension of strings stretching to infinity must be at least somewhat larger than that of the compact string in order to keep the black holes from coalescing. To suppress quantum fluctuations in T_{kk}, and also to justify neglecting the effects of bulk Maxwell fields and linearized gravitons, we can replace each string in figure 5.1 with N strings so long as $\mu r_0^2 \gg 1$ for each string and $N G_N \mu \ll 1$. As in [88], this will be necessary to render our semi-classical treatment in terms of expectation values valid.

To complete our specification of parameters, we further fix any measure of the distance d between the mouths of our wormhole and take the limit where d is much larger than the the radius $r_+ = \sqrt{A/4\pi}$ of the black hole horizon. In this limit, the covering spacetime $\tilde{M}$ can be divided into three overlapping regions: the region near the first black hole where the influence of the second can be treated as a small perturbation, the corresponding region for the second black hole, and the region in between where both black holes cause only small perturbations from flat space. In each region, it is possible to systematically improve the approximation order by order in perturbation theory, but we work in the leading approximation below.

As noted in the introduction, it is possible to compute $\langle T_{kk} \rangle_M$ using the method of images starting in the covering space. However, since we are modeling fluctuations of

[3]Due to the logarithmic divergences of 1+1 field theories noted above, the first condition should really be $\mu r_0^2 \gg \ln n$ where n is a parameter set both by the background spacetime and the manner in which fluctuations are averaged as described in detail below.

the cosmic string as massless 1+1 free fields, they define a 1+1 dimensional conformal field theory. It is thus natural to instead compute $\langle T_{kk} \rangle_M$ by finding a conformal map from the 1+1 spacetime M_{cs} induced on the worldsheet of the compact cosmic string to a piece of the cylinder of circumference 2π, and which simultaneously maps the cosmic string Hartle-Hawking state to the cylinder vacuum. Inverting the transformation will then determine our $\langle T_{kk} \rangle_M$ in terms of the known $\langle T_{ab} \rangle$ on the cylinder and the stress tensor Weyl anomaly associated with this conformal map. Such a map must exist since both the cosmic string Hartle-Hawking state and the cylinder vacuum can be constructed as path integrals over the respective spacetimes. Though we do not explicitly use the method of images to calculate $\langle T_{kk} \rangle_M$, we will still find the quotient construction to be of great use in finding this conformal map. Below, we use $M_{cs}(\tilde{M}_{cs})$ to denote the 1+1 spacetimes induced on the compact cosmic string by $M(\tilde{M})$, with $M_{cs} = \tilde{M}_{cs}/\mathbb{Z}_2$.

We first construct a conformal transformation relating $\tilde{M}_{cs}$ to a piece of a cylinder, and which maps the Hartle-Hawking state on $\tilde{M}_{cs}$ to the cylinder vacuum. The Killing symmetry of $\tilde{M}_{cs}$ means that its Hartle-Hawking state may be characterized as the unique Hadamard state invariant under the symmetry. As a result, the pull-back of the cylinder vacuum under our conformal map will be the Hartle-Hawking state so long as the Killing symmetry of $\tilde{M}_{cs}$ maps to a symmetry of the cylinder vacuum. Choosing locally-Minkowski coordinates ϕ, τ on the cylinder (or equivalently null coordinates $u_c = \tau - \phi$, and $v_c = \tau + \phi$), we take this symmetry to be the 1-parameter subgroup of the vacuum-preserving SO(2,1) symmetry that acts like a boost near the origin $\phi = \tau = 0$ (or $u_c = v_c = 0$) and at appropriate other points that form a periodic array on the cylinder. For convenience after we take the $\mathbb{Z}_2$ quotient, we choose the unusual convention that here ϕ be periodic with period 4π on the cylinder conformal to $\tilde{M}$.

In a static patch of $\tilde{M}_{cs}$ (see figure 5.4) the metric can be written in the form

$$ds^2_{\text{static}} = -f dt^2 + f^{-1} dx^2, \tag{5.1}$$

with $f = f(x)$ and where x ranges over $[0, 2x_0]$. For later use, we also note that in the limit where the separation d between the black holes satisfies $d \gg r_+$, there is a sphere of approximate symmetry passing through x_0 around either black hole, with radius

$$r(x_0) = x_0 + O(r_+) = d/2 + O(r_+), \tag{5.2}$$

where since the symmetry is only approximate the $O(r_+)$ terms depend on precisely how this sphere is defined[4].

To map to the cylinder, we want t, ϕ such that

$$ds^2_{\text{static}} = \Omega^2(-d\tau^2 + d\phi^2) = -\Omega^2 du_c dv_c \tag{5.3}$$

for an appropriate conformal factor Ω. Two such patches will be required to wrap around a piece of a cylinder conformal to $\tilde{M}_{cs}$ (see figure 5.4). Therefore, in our static patch, ϕ ranges over $[0, 2\pi]$. This patch is thus precisely the part of the cylinder with $u_c \in [-2\pi, 0]$, $v_c \in [0, 2\pi]$.

Before constructing the conformal map, we introduce Kruskal coordinates U, V on $\tilde{M}_{cs}$. We build these in the usual way by first introducing the tortoise coordinate

$$x_* = x_{*0} + \int_{x_0}^{x} \frac{1}{f} dx, \tag{5.4}$$

where we will fix the arbitrary parameter x_{*0} below. We then define $u = t - x_*$, $v = t + x_*$,

[4]The second $O(r_+)$ term similarly depends on the precise definition of the separation d.

and finally

$$U = -\kappa_+^{-1} e^{-\kappa_+ u},\ V = \kappa_+^{-1} e^{\kappa_+ v}, \tag{5.5}$$

where κ_+ is the surface gravity of the black hole's outer horizon. In these coordinates, metric becomes

$$ds^2_{\text{static}} = f\left(-dt^2 + dx_*^2\right) = \frac{f}{\kappa_+^2 UV} dU dV. \tag{5.6}$$

Here the region $0 < x < 2x_0$ is mapped to $-\infty < x_* < +\infty$ and thus to $U \in (-\infty, 0)$, $V \in (0, \infty)$. However, the form on the right-hand-side can be analytically continued to all points where both U and V are defined. Comparing (5.3) with (5.6) yields

$$\Omega^2 = -\frac{f}{\kappa_+^2 UV} \frac{dU}{du_c} \frac{dV}{dv_c}. \tag{5.7}$$

Up to an arbitrary scale L, the symmetries determine the map to the cylinder to be

$$U = L \tan(u_c/4), \quad V = L \tan(v_c/4). \tag{5.8}$$

In particular, a map of this form also gives the standard conformal transformation relating the cylinder to 1+1 Minkowski space. Here, we can fix L by using the fact that we want the $\mathbb{Z}_2$ symmetry exchanging the black holes (and corresponding to a π rotation about the non-physical point marked in figure 5.3) to correspond to half a rotation of the cylinder, which here is $\phi \to \phi + 2\pi$; see again figure 5.4. Note that if the $\mathbb{Z}_2$ symmetry on $\tilde{M}_{cs}$ maps the null ray U_1 to the null ray U_2, the Killing symmetry requires that the $\mathbb{Z}_2$ symmetry map λU_1 to U_2/λ. Using (5.8) in addition, we see that the action of this $\mathbb{Z}_2$ is

$$U \to -L^2/U, \quad V \to -L^2/V. \tag{5.9}$$

We can fix L by using time-reversal symmetry to note that the null lines through the point

p (with coordinates $t = 0, x = x_0$) and its image p' under this $\mathbb{Z}_2$ have $U = \pm\kappa_+^{-1} e^{\kappa_+ x_{*0}}$ and have $u_c = -\pi, \pi$, so that $L = \kappa_+^{-1} e^{\kappa_+ x_{*0}}$.

Having constructed the conformal map from $\tilde{M}_{cs}$ to the cylinder with period 4π, it is now straightforward to take the $\mathbb{Z}_2$ quotient and use this same conformal map to relate $M_{cs} = \tilde{M}_{cs}$ to the cylinder with period 2π. Here it is of course critical that we ensured the original conformal map took the $\mathbb{Z}_2$ action on $\tilde{M}_{cs}$ to the action $\phi \to \phi + 2\pi$ on the cylinder. Since the original map related the Hartle-Hawking state on $\tilde{M}_{cs}$ to the 4π cylinder vacuum, the method of images guarantees that it also relates the Hartle-Hawking state on $M_{cs} = \tilde{M}_{cs}$ to the vacuum on the standard cylinder of period 2π as desired.

This map can now be used to compute the integrated null stress tensor $\int T_{kk} d\lambda$ in the Hartle-Hawking state of M_{cs}. To simplify this, we introduce rescaled Kruskal coordinates

$$\bar{U} = \frac{U}{L\kappa_+} = e^{-\kappa_+ x_{*0}} U, \quad \bar{V} = \frac{V}{L\kappa_+} = e^{-\kappa_+ x_{*0}} V. \tag{5.10}$$

Since any Kruskal coordinate is an affine parameter on the horizon, we compute

$$\int T_{\bar{U}\bar{U}} d\bar{U} = \int \frac{du_c}{d\bar{U}} T_{u_c u_c} du_c, \tag{5.11}$$

where the integral is performed over the horizon $V = \bar{V} = 0$. Due to the Weyl anomaly (see e.g. [142] as translated to standard Lorentz signature conventions by [143]), for any null vector $\hat{k}$ the component $T_{\hat{k}\hat{k}}$ is related to the associated components of the cylinder vacuum stress tensor $T^{\text{cyl}}_{\hat{k}\hat{k}} = \hat{k}^a \hat{k}^b T^{\text{cyl}}_{ab}$ by

$$T_{\hat{k}\hat{k}} = T^{\text{cyl}}_{\hat{k}\hat{k}} + \frac{c}{12\pi} \left\{ \nabla_{\hat{k}} \nabla_{\hat{k}} \left(\ln \Omega \right) - \left[\nabla_{\hat{k}} \left(\ln \Omega \right) \right]^2 \right\}, \tag{5.12}$$

where $\nabla_{\hat{k}} = \hat{k}^a \nabla_a$, the covariant derivative is defined by the metric $ds^2_{\text{cyl}} = -du_c dv_c$ on the standard cylinder, and we have used the fact that $\hat{k}^a$ is null.

$T_{u_c u_c}$ is then found by setting $\hat{k}^a \partial_a = \partial_{u_c}$ in (5.12). In particular, in the standard cylinder vacuum we have

$$T^{\rm cyl}_{ab} = \rho (dt_{\rm cyl})_a (dt_{\rm cyl})_b + \rho (d\phi_{\rm cyl})_a (d\phi_{\rm cyl})_b, \tag{5.13}$$

where $\rho = -\frac{c}{24\pi}$ and c is the CFT central charge. Thus

$$T^{\rm cyl}_{u_c u_c} = -\frac{c}{48\pi}. \tag{5.14}$$

Since our bulk spacetime has $3+1$ dimensions, there are two transverse polarizations for oscillations of the string. For our N compact cosmic strings, this yields $c = 2N$.

To compute the remaining terms in (5.12) it is useful to observe that $\nabla_{u_c} = \partial_{u_c}$ since u_c and v_c are affine on the cylinder, and that

$$\partial^2_{u_c} (\ln \Omega) - [\partial_{u_c} (\ln \Omega)]^2 = -\Omega \partial^2_{u_c} \left(\Omega^{-1}\right). \tag{5.15}$$

Since we only need to compute $\langle T_{kk} \rangle_M$ on the horizon $V = \bar{V} = 0$, it is useful to recall that $\frac{f}{UV} = 2 g_{UV}$ is constant over the horizon as required to make U affine there. The factor $\frac{dV}{dv_c}$ is also constant on lines of constant V. The only u_c-dependent factor in (5.7) is thus

$$\frac{dU}{du_c} = \frac{L}{4\cos^2(u_c/4)}, \tag{5.16}$$

so $\Omega^{-1} \propto \cos^2(u_c/4)$ and

$$-\Omega \partial^2_{u_c} \left(\Omega^{-1}\right) = \frac{1}{16}. \tag{5.17}$$

Combining (5.12), (5.14), (5.15), (5.7), and (5.17) yields

$$T_{u_c u_c} = -\frac{c}{64\pi}, \tag{5.18}$$

so that (5.11) yields

$$\int T_{\bar{U}\bar{U}} d\bar{U} = \int_0^{2\pi} 4\kappa_+ \cos^2(u_c/4) \left(-\frac{c}{64\pi}\right) du_c = -\frac{c\kappa_+}{16}, \tag{5.19}$$

and thus

$$\int T_{UU} dU = \int \frac{d\bar{U}}{dU} T_{\bar{U}\bar{U}} d\bar{U} = e^{-\kappa_+ x_{*0}} \int T_{\bar{U}\bar{U}} d\bar{U} = -e^{-\kappa_+ x_{*0}} \frac{c\kappa_+}{16}. \tag{5.20}$$

Finally, it remains to choose the constant x_{*0}. Since this was an arbitrary constant that entered only through the definition of a coordinate, physical results like the back-reaction of quantum fields on the geometry cannot depend on its value. But the value of $\int T_{UU} dU$ does depend on the normalization of U, and it useful to make a choice that illustrates the relevant physics already at this stage. Recall that the null ray through the point x_0 has $U = -\kappa_+^{-1} e^{\kappa_+ x_{*0}}$ at $t = 0$, and this ray passes through an approximate sphere around either black hole of radius $r(x_0) = d/2 + O(r_+)$; see (5.2). Standard dimensionful Reissner-Nordström Kruskal coordinates $U = -\kappa_+^{-1} e^{\kappa_+ (r_* - t)}$ are defined using a tortoise coordinate with $r_* = r + O(\ln \frac{r}{r_+})$, and so we choose

$$x_{*0} = d/2 + O(\ln \frac{d}{r_+}), \tag{5.21}$$

which yields $U(t = 0, x_* = x_{*0}) = -\kappa_+^{-1} e^{\kappa_+ \left(d/2 + O(\ln \frac{d}{r_+})\right)}$.

At finite $\kappa_+ > 0$, the stress-energy is thus exponentially small in the black hole separation d. So while the negative sign in (5.20) should make the wormhole at least formally traversable, this result will be exponentially sensitive to further perturbations – including that from any signal sent through the wormhole. We will return to such issues in section 6.4 after carefully computing the back-reaction from (5.20) in section 6.3. For

now, we simply note that this contrasts sharply with the expectation of a Casimir energy of order $1/d$ for large d at fixed κ_+. The difference is due in part to the fact that the integrated null energy (5.20) differs from the conserved total energy of the quantum field by a factor of ξ^U, the null component of the Killing field which would appear in the latter but does not enter (5.20). As a result, energy that falls across the horizon at late times is exponentially suppressed in (5.20) relative to the conserved total energy.

Before proceeding, we pause to note that the result (5.18) could in fact have been predicted without calculation by combining the following observations. First, the fact that U is affine along the horizon means that we could conformally map our physical spacetime to flat 1+1 Minkowski space using a conformal factor $\tilde{\Omega}$ that is constant on the horizon and which thus has no anomalous contribution to the associated null-null stress-energy. Second, the standard conformal map from 1+1 Minkowski to the cylinder maps the Minkowski vacuum to the cylinder vacuum and thus has an anomaly that precisely cancels the cylinder stress tensor (5.14). However, thirdly, our $\mathbb{Z}_2$ quotient introduces factors of 2 that scale the anomalous contribution by $1/4$, so that it will only partially cancel the cylinder stress-energy. Thus (5.18) is precisely $3/4$ of (5.14). The rest of the computations simply apply this rescaled version of the standard conformal map from the plane to the cylinder. As a result, the final expression (5.20) must in fact be the identical for any other 1+1 background with the same causal structure up to the choice of x_{*0} that determines the overall scale of the effect.

5.3 Back-reaction and Stability

We are now ready to study first-order back-reaction from the quantum stress-energy (5.20), and in turn, study the traversiblity of our wormhole. We first orient ourselves to the appropriate geometry in section 5.3.1 before investigating the linearized Einstein

equations in section 5.3.2.

5.3.1 Geometry and Geodesics

We are primarily interested in following a null geodesic through the throat of our wormhole. As described above, when the wormhole mouths are far apart, the spacetime in the throat is approximately spherically symmetric and thus Reissner-Nordström up to small corrections. At leading order in large d, it thus suffices to study perturbations to Reissner-Nordström sourced by the stress-energy (5.20), and in particular on our null geodesic.

We start with the Reissner-Nordström metric in its static form

$$ds^2 = -f dt^2 + f^{-1} dr^2 + r^2 d\Omega^2, \tag{5.22}$$

where $d\Omega^2$ is the metric on the unit two-sphere. As above, we introduce Kruskal coordinates: the standard tortoise coordinate is

$$r_* = \int \frac{1}{f} dr = r + \frac{1}{2\kappa_+} \ln \frac{|r - r_+|}{r_+} - \frac{1}{2\kappa_-} \ln \frac{|r - r_-|}{r_-} \tag{5.23}$$

where we have chosen the constant of integration such that $r_* = 0$ at $r = 0$. We then introduce $u = t - r_*$, $v = t + r_*$ and thus the dimensionful Kruskal coordinates

$$U = \mp \kappa_+^{-1} e^{\mp \kappa_+ u}, \quad V = \pm \kappa_+^{-1} e^{\pm \kappa_+ v}, \tag{5.24}$$

where the (U, V) signs are $(-, +)$ before the geodesic enters the throat and are $(+, -)$ after it leaves. The metric in these coordinates becomes

$$ds^2 = 2 g_{UV} dU dV + r^2 \left(d\theta^2 + \sin^2 \theta d\phi^2 \right), \tag{5.25}$$

where $r = r(UV)$ is implicitly defined by equations (5.23) and (5.24). As usual, we have

$$g_{UV} = g_{UV}(UV) = \frac{f}{2\kappa_+^2 UV} = -\frac{1}{2}\frac{r_+ r_-}{r^2}\left(\frac{r-r_-}{r_-}\right)^{1+(r_-/r_+)^2} e^{-2\kappa_+ r}. \tag{5.26}$$

The null curve $V = 0$ at constant angles on the S^2 is a geodesic in this background. Following the standard treatment, we wish to understand how this geodesic is displaced under a general metric perturbation h_{ab}. Integrating the geodesic equation gives

$$V(U) = -(2g_{UV}(V=0))^{-1}\int_{-\infty}^{U} \mathrm{d}U h_{kk}, \tag{5.27}$$

where $h_{kk} = h_{ab}k^a k^b$ and where we have used the fact that g_{UV} is constant along the unperturbed horizon at $V = 0$. At $U = +\infty$ one thus finds

$$\Delta V = \frac{r_+}{r_-}\left(\frac{r_+ - r_-}{r_-}\right)^{-1-(r_-/r_+)^2} e^{2\kappa_+ r_+}\int_{-\infty}^{+\infty} \mathrm{d}U h_{kk}. \tag{5.28}$$

So long as this quantity is negative, the geodesic will emerge from the black hole and reach null infinity. As in [144, 132], we will see in section 5.3.2 below that negative h_{kk} follows from the negative $\langle T_{kk}\rangle$ found above in (5.20).

In addition to the binary question of traversability, we can also study the time-delay of this wormhole-traversing null geodesic relative to some standard. For reference purposes, let us consider a non-physical (particularly violating the generalized second law) ultrastatic ($g_{tt} = -1$) spacetime consisting at each time of two copies of Euclidean space, each with a ball of radius r_+ removed around the origin and with the two spheres glued together. A null ray hitting one of these spheres in the first space then instantly teleported to an associated point in the other. Note that Eddington-Finklelstein coordinates on such a space with the above conventions would have $v =$ constant for a radial null ray traveling from one asymptotic region to the other. As a result, if a null geodesic through

our wormhole has $v_{\rm out} = v_{\rm in}$, it is as if the wormhole brought it instantaneously from one mouth to the other. Conversely, with these conventions a null geodesic in Minkowski space that takes a time d to travel the distance d separating the mouths has $v_{\rm out} - v_{\rm in} = d$. As a result, the time delay relative to geodesics that propagate across the same separation in Minkowski space is[5] $t_{\rm delay} = v_{\rm out} - v_{\rm in} - d$, so that it is natural to refer to $v_{\rm out} - v_{\rm in}$ as the transit time $t_{\rm transit}$ required for the signal to traverse the wormhole.

We should thus compute

$$t_{\rm transit} = v_{\rm out} - v_{\rm in} = v(V(U = +\infty)) - v(V(U = -\infty)) \tag{5.29}$$

from (5.28). Due to the exponential relationship between v and V, (5.29) is minimized for a geodesic starting at $V = -\Delta V/2$ and ending at $V = +\Delta V/2$ so that

$$t_{\text{min transit}} = v_{\rm out}\left(-\frac{\Delta V}{2}\right) - v_{\rm in}\left(-\frac{\Delta V}{2}\right) = -\frac{2}{\kappa_+}\ln\left(-\kappa_+\frac{\Delta V}{2}\right). \tag{5.30}$$

From (5.20) – and the fact that we work in linear perturbation theory – we thus expect to find $t_{\text{min transit}} = 2x_{*0} + \text{logs} = d + \text{logs}$ so that the ratio $\frac{t_{\text{min transit}}}{d}$ to the transit time for a geodesic that does not pass through the wormhole becomes 1 in the limit of large d. This expectation will be confirmed below.

5.3.2 Back-reaction

We now study the metric perturbation h_{ab} associated with the quantum stress-energy (5.20). As noted above, at leading order in d it suffices to perturb around the exact Reissner-Nordström metric (5.22), and we consider a general perturbation. We will also

[5] As always for $d = 4$, in our actual background with black holes, propagation through the $1/r$ potential gives an additional logarithmic delay. However, it is still conventional to discuss time delay relative to comparable travel through Minkowski space.

need the Reissner-Nordström electromagnetic field, which in Kruskal coordinates takes the form

$$F_{ab} = -\frac{Q}{2\kappa_+}\left[\frac{1}{V}\partial_U\left(\frac{1}{r}\right) + \frac{1}{U}\partial_V\left(\frac{1}{r}\right)\right](dU)_a \wedge (dV)_b. \tag{5.31}$$

One might expect that we also need to consider the spherically perturbed electromagnetic field $F_{ab} + \delta F_{ab}$. However, because the electromagnetic stress tensor is quadratic in F_{ab}, and since the component $T^{(\mathrm{EM})}_{UU}$ vanishes by symmetry in the unperturbed background, it turns out that to first order one finds simply

$$\delta T^{(\mathrm{EM})}_{UU} = -\frac{Q^2}{8\pi r^4}h_{UU} = -\frac{r_+ r_-}{8\pi r^4}h_{UU} \tag{5.32}$$

which is independent of δF_{ab}. Therefore, on the horizon $V = 0$, the UU component of the linearized Einstein equations becomes

$$\begin{aligned} 8\pi G T^{(\mathrm{scalar})}_{UU} = {} & \frac{\kappa_+}{r_+}\left(2h_{UU} + U\partial_U h_{UU}\right) - \frac{1}{2r_+^2}\partial_U^2\left(h_{\theta\theta} + \frac{1}{\sin^2\theta}h_{\phi\phi}\right) + \frac{1}{2r_+^2}\Big[-\partial_\theta^2 h_{UU} \\ & - \frac{1}{\sin^2\theta}\partial_\phi^2 h_{UU} - \cot\theta\partial_\theta h_{UU} + 2\cot\theta\partial_U h_{U\theta} + \frac{2}{\sin^2\theta}\partial_U\partial_\phi h_{U\phi} + 2\partial_U\partial_\theta h_{U\theta}\Big]. \end{aligned} \tag{5.33}$$

We may then follow [132] in integrating (5.33) over U at each point on the S^2 and applying asymptotically flat boundary conditions to find

$$8\pi G\int\langle T_{kk}\rangle \mathrm{d}U = \left(\frac{\kappa_+}{r_+} + \frac{1}{2r_+^2}(-\partial_\theta^2 - \frac{1}{\sin^2\theta}\partial_\phi^2 - \cot\theta\partial_\theta)\right)\int h_{UU}\mathrm{d}U. \tag{5.34}$$

Because we are interested in solving for the perturbation to the metric in terms of the stress tensor, we can invert this by finding an appropriate Green's function, $H(\Omega, \Omega')$ on S^2:

$$\left(\int dU h_{kk}\right)(\Omega) = 8\pi G\int d\Omega' H(\Omega,\Omega')\int dU\langle T_{kk}\rangle(\Omega'). \tag{5.35}$$

As usual, the general, explicit expression for $H(\Omega, \Omega')$ is rather cumbersome, but here it suffices to consider the response our compact cosmic string, which gives $\langle T_{kk} \rangle(\Omega')$ proportional to a delta-function at a single point on the S^2, which we take to be the north pole $\theta' = 0$. The remaining rotational symmetry then makes H a function only of the polar angle θ, reducing to the known Green's function for the Helmholtz equation [145]:

$$H(\theta) = -\frac{r_+^2}{2\sin(\pi\lambda)} P_\lambda(-\cos\theta) \tag{5.36}$$

for $\lambda = -\frac{1}{2}\left(1 + \sqrt{1 - 8\kappa_+ r_+}\right)$, and $P_l(x)$ the Legendre polynomial, or equivalently,

$$H = \sum_j Y_{m=0,j}(\Omega) H_{mj}, \quad H_{mj} = \sqrt{\frac{2j+1}{4\pi}} \frac{2r_+^2}{2\kappa_+ r_+ + j(j+1)} \tag{5.37}$$

where $Y_{m=0,j}(\Omega) = \sqrt{\frac{2j+1}{4\pi}} P_j(\cos\theta)$ are standard scalar spherical harmonics on S^2 with vanishing azimuthal quantum number. As in [132], we find that the response H_{mj} is largest at small j, and that this effect becomes very strong at small κ_+ in which case $H_{j=0}$ becomes very large.

Note that (5.36) is everywhere positive, and that it is largest at the north pole (where our compact cosmic string resides). The minimal transit time is thus experienced by the geodesic at $\theta = 0$. But for general θ (5.20), (5.30), (5.35), and (5.36) yield

$$t_{\text{min transit}}(\theta) = 2x_{*0} - 4r_+ - \frac{2}{\kappa_+} \ln\left(\frac{\pi G c}{16} \frac{r_-}{r_+^3} \left(\frac{r_+ - r_-}{r_-} \right)^{1-(r_-/r_+)^2} H(\theta) \right). \tag{5.38}$$

While $H(\theta)$ diverges for small theta, the divergence is only logartithmic. Since it also appears inside another log in (5.38), the effect of this divergence is thus rather small and is also independent of d. Using (5.21) thus gives $t_{\text{min transit}}(\theta) \approx d$ up to terms that grow

no faster than logarithmically at large d.

5.4 Discussion

In the above work we studied the back-reaction from quantum fields in their Hartle-Hawking state on a simple classical wormhole solution of general relativity of the form shown in figure 5.1. In the unperturbed solution, both of the wormhole mouths are black holes, and the wormhole interior collapses to a singularity. In particular, since the background respects the NEC, the background wormhole is non-traversable as predicted by topological censorship [83, 84]. The solution of interest is a charged version of that first constructed by Bach and Weyl in 1922 [120], and contains cosmic strings which hold the two mouths of the wormhole apart at some separation d and prevent them from coalescing. Adding charge to the Bach-Weyl solution allows one to adjust the surface gravity κ_+ of the black holes. The solution is asymptotically flat apart from the fact that some of these cosmic strings stretch to infinity. An explicit form for such solutions can be found in [135] based on the implicit solutions in [136]; see also [137, 138, 139, 140] for the simpler extreme limit.

While the wormhole is not traversable, it is infinitesimally close to being so in the sense that one can find two null rays separated by an arbitrarily small amount at $t = 0$ such that one ray begins at past null infinity and enters one mouth of the wormhole while the other exits the other mouth and reaches future null infinity. As a result, an arbitrarily small change in the metric generated by perturbative back-reaction from the stress-energy of quantum fields can render the wormhole traversable, at least for some period of time. In this work we computed the expected stress-energy associated with fluctuations in the locations of the of cosmic strings in their Hartle-Hawking state, as well as the first-order back-reaction of this stress-energy on the metric. When the

number N of such strings is sufficiently large, this expectation value should dominate over any fluctuations in this quantity, and also over contributions from bulk fields (e.g., from linearized gravitons) neglected in this work. However, aside from greybody factors associated with the propagation of such fields into the wormhole throat, it is natural to expect contributions from bulk fields to be qualitatively similar to those found here for cosmic string fluctuations.

As expected on general grounds, here periodic boundary conditions give negative integrated null energy on the horizon. This defocuses null geodesics and slows the collapse of the wormhole, allowing properly chosen causal curves to traverse the wormhole and avoid the singularities. In particular, these curves must begin their traversal of the wormholes at sufficiently early times. Note that we have not computed the full back-reacted metric sourced by our quantum fields, but (following [15]) we have focused on showing that a particular class of causal curves can traverse the perturbed wormhole and on computing the time-advance that defines the associated transit times. For contrast, appendix C describes a 'cosmological wormhole' in which the back-reaction of negative quantum stress-energy causes a time-*delay* instead of the above time-advance. As in [89, 88, 85, 132], the time advance in our asymptotically-flat case becomes large in the limit $\kappa_+ d \to 0$ where the background black holes become extremal. Our perturbative description then breaks down but, at least at large N, it is natural to expect non-perturbative corrections to render the wormhole traversable for all time as in [88].

However, we can more concretely discuss the non-extremal case where perturbation theory is valid. Although the integrated null energy on the horizon remains negative and proportional to N, it also becomes exponentially small in $\kappa_+ d$ (of order $e^{-\kappa_+ d/2}$). The resulting traversability is thus extremely fragile, as an exponentially small positive-energy perturbation will negate this effect and prevent traversability[6].

[6] This includes possible perturbations associated with any signal one might attempt to send through

The exponentially small integrated null energy is due in part to the fact that we integrate affine stress-energy components T_{UU} which are exponentially redshifted for energy that falls into the black hole at late times; i.e., because the Casimir-like energy located at $r \sim d/2$ at $t = 0$ takes a time of order d to fall into the black hole. The effect of positive-energy perturbations is similarly suppressed at late times, so it is only necessary to be exponentially careful with our solution for a time of order d after $t = 0$. At later times a more modest (though still significant) degree of care suffices to allow a signal to pass through, at least modulo the comments of footnote 6.

This exponentially small expected stress-energy may also make one ask again about quantum fluctuations. But as described in [15], the fluctuations of integrated null stress-energy are exactly zero in the Hartle-Hawking state of our double-cover spacetime $\tilde{M}$. While fluctuations on the quotient M will be non-zero due to image terms much like those that give non-vanishing T_{UU}, they will again be exponentially suppressed[7]. So the standard $\sqrt{N}$ suppression of fluctuations relative to the mean will suffice to protect traversability at only moderately large N.

Despite the small integrated stress-energy, the actual transit time through the worm-

the wormhole. Now, a right-moving signal is sensitive to the back-reaction of left-moving stress-energy, and in a pure 1+1 massless theory, a right-moving signal will generate only right-moving stress-energy and so will not interfere with its own attempt to traverse a wormhole. But more generally, right-moving signals will generate some amount of left-moving stress-energy as well. For example, in our model left- and right-moving oscillations of the cosmic strings are coupled via their interactions with the 4-dimensional bulk gravity. However, in the covering space $\tilde{M}$ it is clear that any associated self-delay effect is independent of when the signal is sent into the black hole. As a result, the integrated null stress-energy defined by any fixed affine parameter along the horizon must be exponentially small when a signal enters at early times. As a result, to protect a weak signal entering the left mouth of the wormhole on M from a strongly-blueshifted version of its own back-reaction it suffices to prevent the signal from sending perturbations into the *other* (right) mouth at early times. Nevertheless, it would be interesting to study this back-reaction in detail as was done for GJW wormholes in [131, 85, 146, 147], as this will place fundamental limits on the amount of information that can be transmitted. We thank Eduardo Testé Lino for discussions on this point.

[7]This assumes that we leave the system isolated for a time of order d, and in particular that we do not attempt to detect the signal before this time. The response to sampling the system earlier would involve an integral of T_{UU} supported on only part of the real line, in which case its fluctuations will not vanish even on the covering space $\tilde{M}$. So such sampling could easily provide the exponentially small positive perturbation required to prevent traversability.

hole is rather short. In particular, for a wormhole with mouths separated by a distance d, we find $\frac{t_{\text{min transit}}}{d} \to 1$ as $d \to \infty$; see (5.38). As mentioned in the introduction, general arguments (and in particular the generalized second law) prohibit wormholes from providing the fastest causal curves between distant points [128, 15]. Naively, one might expect this to require $t_{\text{min transit}} \geq d$ for large d. This is the case in $D \geq 5$ spacetime dimensions. There one again has $x_{*0} \approx d/2$, so it is clear that the higher dimensional analogue of our calculation will again give $\frac{t_{\text{min transit}}}{d} \to 1$. So in this sense, at least for $D \geq 5$, perturbative back-reaction on black hole spacetimes far from extremality comes close to saturating the theoretical bound on the shortest possible transit times for traversable wormholes[8].

In contrast, the eternally-traversable MMP wormholes [88] (related to our extremal limits) have $\frac{t_{\text{transit}}}{d} > 2$. Thus, while our non-extremal wormholes are more fragile and while they are traversable only for a limited period of time, for properly-timed signals they can be traversed significantly more quickly than corresponding MMP wormholes. This raises the interesting question of whether excited states of MMP wormholes might also have comparably shortened transit times for properly timed signals. We leave such issues for future investigation.

[8]In a fixed four-dimensional asymptotically flat spacetime (not necessarily satisfying any positive energy condition) of total mass $M > 0$, there is an infrared logarithmic divergence in the Shapiro time-delay for signals sent between distant points. As a result, the fastest causal curve between such points always lies far from the center of mass, no matter what shortcuts might be available closer to this center. This means that, even at large separation d, it is difficult to use arguments about causal curves connecting distant points to rigorously bound wormhole transit times. It would be interesting to understand what bounds might be derived directly from the quantum focusing conjecture [148].

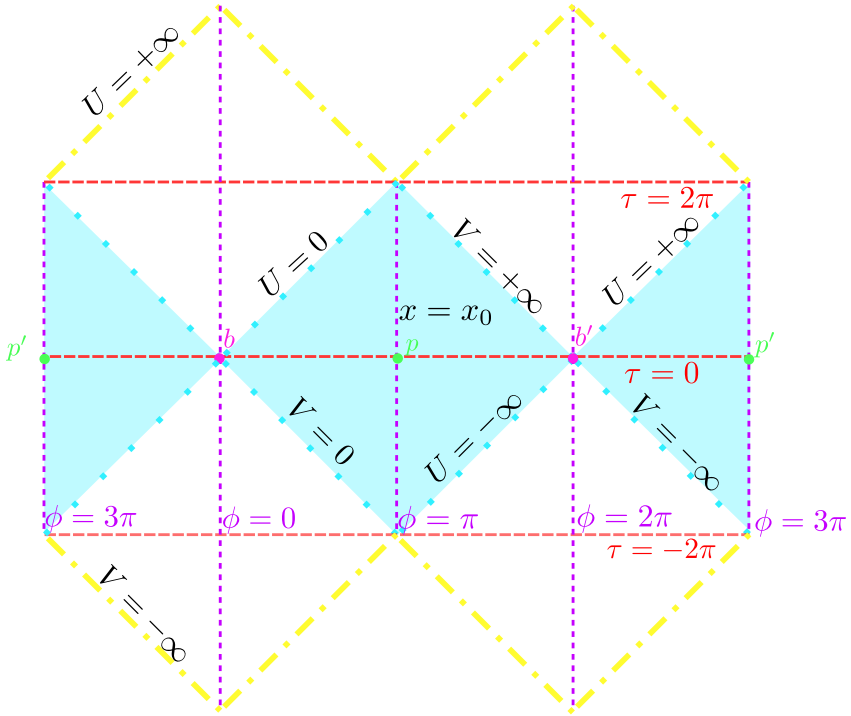

Figure 5.4: A conformal diagram of the two-fold cover $\tilde{M}_{cs}$ of the background spacetime M_{cs} induced on our compact cosmic strings shown in the cylinder conformal frame. Wormholes in this spacetime are not traversable, but are almost so and will be rendered traversable by the back-reaction of quantum fields. The left and right edges of the diagram are to be identified because of the periodicity of ϕ. Here we have truncated the spacetime at the black hole inner horizons (shown as dotted yellow lines) due to the expected instability of such horizons [141]. Blue dots mark the outer horizons, and the shaded regions are the static patches. The diagram is adapted to the cylinder coordinates ϕ, τ as indicated by the horizontal dashed lines showing $\tau = -2\pi, 0, \pi$ and the vertical dashed lines showing $\phi = 0, \pi, 2\pi, 3\pi$. (recall that ϕ has period 4π on $\tilde{M}_{cs}$). The spacetimes has two bifurcation surfaces (points) b, b' at $(\phi, \tau) = (0, 0)$ and $(\phi, \tau) = (2\pi, 0)$. The points p, p' at $(\phi, \tau) = (\pi, 0)$ and $(\phi, \tau) = (3\pi, 0)$ are also marked, as are the right-moving null lines $U = -\infty, 0, +\infty$ and the left-moving null lines $V = -\infty, 0, +\infty$.

Chapter 6

Multi-mouth Wormholes

6.1 Introduction

With natural assumptions, topological censorship theorems forbid traversable wormholes in classical general relativity [83, 84]. In particular, in globally hyperbolic spacetimes obeying the null curvature condition, such theorems require causal curves to be deformable to curves that lie entirely in the boundary of the spacetime, and also that one may choose the deformation so that the relevant curve remains causal throughout the process. Recently, however, it was shown how well-controlled quantum effects can be used to violate the null energy condition in a manner allowing the construction of traversable wormholes [15, 89, 88, 132, 85, 134, 149] that circumvent these theorems; see also [133, 150] for studies of the dynamical production of such traversable wormholes.

Quantum effects in gravity are typically difficult to control unless they are in some sense small. For this reason, one may think of the above constructions of traversable wormholes as starting with background spacetimes that contain an almost traversable wormhole that can be rendered traversable with small corrections. In classical solutions satisfying the null energy condition, this generally requires the background to contain a

bifurcate horizon having no causal shadow[1]; see figure 6.1. Naively then, it might seem as if traversable wormholes are constrained to connect only two regions of spacetime having a single opening, or mouth, in each region. Backgrounds with more interesting connectivity require some sort of finite causal shadow, necessitating a larger amount of negative energy to make the wormhole traversable.

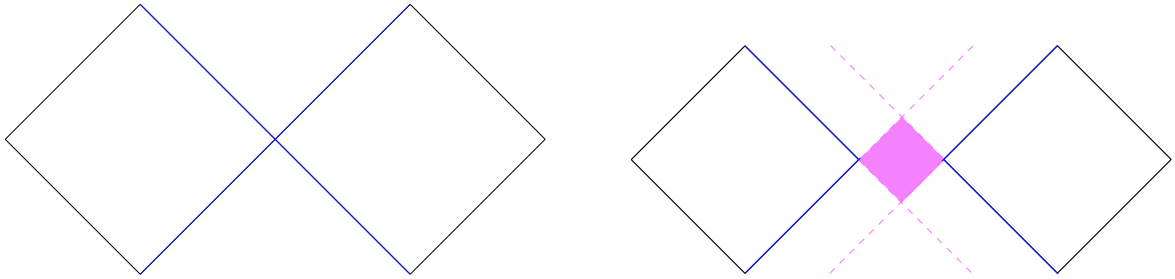

Figure 6.1: **Left:** A bifurcate horizon in a 2-sided asymptotically flat spacetime. **Right:** A spacetime with a causal shadow (shaded in purple).

Nevertheless, we show below that constructions with higher connectivity can still be controlled. Our analysis begins with the more familiar two-mouth asymptotically flat wormholes of [88] or of [149] with the former enhanced by including a large number N_f of 4d massless fermions. This solution is then perturbed by adding a small black hole to our solution deep inside the wormhole throat. Due to the wormhole's inherent fragility and the fact that semiclassical black holes have large masses in Planck units, actively passing this small black hole through a wormhole mouth would destroy traversability. But the extreme redshift deep in the wormhole throat allows semiclassical black holes that leave traversability intact. We take this small black hole to contain an additional wormhole that connects to another distant region of spacetime, and the new wormhole can then be made traversable with further quantum effects in the usual way. The spacetime has fundamental group F_2, the free group on two generators, which differs from the fundamental group F_3 that would be obtained by adding three separate two-mouth wormholes

[1] A causal shadow is defined as a bulk region which is causally disconnected from the boundary, see [151] for more details.

connecting 3 distant regions of spacetime A, B, C in pairs AB, BC, and AC; see figure 6.2.

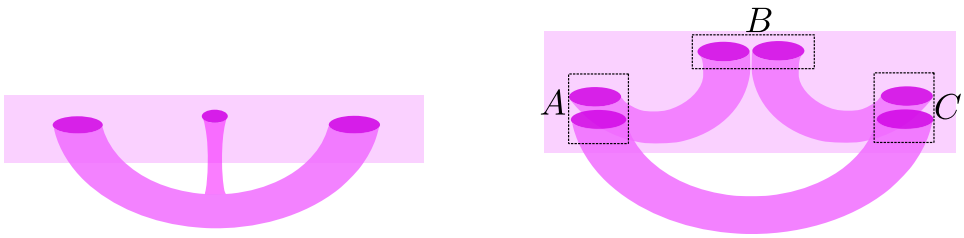

Figure 6.2: **Left:** A 2 dimensional analogue of our spatial topology has two handles. The actual 3 dimensional space has fundamental group F_2, the free group on two generators. **Right:** A space with 3 wormholes connecting regions A, B, C in pairs AB, BC, AC has 3 handles. In 3 dimensions the fundamental group would be F_3.

The above construction also has interesting implications for quantum states of wormholes. First, the ability to add a small black hole to a two-mouth traversable wormhole indicates additional traversable excited states beyond those anticipated in the analyses of [89, 88]. Second, at least when embedded in AdS/CFT, our three-mouth traversable wormhole appears to involve a new entanglement structure different from the TFD-like entanglement associated with two-mouth wormholes.

The paper is organized as follows. Section 6.2 reviews previous constructions of traversable wormholes. Section 6.3 then describes the gravitational construction of our multiboundary traversable wormholes with certain explicit calculations relegated to appendix D. We conclude with a brief discussion in Sec. 6.4, focusing on quantum states and entanglement.

6.2 Review of two-mouth traversable wormhole models

This section reviews two different constructions of two-mouth traversable wormholes in asymptotically flat space. The first [88] uses a magnetic field to localize massless fermions whose Casimir energy then makes the wormhole traversable. The second [134] uses cosmic strings that thread through the wormhole throat and render it traversable. Both models, however, give rise only to metastable wormholes, with [88] having a slightly more stable setup. Nevertheless, the wormholes are long-lived enough to traverse.

Notably, it is expected that the wormhole throat must be longer than the distance between the wormhole mouths, though the wormholes of [149] approximately saturate this bound in certain limits. In $d > 4$, this is a sharp bound that follows from, for example, the Generalized Second Law [152], or in AdS/CFT, from boundary causality [144]. These statements prohibit wormholes from being the fastest causal curves between distant points.[2]

To build a traversable wormhole, we need some source of negative energy since we need null rays to initially converge as they go inside the wormhole throat, but then to diverge as they head out the other mouth. Using Raychaudhuri's equation, we see that positive energy focuses null rays, while negative energy expands them. This is the reason why wormholes were deemed impossible with classical matter, since all of it obeys the null energy condition. The Casimir effect arises when we employ nontrivial boundary conditions for the quantum fields we are studying. Sometimes, these boundary conditions

[2]However, in $d = 4$ asymptotically flat spacetimes, the Shapiro time-delay associated with the wormhole mouths means that the fastest causal curve between two distant points always lies far from the center of mass. Thus, the sharp bounds mentioned above are always trivially satisfied, and a sharp, local bound is lacking for wormhole transit times. Of course, it may be possible to derive sharper local bounds by considering either the quantum focusing conjecture [148], or by considering short wormhole's tendency to form time machines [129].

are such so as to cause depletion of modes in the vacuum, giving us negative energy in return.

6.2.1 Eternal wormholes with magnetic fields

We will first describe the setup proposed in [88]. Let us start with a near-extremal magnetically-charged Reissner-Nordström (RN) black hole and take the near-horizon limit to write the metric

$$ds^2 = r_e^2\big(-(\rho_r^2-1)d\tau_r^2 + \frac{d\rho_r^2}{\rho_r^2-1} + d\Omega^2\big). \tag{6.1}$$

Here r_e is the extremal horizon radius, and ρ_r and τ_r are readily obtained from the usual r and t coordinates as in [88]. This near-horizon metric is global $\mathrm{AdS}_2 \times S^2$, with the AdS_2 factor presented in standard Rindler coordinates. We can of course rewrite the AdS_2 factor in global coordinates, making it appear easy to send causal signals from one side to the other.

Note, however, the S^2 factor has constant size in (6.1). This indicates that the asymptotic regions have been completely detached. To make a traversable wormhole, we must restore these connections by allowing the size of the S^2 to vary slowly. Doing so gives a metric of the form

$$ds^2 = r_e^2\big(-(1+\rho^2+\gamma)dt^2 + (1+\rho^2+\gamma)^{-1}d\rho^2 + (1+\phi)(d\theta^2+\sin^2\theta d\phi^2)\big), \tag{6.2}$$

where ϕ encodes the changing size of the sphere and γ describes the associated backreaction on the AdS_2 factor.

From the Raychaudhuri equation, one finds that $\phi(\rho)$ must be monotonic in spacetimes of the form (6.2) satisfying the null curvature condition. But making a wormhole

that connects to asymptotic regions at both ends requires ϕ to grow in both directions at large $|\rho|$. Completing the construction in a solution of Einstein-Hilbert gravity thus requires the introduction of negative energy.

One way to obtain negative energy is to exploit the Casimir effect. The construction of [88] does so by using the magnetic field of the black hole and a 3+1 massless charged fermion field. The magnetic field creates localized Landau levels near each field line, which gives a large number q of effective 1+1 massless fermions. As shown in figure 6.3, field lines that loop through the wormhole yield 1+1 theories on $S^1 \times \mathbb{R}$ whose Casmir stress-energy is readily computed. Since constant ϕ yields the exact solution (6.1) with vanishing stress-energy, a small negative stress-energy suffices to allow growth of ϕ at large positive and negative ρ so long as the negative stress-energy threads the entire wormhole and this growth is correspondingly slow.

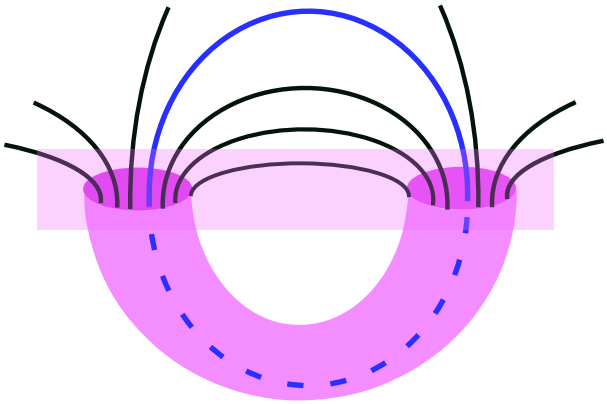

Figure 6.3: The traversable wormhole of [88]. Magnetic field lines thread the wormhole. Fermions localize into their lowest Landau level near each field line. For field lines that form closed loops, this creates effective 1+1 dimensional massless theories on $S^1 \times \mathbb{R}$ whose Casimir energy makes the wormhole traversable.

We emphasize that the loops must close in order to generate the Casimir energy. This requires that both wormhole mouths be placed in the same asympotic region of spacetime. As a result, the mouths attract each other gravitationally, and some feature must be added to keep them from coalescing into a single black hole. For example, one

can add angular momentum to slow this coalescence and make the wormhole long-lived as in [88].

6.2.2 Perturbative wormholes with cosmic strings

In contrast to the wormholes described above, [132, 149, 134] used a perturbative framework to give a general method of constructing traversable wormholes with both mouths in the same asymptotic region. As above, in this construction we start with a classical background containing a pair of charged, RN-like black holes. These black holes are held apart by the tension of a cosmic string that threads the wormhole and stretches to infinity. A second cosmic string wraps the non-contractible compact cycle through the wormhole. The quantum fluctuations of this compact string generate the negative Casimir energy needed for traversability. This wormhole will generally be strongly time-dependent, and can be traversed by curves only if they leave past null infinity at sufficiently early times.

We can think of these wormholes as coming from a quotienting process, starting with a classical geometry $\tilde{M}$ with a bifurcate Killing horizon and one asymptotic region on each side of the horizon. We can then think of $\tilde{M}$ as an *almost* traversable wormhole with two asymptotic regions. However, the horizon generating Killing field forces the null stress-energy of any perturbation respecting this symmetry to be zero. Suppose this spacetime admits a $\mathbb{Z}_2$ isometry J exchanging the right and left asymptotic regions and preserving the time orientation. Then quotienting by this isometry $M = \tilde{M}/J$ gives an *almost* traversable wormhole with a single asymptotic region. In M, the horizon generating Killing symmetry is broken by the quotient by J: it maps the horizon-generating Killing field ξ to $-\xi$, by identifying the right and left regions and preserving the time-orientation of the spacetime. Thus, on the quotient spacetime, small perturbations can render the

quotient wormhole traversable.

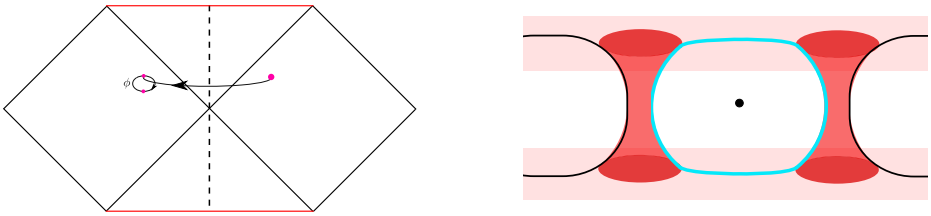

Figure 6.4: Left: The background spacetime and quotient necessary to make an $\mathbb{RP}^3$ geon. The horizon generating killing field is shown in light blue, and the quotient identifies a point in right asymptotic region with a point at the same time and radius on the left, with an additional antipodal shift on the internal sphere. Right: The quotient that creates a wormhole similar to Fig. 6.3 starts with two maximally extended black holes, held apart by cosmic strings that run off to infinity (black). A point is identified with the point given by swapping the black hole mouths and the asymptotic regions, e.g. it can be thought of as identifying a point with its π rotation about the black dot in the figure. Quantum fluctuations of the light blue compact string will generate negative energy.

The simplest example of such quotient wormholes is the $\mathbb{RP}^3$ geon [92, 91, 83] shown in Fig. 6.4. The traversability of simple examples AdS geons were explored in [132, 134]. Examples that took the more familiar form shown in Fig. 6.3 were studied in [149]. There, the covering space $\tilde{M}$ contains a pair of maximally-extended black holes, as in Fig. 6.4. The quotient M is obtained by identifying a point with the point obtained by swapping the black hole mouths and the asymptotic regions. In the covering space $\tilde{M}$, there are three cosmic strings. Under quotienting, the compact cosmic string in $\tilde{M}$ becomes a shorter compact cosmic string in M, while the strings stretching to infinity in $\tilde{M}$ becomes a single string that goes through the wormhole mouth and stretches to infinity on either side.

Once we have formed our classical backgrounds, we can understand the back-reaction from quantum fields sitting on the spacetime. As explained in [132], if quantum fields on $\tilde{M}$ have a well-defined Hartle-Hawking state, there will be a corresponding Hartle-Hawking-like state on M, defined by the path integral over the appropriate quotient

of the Euclidean geometry of $\tilde{M}$. For linear fields, this state can also be constructed by applying the method of images to the Hartle-Hawking state on $\tilde{M}$. The expression for $\langle T_{kk} \rangle_M$ (where k present the null vectors along the horizon) depends on whether the quantum field is periodic or anti-periodic around the non-contractible cycle created by the quotient, and the two choices differ only by an overall sign. Barring surprising cancellations, then, we can tune the boundary conditions of our fields to render the wormhole traversable.

Here the quantum fluctuations will be given by the cosmic strings. Since the cosmic strings lie along the horizon, they will be tangent to k. Thus, the classical cosmic string stress tensor, which is proportional to the induced metric, will not contribute to $\langle T_{kk} \rangle_M$. Quantum fluctuations of the string will contribute, however. In [149], these fluctuations were modelled as 1+1 dimensional massless free scalar fields.

For the string stretching to infinity in M, the points (x, Jx) in the covering space $\tilde{M}$ will lie on two distinct non-compact strings. The fluctuations on two different strings will be uncorrelated, and so the quantum fluctuations of the non-compact string will not contribute to $\int \langle T_{kk} \rangle_M d\lambda$. However, the contributions from quantum fluctuations of the compact string are non-zero.

In the extremal limit of RN black holes of the classical backgrounds, the back-reaction becomes large. Thus, our ability to treat the back-reaction perturbatively will break down. However, we take the divergence as an indication that a non-perturbative calculation would give an long lived traversable wormhole like those of [88].

6.3 Gravitational Construction

Our idea for constructing multiboundary traversable wormholes is simple: start with a two-mouth wormhole, place a small, near-extremal black hole in the throat, and extend

it into a wormhole with another small mouth in the same asymptotic region as the larger mouths. Technically, the insertion of the two small mouths in the initial large wormhole solution is a straightforward (if possibly tedious) problem of matched asymptotic expansions: the small mouths can be treated as perturbations of, respectively, the throat and the asymptotic region, while the effects of the latter on the mouths are incorporated as tidal perturbations of the near-extremal Reissner-Nordström black hole. Here we will be content with working at the lowest order in the matched asymptotic expansion, in which the backreaction of the mouths is neglected.

While the insertion of the small mouths is a generic and unproblematic part of the construction, there are other aspects that must be dealt with more carefully. One of them, still fairly simple, is the question of mechanical equilibrium (and possibly stability) of the new configuration, which actually arises at the first orders in the matched asymptotic expansion. A more involved problem is how to achieve the negative energies that make the throats traversable. The answers to these questions vary depending on the details of the model we choose—in other words, on the tools that we avail ourselves of for the construction. We may restrict ourselves to working within the same theory as [88], with only fields and matter available in the Standard Model (specifically, a Maxwell field and light fermions electrically coupled to it, in addition to gravity), to prove that the latter allows for multiboundary traversable wormholes. Or, instead, we may resort to a larger set of tools, as [149] did (with cosmic strings as appear in, say, grand unified theories), and aim at a 'proof of principle' that such wormholes are possible with reasonable matter and field content, e.g., satisfying basic energy conditions, and possibly within the landscape of string theory. Allowing only SM tools of course makes the task more difficult.

6.3.1 Multiwormhole construction guide

Let us then begin by discussing mechanical equilibrium. For a two-mouth wormhole this can be achieved by introducing an external magnetic field (in GR, this would be a Melvin flux tube [153]) tuned to keep the mouths apart, or by attaching cosmic strings that pull them, as explained above (exact solutions exist for both mechanisms [140, 135]). Alternatively, instead of balancing them into exact equilibrium, one can set the mouths into a long-lived Keplerian orbit around each other, or even, simply let them fall towards one another: the time to the merger from an initial separation d_{out} between the two mouths is $\sim d_{out}^{3/2}$. If the transit time along the throat is parametrically $O(d_{out})$ (it cannot be shorter) then the wormhole will remain open for long enough to cross it before collapsing.

When introducing a third mouth in the model of [88], where all black holes are near-extremal magnetic RN solutions, the option of equilibrium with a magnetic field background should not be hard to achieve: just like a uniform magnetic field can be approximated by the field in between two large, static magnetic sources (even nonlinearly in GR [154]), by adding a third source we can expect to achieve a magnetic field background where the three wormhole mouths are in (unstable) equilibrium. The other possibilities—cosmic strings, three-body orbits, or free-fall collapse—are equally workable. Another interesting, mechanically simpler possibility is to let the small black hole be charged under a different $U(1)$ gauge field than the bigger mouths, and then placing it at midpoint between the latter. Even if these configurations are unstable, the argument above guarantees that they can be long-enough lived to traverse the throats.

Now we move on to the problem of achieving the negative Casimir energies that thread the wormhole, beginning within the strict set up of the magnetic line model of [88]. The effective two-dimensional massless fermions will still travel along magnetic

field lines, which form loops along the non-contractible cycles of the wormhole and thus provide negative Casimir energies. There might be complications if the wavefunctions of the fermions along neighboring flux lines of different loops overlap. However, this overlap can be made parametrically small. The fermion modes bound to a given flux line can be arranged in a basis of Landau levels, which damp exponentially away from the flux line on which they are centered. The damping lengths in the two orthogonal directions multiply to give an area equal to a flux quantum. There are q flux quanta spread over the sphere, whose area is proportional to some r_w. So the linear extent of any Landau level is of order $q^{-1/2}r_w$. Since the structure of the flux lines varies on a scale set by r_w, for $q \gg 1$ this structure varies adiabatically as one moves from one flux line to another.

The analysis can be made much simpler by enlarging our toolbox beyond the Standard Model. One possibility, still using the magnetic line mechanism of [88], is to allow for three $U(1)$ gauge fields, and three flavors of fermions electrically coupled to each of the gauge fields. Then, with each pair of the mouths having opposite magnetic charges under one of the $U(1)$'s,[3] the fermions travel along field lines in an independent manner.[4]

The cosmic string model, where zero modes traveling along loops of string provide the requisite Casimir energy, is more versatile. We may use it in a hybrid fashion, by adding the third mouth to the magnetic-line model of [88] and thread it with two cosmic strings, each separately linked to the two big mouths; or else, if that hybrid is deemed too ugly to regard, directly work with the cosmic string wormhole model of [149] and add two new cosmic strings, one along each new cycle.

[3] I.e., the two big mouths have charges $(Q_1, Q_2, 0)$, $(-Q_1, 0, Q_3)$ and the small one $(0, -Q_2, -Q_3)$, with $|Q_1| \gg |Q_2|, |Q_3|$. This also allows easily for symmetric equilibrium positions for the small mouth.

[4] This is not entirely without issues. First, now the magnetic charge of a mouth, which controls the effective number of two-dimensional fermions, is not the same as the radius of the S^2 of the mouth. Second, we do not know of any explicit solutions (analytic or numerical) for black holes with charges under two (out of three) gauge fields and no other fields. Known solutions also involve dilatonic scalars and have singular extremal limits. Nevertheless, it seems plausible that, in a theory with several gauge fields and no dilatons one can take a RN solution with one type of charge, and perturbatively add a small charge under another gauge field keeping horizon regularity for a time long enough for our purposes.

We conclude that the cosmic string method of [149], possibly augmented with additional gauge fields, serves to prove that it is possible to construct multiboundary wormholes sufficiently long-lived to be traversable. Their existence within the Standard Model, following the methods of [88], also seems likely, but its detailed investigation is more complicated.

6.3.2 Signaling across mouths

Suppose A and B are using the wormhole with two big mouths to exchange messages. What are the consequences of inserting a third, small mouth operated by c? From the gravitational perspective, there are two different kinds of effects. First, the message sent by A (a particle or a wave) may be partly absorbed by the small mouth and thus be received by c and not B. The wormhole has then become a leaky pipeline. The absorption probability is proportional to the area of the small mouth, and can also have a dependence on the small mouth's angular position in the S^2 of the large throat. In a qubit (or qudit) model of quantum teleportation, the leakiness of the line can presumably be easily reproduced. The absorption probability, proportional to the number of degrees of freedom that c holds, may also be plausible, while the effect of the angular dependence seems to require a more detailed understanding of the localization of the qubits of c in the teleportation channel. On the other hand, having information about this angular position is essential for A and B if they intend to communicate efficiently with c. It means that they must have a detailed enough understanding of the entanglement structure of their many qubit system such that they can operate on the sectors of it that hold the entanglement with c in order to teleport a message to it.

A second effect is due to the Shapiro time delay that the signal will experience as it travels in the vicinity of the small mouth within the throat. That is, if the small mouth

is placed at a distance ρ_s in the throat geometry (6.2), then the signal that A sends to be B will take an additional time

$$\delta t \approx 2m \log(\frac{4l^2}{b^2}) \tag{6.3}$$

to arrive. Here b is the distance of closest approach of the null geodesic (for the signal) to the small mouth, which translates into an angular difference between the positions in S^2 of the mouth and the initial signal. Although, again, this angular information may not be easily reproduced in a toy quantum-mechanical model, the existence of a signaling delay may admit a simpler interpretation. Loosely, the increased travel-time may be correlated with an increased complexity in decoding the teleported message. This time delay must be corrected in the case of the AdS_2 throat (the magnetic model) to account for the redshift between the two large mouths and the position of the small mouth in the throat.

Now, instead, say that A and c want to communicate among themselves and not with B. What are the effects of having a good portion of the channel constituted by a big throat?

6.3.3 Size limits on the third mouth

The constructions above work well in the limit where the third mouth is much smaller than the other two, but we can ask ourselves how large this mouth can be. Even though the approximations we have employed do not rigorously apply, we can still use them in order to obtain parametric estimates.

There are several effects that can limit the size of the third mouth. In the cosmic string model, the original wormhole remains open for only a limited amount of (retarded)

time. We note that from [149],

$$\Delta V = \frac{r_+}{r_-}\left(\frac{r_+ - r_-}{r_-}\right)^{-1-(r_-/r_+)^2} e^{2\kappa_+ r_+} \int_{-\infty}^{+\infty} \mathrm{d}U h_{kk}, \tag{6.4}$$

where

$$\left(\int dU h_{kk}\right)(\Omega) = 8\pi G \int d\Omega' H(\Omega,\Omega') \int dU \langle T_{kk}\rangle(\Omega'), \tag{6.5}$$

$$\int \langle T_{UU}\rangle dU = -e^{-\kappa_+ d/2}\frac{c\kappa_+}{16 r_+^2}, \tag{6.6}$$

and

$$H = \sum_j Y_{m=0,j}(\Omega) H_{mj}, \quad H_{mj} = \sqrt{\frac{2j+1}{4\pi}}\frac{2r_+^2}{2\kappa_+ r_+ + j(j+1)} \tag{6.7}$$

for $Y_{m=0,j}(\Omega) = \sqrt{\frac{2j+1}{4\pi}} P_j(\cos\theta)$ are standard scalar spherical harmonics on S^2 with vanishing azimuthal quantum number.

Putting this all together, we find

$$\Delta V = -\frac{G_N c\pi\kappa_+}{2}\frac{1}{r_+ r_-}\left(\frac{r_+ - r_-}{r_-}\right)^{-1-(r_-/r_+)^2} e^{\kappa_+(2r_+ - d/2)} \int d\Omega' H(\Omega,\Omega'). \tag{6.8}$$

For concreteness, we can choose a geodesic at $\theta = \pi/2$, and keep just the lowest term in 6.7, which dominates at small κ_+:

$$\Delta V = -\frac{G_N c\pi}{2}\frac{1}{r_-}\left(\frac{r_+ - r_-}{r_-}\right)^{-1-(r_-/r_+)^2} e^{\kappa_+(2r_+ - d/2)}, \tag{6.9}$$

where c is the central charge associated with quantum fluctuations of the compact cosmic string, where we've chosen a geodesic through $\theta = \pi/2$, and where U and V are

defined such that the metric on the bifurcation surface is

$$ds^2 = \frac{r_-}{r_+}\left(\frac{r_+ - r_-}{r_-}\right)^{1+(r_-/r_+)^2} e^{-2\kappa_+ r_+} dU dV. \tag{6.10}$$

Then, if the time (6.3) became longer than this available crossing time, a signal would be delayed by the presence of the third mouth for too long to make it across the wormhole. Considering the case that $b \sim r_e/2$, this leads to a bound

$$\Delta v = \delta t \left(\frac{r_-}{r_+}\left(\frac{r_+ - r_-}{r_-}\right)^{1+(r_-/r_+)^2} e^{-2\kappa_+ r_+}\right)^{\frac{3}{2}} \lesssim \Delta V, \tag{6.11}$$

which then gives

$$m \lesssim \frac{c\pi}{4\log\left(\frac{4d^2}{r_+^2}\right)} \frac{r_+^{1/2}}{r_-^{3/2}} \left(\frac{r_+ - r_-}{r_-}\right)^{-3/2-3/2(r_-/r_+)^2} e^{\kappa_+(3r_+ - d/2)}. \tag{6.12}$$

The magnetic wormhole model does not suffer from this problem since in principle it can remain open for an arbitrarily long time. Nevertheless, there is another effect that can limit the size of a third mouth inserted in it. The positive mass of this mouth will create a focusing effect within the wormhole that will counter against the defocusing effect of the negative Casimir energy that is responsible for keeping it open. The backreaction of the third mouth on the wormhole width can be incorporated in the construction of [88] if we model it as a delta-function mass source. The size of the S^2 along the throat is controlled by a scalar field ϕ, and the overall effect of the source on it is obtained by smearing it over the S^2 to get a codimension one defect. We find

$$\phi_\tau(\rho) = \alpha(1 + \rho \arctan\rho) + c_1\sqrt{1+\rho^2} - \beta\rho\Theta(\rho), \tag{6.13}$$

which gives

$$\phi''_\tau(\rho) = \frac{2\alpha}{(1+\rho^2)^2} + \frac{c_1}{(1+\rho^2)^{3/2}} - \beta\delta(\rho). \tag{6.14}$$

Then, in order for the S^2 not to collapse, we need $\frac{\beta}{\alpha} \sim 1$, which in turn gives

$$M_0 < \frac{qN_f}{8\pi r_e} = \frac{N_f g r_e}{8\pi^{3/2}\ell_p d}. \tag{6.15}$$

To compute the energy of this mass (as seen from outside the wormhole), we include a redshift factor of $\frac{r_e}{d}$, giving

$$E_{bh} < \frac{qN_f}{8\pi r_e} = \frac{N_f g}{8\pi^{3/2}\ell_p}. \tag{6.16}$$

or,

$$E_{bh} < \frac{2}{\pi} E_{min} \tag{6.17}$$

where E_{min} is the energy gap between traversable and non-traversable wormholes. We see that this is comparable to the Casimir energy.

6.4 Discussion

In the above work we constructed a multiboundary traversable wormhole. This was done by starting with a two mouthed traversable wormhole of the form of either [88, 149]. We then perturbed this solution by adding a small black hole in the throat of the larger wormhole. As long as this black hole is much smaller than the wormhole mouths, the original wormhole will remain traversable. This small black hole can be placed in mechanical equilibrium through the proper placement of cosmic strings. Additional compact cosmic strings can be used to make all mouths traversable.

This construction shows that the number of bound states of traversable wormhole

solutions is much larger than previously thought.

While two-mouth traversable wormholes are associated with TFD-like entanglement [89], our three-mouth wormholes will require a new entanglement structure – a concept that can be made precise by embedding our construction in an AdS/CFT context. A full exploration of this topic is beyond the scope of this work. However, it is useful to briefly consider the locations of extremal surfaces homologous to the individual mouths of our wormholes. If the mouths of our wormholes were embedded in AdS, these extremal surfaces would be candidate entangling surfaces for associated regions of the boundary.

In [155, 17], it was found that narrowing of the 'entanglement shadow' region between these three surfaces, so that the separation between some two of these surfaces becomes small relative to their distance to the third, was indicative of a region of mostly bipartite entanglement between the corresponding boundaries. In contrast, regions where the distance between the various entangling surfaces is roughly the same between each pair of surfaces might naturally be taken as a signal of tripartite entanglement. In particular, [17] associated large amounts of multipartite entanglement AdS black holes whose temperature was small compared to the AdS scale while [155] showed that states dual to hot black holes are well-approximated by sewing together various copies of $|TFD\rangle$ states. See figure 6.5 below.

We again consider a wormhole with three mouths, A, B, and C. Recall that our analysis of back-reaction suggested that one mouth C must remain small relative to the other two. We thus assume that this is so. Before we add in C, the extremal surfaces associated with A and B coincide and lie at the bottom of the AB throat. In the limit where C is much smaller than A and B, it will have little effect on the geometry far from C. Thus the extremal surfaces associated with A and B will remain close over most of their area, and in particular at the top of the wormhole in 6.6 below. Furthermore, the extremal surface associated with C will remain close to the bottom of of the small

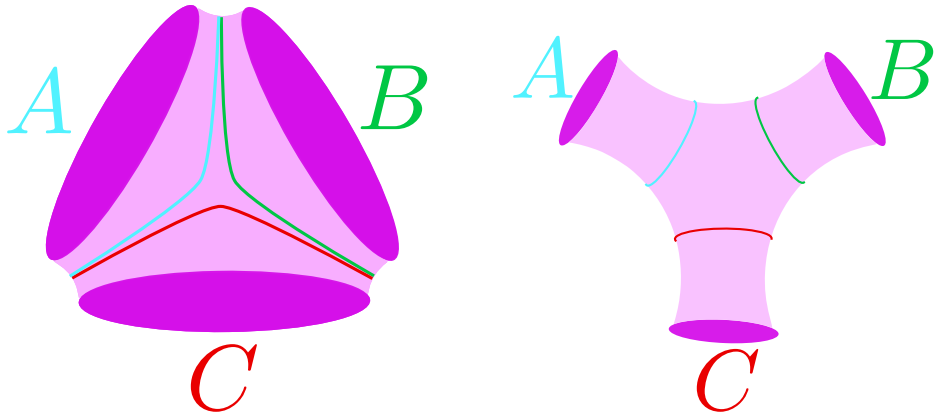

Figure 6.5: Left: A hot AdS_3 3-mouth wormhole. The entanglement shadow becomes very narrow in regions where pairs of extremal surfaces approach each other, indicating regions of strong bipartiate entanglement. Right: A cold AdS_3 3-mouth wormhole. At any point on one entangling surface, the distance to the other two entangling surfaces is roughly the same. This suggests strongly tripartite entanglement.

wormhole throat, and thus far away from the other two surfaces. We may thus expect large bipartite entanglement to remain between A and B, with C being entangled with the AB system in a very non-local way, and presumably in a manner that involves significant 3-party entanglement.

The large bipartite entanglement between A and B is consistent with the idea that C has little effect on signals being sent between A and B. But it would be interesting to consider quantum mechanical duals in more detail, as well as the quantum teleportation protocols associated with traversing the wormhole in the bulk in analogy with the discussions of e.g. [15, 131, 147, 156]. In particular, if the entanglement of C with A and B is indeed mostly of the multi-party sort, then the dual description of sending a signal from C to either one of A or B must necessarily involve all three systems. While this idea may at first seem unfamiliar, it is consistent with the fact that the asymptotically flat region of our gravitational solution does in fact provide interactions between each pair of mouths AB, AC, and BC.

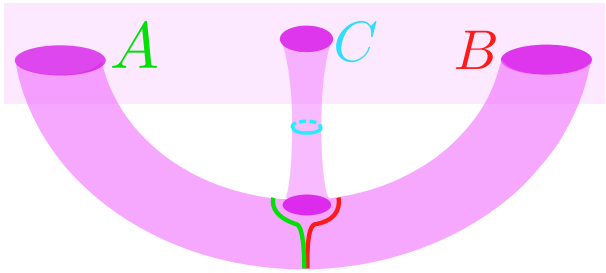

Figure 6.6: Extremal surfaces in our three boundary wormholes. Here, the small size of C guarantees that the extremal surfaces associated with A and B stay close together, suggesting that A and B retain a large amount of bipartite entanglement. C, however, stays comparably far from both A and B, and presumably its is entanglement with A and B in some non-local way containing tripartite entanglement.

Appendix A

$\mathrm{Mm}_\gamma(A)$ is mostly contained in the interior of $D(\gamma)$ and in γ itself

This appendix contains some addition results concerning the possible intersections of restricted maximin surfaces with $\partial D(\gamma)$ that can be easily proven using the techniques of section 3.4, but which are not required for our main results. In particular, we saw in the first example from section 3.3.1 that $\mathrm{Mm}_\gamma(A)$ can intersect γ. The proofs of the claims below establish that, up to possible sets of measure zero, $\mathrm{Mm}_\gamma(A)$ is contained in the union of the interior of $D(\gamma)$ and γ itself. We focus below on excluding open sets of $\mathrm{Mm}_\gamma(A)$ from L^+, but analogous arguments clearly also hold for L^-.

Claim 4. Suppose that $p \in L^+$ has $\theta_+ \geq 0$ (where θ_+ is the expansion of the null generators of L^+). For any boundary region A, there does not exist a subset $V \subset \mathrm{Mm}_\gamma(A)$, open in $\mathrm{Mm}_\gamma(A)$, such that $p \in V$ and $V \subset L^+$.

Proof: Suppose that such regions A and V exist. There must exist a surface $\Sigma \in \mathcal{C}_\gamma$ such that $\mathrm{Mm}_\gamma(A) = \min(A, \Sigma)$. Because Σ is an achronal surface containing $V \subset L^+$ and γ, Σ must contain the part of the null generator of L^+ containing p that lies to the past of p. Because $\theta_+ \geq 0$ at p, the null generic condition requires $\theta_+ > 0$ for any point in L^+ to the past of p. But since Claim 1 forbids $\mathrm{Mm}_\gamma(A)$ from lying along this generator of L^+, we see that deforming $\mathrm{Mm}_\gamma(A)$ in the $-k$ direction at the point p keeps the surface in Σ and that this deformation reduces its area (since $\theta_+ > 0$). This contradicts the fact that $\mathrm{Mm}_\gamma(A) = \min(A, \Sigma)$, so A, V cannot exist.

Claim 5. Suppose that $p \in L^+$ has $\theta_+ < 0$. Then p cannot be in $\mathrm{Mm}_\gamma(A)$ for any A.

Proof:

Let Σ be a Cauchy surface on which $\mathrm{Mm}_\gamma(A)$ is minimal, and consider the future-ingoing directed null congruence N orthogonal to $\mathrm{Mm}_\gamma(A)$. Since it is nowhere to the future of L^+ and $\theta_+ < 0$, we must have $\theta_{k,N} < 0$ by Corollary zero. But any $p \in \mathrm{Mm}_\gamma(A)$ must have $\theta_{k,N} = 0$ by Claim 2. So p cannot lie in L^+.

In fact, the argument for Claim 5 also applies at caustics or nonlocal intersections (i.e., at all points where θ_+ is ill defined). In such cases, deforming Σ to the past again causes

the area of any surface $\min(A, \Sigma_\epsilon)$ to exceed $\mathrm{Mm}_\gamma(A)$, contradicting the maximization step of the maximin procedure. We formalize this result in the following statement

Claim 6. Suppose θ_+ is ill defined or diverges at $p \in L^+$. Thus $p \in L^+$ lies on a caustic or nonlocal self intersection of L^+ by Theorem 1 of [73]. Then for any boundary region A, there does not exist a subset $V \subset \mathrm{Mm}_\gamma(A)$ open in $\mathrm{Mm}_\gamma(A)$ such that $p \in V$ and $V \subset L^+$.

Proof: Same as above.

Appendix B

First-order traversability requires a stationary horizon

We show here that any background spacetime obeying the null convergence condition $R_{ab}k^a k^b \geq 0$ which can yield a traversable wormhole after first-order backreaction of a quantum field must be a quotient of a spacetime with a stationary (divergence-free and shear-free) horizon.

We phrase the argument for a spacetime $\tilde{m}$ with a single boundary[1], but the argument for multiple boundaries is identical. Consider any curve that starts and ends at the boundary but is not smoothly deformable (with fixed endpoints) to lie entirely in the boundary. Let us now deform this curve by moving one endpoint to the far future on the boundary and the other to the far past on the boundary. If the limiting curve could be causal with any timelike segment, there would be a faster causal curve through the wormhole (i.e., not deformable to lie in the boundary) which starts and ends on the boundary at finite times. This is impossible since the wormhole is not traversable in the background [83, 84]).

Consider then the class of limiting curves that consist only of null and spacelike segments. If the proper length of all such curves is bounded below, then no such curve can be rendered causal by an arbitrarily small perturbation. Allowing timelike segments does not help, as that will necessarily make the spacelike segments longer. So if the wormhole can be rendered traversable by an arbitrarily small perturbation, there must be a sequence of such limiting curves whose proper length approaches zero. The limiting of this sequence is then a curve that is everywhere null. (We assume the spacetime to be sufficiently regular so that this sequence is guaranteed to converge.) It must also be a geodesic, else there would be a timelike curve that traverses the wormhole. And since it runs from the boundary to the boundary, it is a complete null curve (having infinite affine parameter).

Now, since the spacetime contains a wormhole, it has some non-trivial wormhole

[1]We use this term to refer to the regular part of the boundary; i.e., the part that is asymptotically flat or AdS and not the part of the conformal boundary describing spacetime singularities.

homotopy group (see footnote 4) that we can use to define a multiple cover M of the original spacetime $\tilde{M}$. The order of this cover does not matter. In the cover, our complete null curve lifts to at least one complete null curve that starts one connected component of the boundary and ends on another. That curve must be achronal, else the two boundaries would be causally connected (violating topological censorship [83, 84]). But since the original background (and thus the covering space) satisfies the null convergence condition, Galloway's splitting theorem (theorem 4.1 of [157]) requires the geodesic to lie on a stationary null surface. The projection of this surface to the original spacetime (a quotient of the cover) is thus stationary and null as well.

Appendix C

Counterpoint: Negative Energy causes collapse of cosmological wormholes

In order to contrast with our analysis above, and also because it provides a convenient exactly solvable model, we now briefly discuss analogous computations for what one may call a cosmological wormhole. Here we again consider a $\mathbb{Z}_2$ quotient of a covering spacetime $\tilde{M}$ having a globally-defined Killing symmetry, which in this case we take to be exact de Sitter space dS_d. In particular, in global coordinates we take the $\mathbb{Z}_2$ identification to be the antipodal map on the spheres at each global time. This is clearly a cosmological analogue of the $\mathbb{RP}_3$ geon. It is thus natural to think of it as a cosmological wormhole, though we will not attempt to introduce a general definition of this term.

As is well known, in de Sitter space perturbations satisfying the NEC tend to make the conformal diagram taller so that – at least in the natural sense defined by global coordinates – wormholes become *more* traversable; see figure C.1. This is evident from the classic Einstein static universe solution, in which the addition of positive energy dust to an otherwise-empty de Sitter space removes the cosmological expansion and leaves a static cylinder that can be circled by causal curves arbitrarily many times. That a similar effect occurs from general perturbations satisfying the NEC also follows from [144]. One thus expects the analogue of (5.28) to have the opposite sign. And since periodic scalars in the Hartle-Hawking state should again violate the null energy condition, they should *not* make our cosmological wormhole traversable. Indeed, they should make it more *non*-traversable than before. All of these expectations will be explicitly realized below.

In particular, it is straightforward to compute the analogue of (5.28), showing the effect of back-reaction. For simplicity, we treat only the rotationally symmetric case.

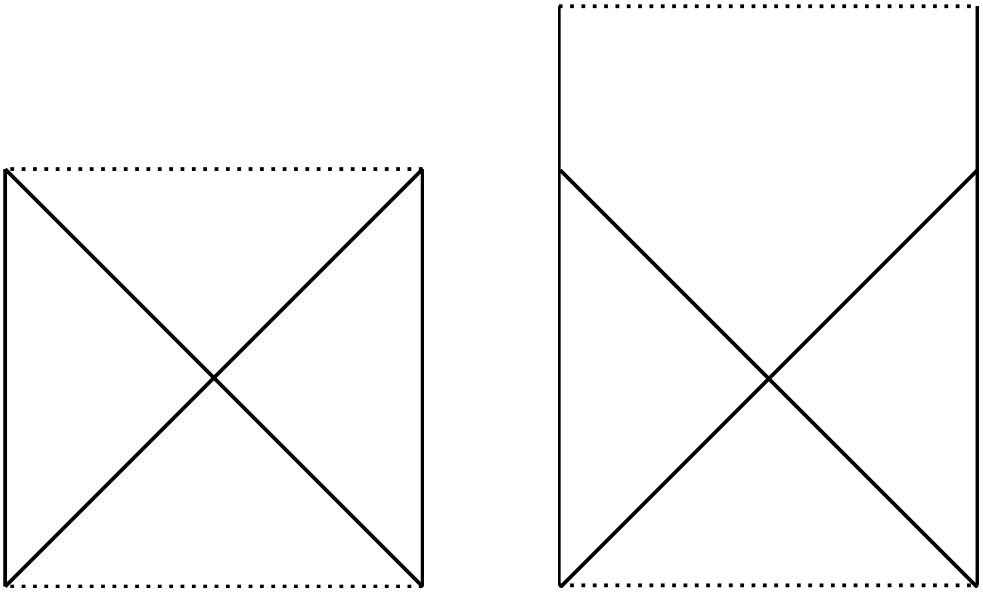

Figure C.1: (Left) A conformal diagram of dS_d showing time and the polar angle on the S^{d-1} (the other $d-2$ angles are suppressed). The left edge is the south pole of the S^{d-1} and the right edge is the north pole. The diagonal lines denote light rays. (Right) Perturbations satisfying the NEC generically make the diagram taller so that light rays can travel from the north pole to the south pole in finite time. Here for simplicity we consider perturbations that preserve spherical symmetry.

The dS_d metric with a general spherical perturbation is

$$ds^2 = \ell^2 \frac{-4dUdV + (1+UV)^2 d\Omega_{d-2}^2}{(1-UV)^2} + h_{UU}dU^2 + 2h_{UV}dUdV + h_{VV}dV^2 + h_{\Omega\Omega}d\Omega_{d-2}^2, \tag{C.1}$$

where $d\Omega_{d-2}^2$ is the standard metric on the unit S^{d-2} and where h_{UU}, h_{UV}, h_{VV}, $h_{\Omega\Omega}$ are functions of U, V. On the horizon $V = 0$, the linearized Einstein equation (with cosmological constant) yields

$$8\pi G T_{UU} = -\frac{d-2}{2\ell^2}\left(2h_{UU} + U\partial_U h_{UU} + \partial_U^2 h_{\Omega\Omega}\right). \tag{C.2}$$

The negative sign in the above expression shows that positive null-energy gives a time-advance, while negative null-energy gives a time-delay. In particular, we find

$$\Delta V = \frac{1}{8\ell^2}\int_{-\infty}^{\infty} h_{UU}dU = -\frac{\pi G}{d-2}\int_{-\infty}^{\infty} T_{UU}dU. \tag{C.3}$$

Since scalar two-point functions on dS_d are known in closed form for any mass $m \geq 0$ and dimension d, we may dispense with any cosmic strings and simply study scalars on $M = \mathrm{dS}_d/\mathbb{Z}_2$ coupled to pure Einstein-Hilbert gravity with a cosmological constant.

For simplicity, we ignore quantum effects from linearized gravitons. Neglecting such contributions is justified in the presence of a large number N of bulk scalar fields.

The scalar two-point function in the dS_d Hartle-Hawking state (also known as the Bunch-Davies vacuum or the Euclidean vacuum) takes the closed form expression [158, 159]

$$\begin{aligned} G\left(x,x'\right) =& \frac{1}{\left(4\pi\right)^{d/2}\ell^{d-2}}\frac{\Gamma\left(\frac{d-1}{2}-i\mu\right)\Gamma\left(\frac{d-1}{2}+i\mu\right)}{\Gamma\left(\frac{d}{2}\right)} \\ & \times {}_2F_1\left(\frac{d-1}{2}-i\mu,\frac{d-1}{2}+i\mu;\frac{d}{2};1-\frac{D\left(x,x'\right)}{4\ell^2}\right), \end{aligned} \tag{C.4}$$

where $\mu \equiv \sqrt{m^2\ell^2-\frac{1}{4}}$, and $D\left(x,x'\right)$ is the (squared) distance between x and x' in the $(d+1)$-dimensional Minkowski spacetime into which dS_d is naturally embedded. In some references, $D\left(x,x'\right)$ is called the 'chordal distance' between x and x'.

In global coordinates, the de Sitter line element is

$$ds_d^2 = \frac{\ell^2}{\cos^2\eta}\left(-d\eta^2+d\theta^2+\sin^2\theta d\Omega_{d-2}^2\right), \tag{C.5}$$

with $\theta\in[0,\pi]$. The $\mathbb{Z}_2$ quotient identifies each point (η,θ,Ω) with point $(\eta,\pi-\theta,a(\Omega))$ where $\Omega\in S^{d-2}$ and $a(\Omega)$ denotes the S^{d-2} antipodal map. We want to compute the two point function $G\left(U,U'\right)$ when the first point lies on horizon $\eta=\theta$ and has affine parameter U and the second point lies on the image horizon $\eta=\pi-\theta$ with affine parameter U'. The affinely-parametrized horizon is

$$\eta\left(U\right)=\arctan U,\ \theta\left(U\right)=\arctan U, \tag{C.6}$$

which becomes

$$T\left(U\right)=\ell U, X\left(U\right)=\ell, \vec{Y}\left(U\right)=\ell U\vec{z}, \tag{C.7}$$

in terms of the $d+1$ standard embedding coordinates $T,X,\vec{Y}$ such that $T^2-X^2-|\vec{Y}|^2=-\ell^2$. Here, $\vec{z}$ is a unit vector describing a S^{d-2}. The affine-parametrized image horizon is

$$T'\left(U'\right)=\ell U', X'\left(U'\right)=-\ell, \vec{Y}'\left(U'\right)=-\ell U'\vec{z}. \tag{C.8}$$

Thus, the chordal distance is

$$D\left(U,U'\right)=-(T-T')^2+(X-X')^2+|\vec{Y}-\vec{Y}'|^2=4\ell^2\left(1+UU'\right), \tag{C.9}$$

and the two point function is

$$\begin{aligned} G\left(U,U'\right) =& \frac{1}{\left(4\pi\right)^{d/2}\ell^{d-2}}\frac{\Gamma\left(\frac{d-1}{2}-i\mu\right)\Gamma\left(\frac{d-1}{2}+i\mu\right)}{\Gamma\left(\frac{d}{2}\right)} \\ & \times {}_2F_1\left(\frac{d-1}{2}-i\mu,\frac{d-1}{2}+i\mu;\frac{d}{2};-UU'\right). \end{aligned} \tag{C.10}$$

The stress tensor is then

$$\begin{aligned}T_{UU}(U) =& \lim_{U'\to U}\partial_U\partial_{U'}G(U,U') \\ =&\frac{1}{2^{d+2}\ell^{d-2}\pi^{d/2}}\frac{(d-1-2i\mu)(d-1+2i\mu)}{d(d+2)}\frac{\Gamma\left(\frac{d-1-2i\mu}{2}\right)\Gamma\left(\frac{d-1+2i\mu}{2}\right)}{\Gamma\left(\frac{d}{2}\right)} \\ &\times\left[-2(d+2)\,{}_2F_1\left(\frac{d+1-2i\mu}{2},\frac{d+1+2i\mu}{2};\frac{d+2}{2};-U^2\right)\right. \\ &\left.+U^2\left(d^2+2d+1+4\mu^2\right){}_2F_1\left(\frac{d+3-2i\mu}{2},\frac{d+3+2i\mu}{2};\frac{d+4}{2};-U^2\right)\right].\end{aligned} \tag{C.11}$$

Its integral is

$$\int_{-\infty}^{\infty}T_{UU}(U)\,dU=-\frac{\Gamma\left(\frac{d}{2}+1\right)\Gamma\left(\frac{d}{2}-i\mu\right)\Gamma\left(\frac{d}{2}+i\mu\right)}{2\ell^{d-2}\pi^{d/2}\Gamma(d+1)}<0. \tag{C.12}$$

Using the identity $\Gamma(1-z)\Gamma(z)=\frac{\pi}{\sin(\pi z)}$ one can rewrite the right-hand-side of (C.12) as a d-dependent polynomial in μ divided by $\sinh(\mu+i\pi\frac{d}{2})$ (i.e., divided by either $\sinh(\mu)$ or $\cosh(\mu)$ depending on whether d is even or odd). The polynomial has a definite sign such that the overall expression is negative for all allowed μ, and the factor of $\sinh(\mu+i\pi\frac{d}{2})$ in the denominator means that it decreases exponentially at large μ.

Appendix D

Constructing the wormhole

In this section, we will explicitly construct the wormhole solution in the case of [88], by perturbing the original solution with a point mass delta function source for the small black hole. As we have seen, we are considering two RN black holes, whose throats we have replaced with a single global $AdS_2 \times S^2$ metric. However, this approximation is valid around $\rho = 0$ point, which corresponds to "the middle of the throat", but as we are climbing up the throat, the spheres are becoming larger and so we have to account for that effect. Hence, instead of putting the sizes of the spheres to be constant, $r_e^2 d\Omega^2$, we will perturb them a little bit and solve for the small parameter as a function of ρ - now we will have $r_e^2(1+\phi)d\Omega^2$. Similarly, we modify $g_{\tau\tau}$ and $g_{\rho\rho}$ components - we will add a small parameter $\gamma = \gamma(\rho)$, which will describe the departure from the $AdS_2 \times S^2$ metric. So, our ansatz will have the following form:

$$ds^2 = r_e^2[-(1+\rho^2+\gamma)d\tau^2 + \frac{d\rho^2}{1+\rho^2+\gamma} + (1+\phi)d\Omega^2]. \tag{D.1}$$

Since the parameters γ and ϕ are small, we can expand the denominator ($g_{\rho\rho}$) in terms of γ:

$$\frac{1}{1+\rho^2+\gamma} \simeq \frac{1}{1+\rho^2}\left(1 - \frac{\gamma}{1+\rho^2}\right). \tag{D.2}$$

When computing the Einstein tensor, we will neglect all second order quantities in ϕ and γ. After some algebra, we get the Einstein tensor by components:

$$G_{\tau\tau} = \gamma - (1+\rho^2)(-1+\rho\phi' + (1+\rho^2)\phi'') - (1+\rho^2)\phi + ... \tag{D.3}$$

$$G_{\rho\rho} = (1+\rho^2)^{-2}(\gamma + (1+\rho^2)(-1+\phi+\rho\phi')) + ... \tag{D.4}$$

$$G_{\theta\theta} = \frac{1}{2}(2 + 2\phi + 2\rho\phi' + (1+\rho^2)\phi'' + \gamma'') + ... \tag{D.5}$$

$$G_{\Phi\Phi} = \frac{1}{2}\sin^2\theta(2 + 2\phi + 2\rho\phi' + (1+\rho^2)\phi'' + \gamma'') + ... \tag{D.6}$$

For our purposes, it is enough to consider only the second equation (D.4). The ρ-component of the stress energy tensor will have three contributions - one coming from the Maxwell field, another from the Dirac fermions and the third one is the small black hole contribution.

The Maxwell stress energy tensor has the following form:

$$T_{\mu\nu} = \frac{1}{g^2}(F_{\mu\sigma}F_{\nu}^{\ \sigma} - \frac{1}{4}g_{\mu\nu}F^2). \tag{D.7}$$

Since Maxwell field strength is given as $F = -\frac{q}{2}\sin\theta d\theta d\phi$, we only have two components of the field strength, $F_{\theta\phi} = F_{\phi\theta}$. Hence, only the second part of (D.7) stays:

$$\begin{aligned} F^2 &= F_{\mu\nu}F^{\mu\nu} = F_{\theta\phi}F^{\theta\phi} + F_{\phi\theta}F^{\phi\theta} \\ &= 2g^{\theta\theta}g^{\phi\phi}F_{\theta\phi}^2 = \frac{1}{r_e^4(1+\phi)^2\sin^2\theta}\frac{2q^2}{4}\sin^2\theta \\ &= \frac{q^2}{2r_e^4}(1-2\phi), \end{aligned} \tag{D.8}$$

where we have used the fact that the parameter ϕ is small. Now, the whole tensor can be written as:

$$\begin{aligned} T_{\rho\rho}^M &= -\frac{1}{4g^2}g_{\rho\rho}F^2 = -\frac{1}{4g^2}\frac{r_e^2}{1+\rho^2+\gamma}\frac{q^2}{2r_e^4}(1-2\phi) \\ &= -\frac{q^2}{8g^2r_e^2}\frac{1}{1+\rho^2}\left(1-2\phi-\frac{\gamma}{1+\rho^2}\right). \end{aligned} \tag{D.9}$$

If we recall now that $r_e^2 = \pi q^2 G_N g^{-2}$, we get:

$$8\pi G_N\frac{q^2}{8g^2}\frac{g^2}{\pi q^2 G_N} = 1, \tag{D.10}$$

and so, from

$$G_{\rho\rho} = 8\pi G_N(T_{\rho\rho}^M + T_{\rho\rho}^F + T_{\rho\rho}^\delta), \tag{D.11}$$

we get:

$$\rho\phi' - \phi = 8\pi G_N(1+\rho^2)(T_{\rho\rho}^F + T_{\rho\rho}^\delta). \tag{D.12}$$

We take the fermion contribution to be the same as in [88], and so

$$8\pi G_N T_{\rho\rho}^F = -\frac{\alpha}{(1+\rho^2)^2}, \qquad \alpha \equiv \frac{qG_N}{4\pi r_e^2}. \tag{D.13}$$

Putting the delta function source in the energy equation, that is $G_{\tau\tau}$ and solving for

ϕ, we find,

$$\phi_\tau(\rho) = \alpha(1 + \rho \arctan \rho) + c_1\sqrt{1+\rho^2} + ic_2\rho - \beta\rho\Theta(\rho), \tag{D.14}$$

where we can put $c_2 = 0$. Computing the second derivative, we obtain

$$\phi''_\tau(\rho) = \frac{2\alpha}{(1+\rho^2)^2} + \frac{c_1}{(1+\rho^2)^{3/2}} - \beta\delta(\rho). \tag{D.15}$$

Therefore, in the case where β dominates over α and c_1, we have a change in the sign of the derivative of the expansion scalar, and hence, we no longer have the defocusing effect, only focusing. This will also tell us what is the maximum size of the small black hole that we can put in the wormhole. In order to determine the size, let us first set c_1 to zero[1] and let us look at the equation (D.15) near $\rho = 0$. We see that the change in the sign is determined by the ratio α/β, since if α is bigger than β, then the small black hole does not change the inner dynamics of the wormhole. If it is smaller, the small black hole becomes too large and our construction breaks down. From this ratio, we can therefore determine the maximal mass of the small black hole, M_0. However, before we get to the trivial algebra, we must set the units correctly. We are working in units where energy is proportional to the inverse of the length and where we have extracted the length scale out of the metric like r_e^2. Hence, $G_{\tau\tau}$ is dimensionless. We see that α is set in correct units already then since $\alpha = \frac{qG}{4\pi r_e^2}$, where $G = \ell_p^2$. The coefficient β is of order r_e^{-1} which with $\delta(r_e\rho) = \frac{\delta(\rho)}{r_e}$ makes it of order of inverse squared length. So, in order to make it dimensionless, we have to multiply by r_e^2. Now we can see the ratios:

$$\frac{\beta}{\alpha} = \frac{2G_N M_0}{r_e^2} \times \frac{1}{r_e} \times r_e^2 \times \frac{4\pi r_e^2}{qG_N} \tag{D.16}$$

The critical case is when this ratio is of order 1, and so we get a bound on the mass as

$$M_0 = \frac{q}{8\pi r_e} = \frac{qg}{8\pi^{3/2} q\ell_p} \propto \frac{g}{\ell_p} \tag{D.17}$$

Adding N_f flavors gives

$$M_0 < \frac{qN_f}{8\pi r_e} = \frac{N_f g}{8\pi^{3/2}\ell_p}. \tag{D.18}$$

To compute the effect on the energy as seen from the outside, however, we include an

[1] In [88], solution for ϕ was obtained from the $G_{\rho\rho}$ equation which satisfies the symmetry $\rho \to -\rho$. From here, all the constants go to zero (except for α) and such a solution automatically obeys the $G_{\tau\tau}$ equation. Here we were solving first in the energy equation, where we cannot apply the symmetry argument. Nevertheless, $c_1 = 0$ is compatible with the wormhole construction and it makes the analysis for the size of the small black hole easier to understand.

additional redshift factor, r_e/d, bringing the energy to

$$E_{bh} < \frac{r_e g N_f}{8\pi^{3/2}\ell_p d} \tag{D.19}$$

We can compare this to

$$E_{min} = \frac{r_e g N_f}{16\pi^{1/2}\ell_p d} \tag{D.20}$$

so that $E_{bh} < \frac{2}{\pi} E_{min}$.

Bibliography

[1] S. Hawking, *Black hole explosions*, *Nature* **248** (1974) 30–31.

[2] J. D. Bekenstein, *Generalized second law of thermodynamics in black hole physics*, *Phys. Rev. D* **9** (1974) 3292–3300.

[3] R. M. Wald, *General Relativity*. Chicago Univ. Pr., Chicago, USA, 1984.

[4] S. W. Hawking, *Particle creation by black holes*, *Comm. Math. Phys.* **43** (1975), no. 3 199–220.

[5] R. Bousso, *A Covariant entropy conjecture*, *JHEP* **07** (1999) 004, [hep-th/9905177].

[6] R. Bousso, *The Holographic principle*, *Rev. Mod. Phys.* **74** (2002) 825–874, [hep-th/0203101].

[7] R. Bousso and N. Engelhardt, *Proof of a New Area Law in General Relativity*, *Phys. Rev. D* **92** (2015), no. 4 044031, [arXiv:1504.0766].

[8] R. Bousso and N. Engelhardt, *New Area Law in General Relativity*, *Phys. Rev. Lett.* **115** (2015), no. 8 081301, [arXiv:1504.0762].

[9] S. Ryu and T. Takayanagi, *Holographic derivation of entanglement entropy from AdS/CFT*, *Phys. Rev. Lett.* **96** (2006) 181602, [hep-th/0603001].

[10] M. Headrick and T. Takayanagi, *A Holographic proof of the strong subadditivity of entanglement entropy*, *Phys. Rev. D* **76** (2007) 106013, [arXiv:0704.3719].

[11] A. Lewkowycz and J. Maldacena, *Generalized Gravitational Entropy*, *JHEP* **08** (2013) 090, [arXiv:1304.4926].

[12] V. E. Hubeny, M. Rangamani, and T. Takayanagi, *A Covariant holographic entanglement entropy proposal*, *JHEP* **07** (2007) 062, [arXiv:0705.0016].

[13] A. C. Wall, *Maximin Surfaces, and the Strong Subadditivity of the Covariant Holographic Entanglement Entropy*, *Class. Quant. Grav.* **31** (2014), no. 22 225007, [arXiv:1211.3494].

[14] N. Engelhardt and A. C. Wall, *Decoding the Apparent Horizon: Coarse-Grained Holographic Entropy*, *Phys. Rev. Lett.* **121** (2018), no. 21 211301, [arXiv:1706.0203].

[15] P. Gao, D. L. Jafferis, and A. Wall, *Traversable Wormholes via a Double Trace Deformation*, *JHEP* **12** (2017) 151, [arXiv:1608.0568].

[16] J. Maldacena and L. Susskind, *Cool horizons for entangled black holes*, *Fortsch. Phys.* **61** (2013) 781–811, [arXiv:1306.0533].

[17] V. Balasubramanian, P. Hayden, A. Maloney, D. Marolf, and S. F. Ross, *Multiboundary Wormholes and Holographic Entanglement*, *Class. Quant. Grav.* **31** (2014) 185015, [arXiv:1406.2663].

[18] B. Grado-White, D. Marolf, and S. J. Weinberg, *Radial Cutoffs and Holographic Entanglement*, arXiv:2008.0702.

[19] J. M. Maldacena, *The Large N limit of superconformal field theories and supergravity*, *Int. J. Theor. Phys.* **38** (1999) 1113–1133, [hep-th/9711200].

[20] N. Engelhardt and A. C. Wall, *Extremal Surface Barriers*, *JHEP* **03** (2014) 068, [arXiv:1312.3699].

[21] A. Ashtekar and B. Krishnan, *Dynamical horizons and their properties*, *Phys. Rev. D* **68** (2003) 104030, [gr-qc/0308033].

[22] S. Hayward, *General laws of black hole dynamics*, *Phys. Rev. D* **49** (1994) 6467–6474.

[23] F. Sanches and S. J. Weinberg, *Holographic entanglement entropy conjecture for general spacetimes*, *Phys. Rev. D* **94** (2016), no. 8 084034, [arXiv:1603.0525].

[24] V. E. Hubeny and M. Rangamani, *Causal Holographic Information*, *JHEP* **06** (2012) 114, [arXiv:1204.1698].

[25] B. Freivogel and B. Mosk, *Properties of Causal Holographic Information*, *JHEP* **09** (2013) 100, [arXiv:1304.7229].

[26] W. R. Kelly and A. C. Wall, *Coarse-grained entropy and causal holographic information in AdS/CFT*, *JHEP* **03** (2014) 118, [arXiv:1309.3610].

[27] N. Engelhardt and A. C. Wall, *No Simple Dual to the Causal Holographic Information?*, *JHEP* **04** (2017) 134, [arXiv:1702.0174].

[28] W. Bunting, Z. Fu, and D. Marolf, *A coarse-grained generalized second law for holographic conformal field theories*, *Class. Quant. Grav.* **33** (2016), no. 5 055008, [arXiv:1509.0007].

[29] C. Fefferman and R. Graham, *Conformal invariants*, *Elie Cartan et les Mathematiques d'aujourd'hui, Asterisque* (1985) 95.

[30] R. Bousso, *Holography in general space-times*, *JHEP* **06** (1999) 028, [hep-th/9906022].

[31] T. Faulkner, A. Lewkowycz, and J. Maldacena, *Quantum corrections to holographic entanglement entropy*, *JHEP* **11** (2013) 074, [arXiv:1307.2892].

[32] D. L. Jafferis, A. Lewkowycz, J. Maldacena, and S. J. Suh, *Relative entropy equals bulk relative entropy*, *JHEP* **06** (2016) 004, [arXiv:1512.0643].

[33] X. Dong and A. Lewkowycz, *Entropy, Extremality, Euclidean Variations, and the Equations of Motion*, *JHEP* **01** (2018) 081, [arXiv:1705.0845].

[34] L. McGough, M. Mezei, and H. Verlinde, *Moving the CFT into the bulk with $T\overline{T}$*, *JHEP* **04** (2018) 010, [arXiv:1611.0347].

[35] M. Taylor, *TT deformations in general dimensions*, arXiv:1805.1028.

[36] T. Hartman, J. Kruthoff, E. Shaghoulian, and A. Tajdini, *Holography at finite cutoff with a T^2 deformation*, *JHEP* **03** (2019) 004, [arXiv:1807.1140].

[37] M. Guica and R. Monten, *$T\bar{T}$ and the mirage of a bulk cutoff*, arXiv:1906.1125.

[38] B. Swingle, *Entanglement Renormalization and Holography*, *Phys. Rev.* **D86** (2012) 065007, [arXiv:0905.1317].

[39] X.-L. Qi, *Exact holographic mapping and emergent space-time geometry*, arXiv:1309.6282.

[40] G. Evenbly and G. Vidal, *Tensor network states and geometry*, *Journal of Statistical Physics* **145** (Nov, 2011) 891–918.

[41] J. Molina-Vilaplana and P. Sodano, *Holographic View on Quantum Correlations and Mutual Information between Disjoint Blocks of a Quantum Critical System*, *JHEP* **10** (2011) 011, [arXiv:1108.1277].

[42] B. Swingle, *Constructing holographic spacetimes using entanglement renormalization*, arXiv:1209.3304.

[43] H. Matsueda, M. Ishihara, and Y. Hashizume, *Tensor network and a black hole*, *Phys. Rev.* **D87** (2013), no. 6 066002, [arXiv:1208.0206].

[44] F. Pastawski, B. Yoshida, D. Harlow, and J. Preskill, *Holographic quantum error-correcting codes: Toy models for the bulk/boundary correspondence*, *JHEP* **06** (2015) 149, [arXiv:1503.0623].

[45] P. Hayden, S. Nezami, X.-L. Qi, N. Thomas, M. Walter, and Z. Yang, *Holographic duality from random tensor networks*, *JHEP* **11** (2016) 009, [arXiv:1601.0169].

[46] M. Miyaji and T. Takayanagi, *Surface/State Correspondence as a Generalized Holography*, *PTEP* **2015** (2015), no. 7 073B03, [arXiv:1503.0354].

[47] T. Takayanagi and K. Umemoto, *Entanglement of purification through holographic duality*, *Nature Phys.* **14** (2018), no. 6 573–577, [arXiv:1708.0939].

[48] P. Nguyen, T. Devakul, M. G. Halbasch, M. P. Zaletel, and B. Swingle, *Entanglement of purification: from spin chains to holography*, *JHEP* **01** (2018) 098, [arXiv:1709.0742].

[49] N. Bao, G. Penington, J. Sorce, and A. C. Wall, *Beyond Toy Models: Distilling Tensor Networks in Full AdS/CFT*, arXiv:1812.0117.

[50] N. Bao, G. Penington, J. Sorce, and A. C. Wall, *Holographic Tensor Networks in Full AdS/CFT*, arXiv:1902.1015.

[51] C. Krishnan, *Bulk Locality and Asymptotic Causal Diamonds*, *SciPost Phys.* **7** (2019), no. 4 057, [arXiv:1902.0670].

[52] C. Krishnan, V. Patil, and J. Pereira, *Page Curve and the Information Paradox in Flat Space*, arXiv:2005.0299.

[53] S. Ryu and T. Takayanagi, *Aspects of Holographic Entanglement Entropy*, *JHEP* **08** (2006) 045, [hep-th/0605073].

[54] W. Donnelly and V. Shyam, *Entanglement entropy and $T\overline{T}$ deformation*, *Phys. Rev. Lett.* **121** (2018), no. 13 131602, [arXiv:1806.0744].

[55] A. Lewkowycz, J. Liu, E. Silverstein, and G. Torroba, *$T\bar{T}$ and EE, with implications for (A)dS subregion encodings*, arXiv:1909.1380.

[56] H. Geng, *Some Information Theoretic Aspects of De-Sitter Holography*, *JHEP* **02** (2020) 005, [arXiv:1911.0264].

[57] Y. Nomura, P. Rath, and N. Salzetta, *Pulling the Boundary into the Bulk*, *Phys. Rev. D* **98** (2018), no. 2 026010, [arXiv:1805.0052].

[58] C. Murdia, Y. Nomura, and P. Rath, *Coarse-Graining Holographic States: A Semiclassical Flow in General Spacetimes*, arXiv:2008.0175.

[59] D. Marolf, A. C. Wall, and Z. Wang, *Restricted Maximin surfaces and HRT in generic black hole spacetimes*, *JHEP* **05** (2019) 127, [arXiv:1901.0387].

[60] P. Hayden, M. Headrick, and A. Maloney, *Holographic Mutual Information is Monogamous*, *Phys. Rev.* **D87** (2013), no. 4 046003, [arXiv:1107.2940].

[61] G. Penington, *Entanglement Wedge Reconstruction and the Information Paradox*, arXiv:1905.0825.

[62] A. Almheiri, N. Engelhardt, D. Marolf, and H. Maxfield, *The entropy of bulk quantum fields and the entanglement wedge of an evaporating black hole*, *JHEP* **12** (2019) 063, [arXiv:1905.0876].

[63] A. Almheiri, R. Mahajan, J. Maldacena, and Y. Zhao, *The Page curve of Hawking radiation from semiclassical geometry*, arXiv:1908.1099.

[64] A. Almheiri, R. Mahajan, and J. Maldacena, *Islands outside the horizon*, arXiv:1910.1107.

[65] M. Rozali, J. Sully, M. Van Raamsdonk, C. Waddell, and D. Wakeham, *Information radiation in BCFT models of black holes*, arXiv:1910.1283.

[66] H. Z. Chen, Z. Fisher, J. Hernandez, R. C. Myers, and S.-M. Ruan, *Information Flow in Black Hole Evaporation*, arXiv:1911.0340.

[67] R. Bousso and M. Tomaˇ sević, *Unitarity From a Smooth Horizon?*, arXiv:1911.0630.

[68] A. Almheiri, R. Mahajan, and J. E. Santos, *Entanglement islands in higher dimensions*, arXiv:1911.0966.

[69] A. Almheiri, T. Hartman, J. Maldacena, E. Shaghoulian, and A. Tajdini, *Replica Wormholes and the Entropy of Hawking Radiation*, arXiv:1911.1233.

[70] G. Penington, S. H. Shenker, D. Stanford, and Z. Yang, *Replica wormholes and the black hole interior*, arXiv:1911.1197.

[71] M. Headrick and V. Hubeny. To appear.

[72] H. Casini and M. Huerta, *A c-theorem for the entanglement entropy*, *J. Phys.* **A40** (2007) 7031–7036, [cond-mat/0610375].

[73] C. Akers, R. Bousso, I. F. Halpern, and G. N. Remmen, *Boundary of the future of a surface*, *Phys. Rev.* **D97** (2018), no. 2 024018, [arXiv:1711.0668].

[74] M. Rota and S. J. Weinberg, *New constraints for holographic entropy from maximin: A no-go theorem*, *Phys. Rev. D* **97** (2018), no. 8 086013, [arXiv:1712.1000].

[75] P. T. Chrusciel, E. Delay, G. J. Galloway, and R. Howard, *The Area theorem*, *Annales Henri Poincare* **2** (2001) 109–178, [gr-qc/0001003].

[76] S. W. Hawking, *Gravitational Radiation from Colliding Black Holes*, *Phys. Rev. Lett.* **26** (1971) 1344–1346.

[77] X. Dong, A. Lewkowycz, and M. Rangamani, *Deriving covariant holographic entanglement*, *JHEP* **11** (2016) 028, [arXiv:1607.0750].

[78] W. Donnelly, E. LePage, Y.-Y. Li, A. Pereira, and V. Shyam, *Quantum corrections to finite radius holography and holographic entanglement entropy*, *JHEP* **05** (2020) 006, [arXiv:1909.1140].

[79] C. Murdia, Y. Nomura, P. Rath, and N. Salzetta, *Comments on holographic entanglement entropy in TT deformed conformal field theories*, *Phys. Rev. D* **100** (2019), no. 2 026011, [arXiv:1904.0440].

[80] A. Einstein and N. Rosen, *The Particle Problem in the General Theory of Relativity*, *Phys. Rev.* **48** (1935) 73–77.

[81] J. C. Graves and D. R. Brill, *Oscillatory Character of Reissner-Nordstrom Metric for an Ideal Charged Wormhole*, *Phys. Rev.* **120** (1960) 1507–1513.

[82] M. S. Morris, K. S. Thorne, and U. Yurtsever, *Wormholes, Time Machines, and the Weak Energy Condition*, *Phys. Rev. Lett.* **61** (1988) 1446–1449.

[83] J. L. Friedman, K. Schleich, and D. M. Witt, *Topological censorship*, *Phys. Rev. Lett.* **71** (1993) 1486–1489, [gr-qc/9305017]. [Erratum: Phys. Rev. Lett.75,1872(1995)].

[84] G. J. Galloway, K. Schleich, D. M. Witt, and E. Woolgar, *Topological censorship and higher genus black holes*, *Phys. Rev.* **D60** (1999) 104039, [gr-qc/9902061].

[85] E. Caceres, A. S. Misobuchi, and M.-L. Xiao, *Rotating traversable wormholes in AdS*, arXiv:1807.0723.

[86] C. Bachas and I. Lavdas, *Quantum Gates to other Universes*, *Fortsch. Phys.* **66** (2018), no. 2 1700096, [arXiv:1711.1137].

[87] A. Almheiri, A. Mousatov, and M. Shyani, *Escaping the Interiors of Pure Boundary-State Black Holes*, arXiv:1803.0443.

[88] J. Maldacena, A. Milekhin, and F. Popov, *Traversable wormholes in four dimensions*, arXiv:1807.0472.

[89] J. Maldacena and X.-L. Qi, *Eternal traversable wormhole*, arXiv:1804.0049.

[90] Z. Fu, D. Marolf, and E. Mefford, *Time-independent wormholes*, *JHEP* **12** (2016) 021, [arXiv:1610.0806].

[91] D. Giulini. PhD thesis, University of Cambridge, 1989.

[92] C. W. Misner and J. A. Wheeler, *Classical physics as geometry: Gravitation, electromagnetism, unquantized charge, and mass as properties of curved empty space*, *Annals Phys.* **2** (1957) 525–603.

[93] A. C. Wall, *Proving the Achronal Averaged Null Energy Condition from the Generalized Second Law*, *Phys. Rev.* **D81** (2010) 024038, [arXiv:0910.5751].

[94] A. C. Wall, *A proof of the generalized second law for rapidly changing fields and arbitrary horizon slices*, *Phys. Rev.* **D85** (2012) 104049, [arXiv:1105.3445]. [Erratum: Phys. Rev.D87,no.6,069904(2013)].

[95] R. Bousso, Z. Fisher, J. Koeller, S. Leichenauer, and A. C. Wall, *Proof of the Quantum Null Energy Condition*, *Phys. Rev.* **D93** (2016), no. 2 024017, [arXiv:1509.0254].

[96] T. Faulkner, R. G. Leigh, O. Parrikar, and H. Wang, *Modular Hamiltonians for Deformed Half-Spaces and the Averaged Null Energy Condition*, *JHEP* **09** (2016) 038, [arXiv:1605.0807].

[97] T. Hartman, S. Kundu, and A. Tajdini, *Averaged Null Energy Condition from Causality*, *JHEP* **07** (2017) 066, [arXiv:1610.0530].

[98] S. Balakrishnan, T. Faulkner, Z. U. Khandker, and H. Wang, *A General Proof of the Quantum Null Energy Condition*, arXiv:1706.0943.

[99] J. Louko and D. Marolf, *Single exterior black holes and the AdS / CFT conjecture*, *Phys. Rev.* **D59** (1999) 066002, [hep-th/9808081].

[100] J. Louko, R. B. Mann, and D. Marolf, *Geons with spin and charge*, *Class. Quant. Grav.* **22** (2005) 1451–1468, [gr-qc/0412012].

[101] T. Hartman and J. Maldacena, *Time Evolution of Entanglement Entropy from Black Hole Interiors*, *JHEP* **05** (2013) 014, [arXiv:1303.1080].

[102] J. Louko and D. Marolf, *Inextendible Schwarzschild black hole with a single exterior: How thermal is the Hawking radiation?*, *Phys. Rev.* **D58** (1998) 024007, [gr-qc/9802068].

[103] R. M. Wald, *Quantum Field Theory in Curved Space-Time and Black Hole Thermodynamics*. Chicago Lectures in Physics. University of Chicago Press, Chicago, IL, 1995.

[104] J. M. Maldacena, *Eternal black holes in anti-de Sitter*, *JHEP* **04** (2003) 021, [hep-th/0106112].

[105] S. Sachdev and J. Ye, *Gapless spin-fluid ground state in a random quantum Heisenberg magnet*, *Physical Review Letters* **70** (May, 1993) 3339–3342, [cond-mat/9212030].

[106] A. Kitaev, "A simple model of quantum holography." http://online.kitp.ucsb.edu/online/entangled15/kitaev/,http://online.kitp.ucsb.edu/online/entangled15/kitaev2/. Talks at KITP, April 7, 2015 and May 27, 2015.

[107] J. Maldacena, D. Stanford, and Z. Yang, *Conformal symmetry and its breaking in two dimensional Nearly Anti-de-Sitter space*, *PTEP* **2016** (2016), no. 12 12C104, [arXiv:1606.0185].

[108] T. Andrade and D. Marolf, *AdS/CFT beyond the unitarity bound*, *JHEP* **01** (2012) 049, [arXiv:1105.6337].

[109] I. Ichinose and Y. Satoh, *Entropies of scalar fields on three-dimensional black holes*, *Nucl. Phys.* **B447** (1995) 340–372, [hep-th/9412144].

[110] J. Louko, D. Marolf, and S. F. Ross, *On geodesic propagators and black hole holography*, *Phys. Rev.* **D62** (2000) 044041, [hep-th/0002111].

[111] D. Marolf, *The dangers of extremes*, *Gen. Rel. Grav.* **42** (2010) 2337–2343, [arXiv:1005.2999].

[112] D. Marolf and A. Ori, *Outgoing gravitational shock-wave at the inner horizon: The late-time limit of black hole interiors*, *Phys. Rev.* **D86** (2012) 124026, [arXiv:1109.5139].

[113] S. Aretakis, *Stability and Instability of Extreme Reissner-Nordström Black Hole Spacetimes for Linear Scalar Perturbations I*, *Commun. Math. Phys.* **307** (2011) 17–63, [arXiv:1110.2007].

[114] S. Aretakis, *Stability and Instability of Extreme Reissner-Nordstrom Black Hole Spacetimes for Linear Scalar Perturbations II*, *Annales Henri Poincare* **12** (2011) 1491–1538, [arXiv:1110.2009].

[115] S. Aretakis, *Decay of Axisymmetric Solutions of the Wave Equation on Extreme Kerr Backgrounds*, *J. Funct. Anal.* **263** (2012) 2770–2831, [arXiv:1110.2006].

[116] S. Aretakis, *Horizon Instability of Extremal Black Holes*, *Adv. Theor. Math. Phys.* **19** (2015) 507–530, [arXiv:1206.6598].

[117] J. Lucietti and H. S. Reall, *Gravitational instability of an extreme Kerr black hole*, *Phys. Rev.* **D86** (2012) 104030, [arXiv:1208.1437].

[118] M. Casals, S. E. Gralla, and P. Zimmerman, *Horizon Instability of Extremal Kerr Black Holes: Nonaxisymmetric Modes and Enhanced Growth Rate*, *Phys. Rev.* **D94** (2016), no. 6 064003, [arXiv:1606.0850].

[119] H. Weyl, *Zue gravitationstheorie*, *Ann. der Physik* **54** (1917) 117–145.

[120] R. Bach and H. Weyl, *Neue lösungen der einsteinschen gravitationsgleichungen*, *Math Z.* **13** (1922) 134.

[121] W. Israel and K. A. Khan, *Collinear particles and bondi dipoles in general relativity*, *Il Nuovo Cimento (1955-1965)* **33** (Jul, 1964) 331–344.

[122] F. Dowker, J. P. Gauntlett, D. A. Kastor, and J. H. Traschen, *Pair creation of dilaton black holes*, *Phys. Rev.* **D49** (1994) 2909–2917, [hep-th/9309075].

[123] F. Dowker, J. P. Gauntlett, S. B. Giddings, and G. T. Horowitz, *On pair creation of extremal black holes and Kaluza-Klein monopoles*, *Phys. Rev.* **D50** (1994) 2662–2679, [hep-th/9312172].

[124] H. Stephani, D. Kramer, M. A. H. MacCallum, C. Hoenselaers, and E. Herlt, *Exact solutions of Einstein's field equations*. Cambridge Monographs on Mathematical Physics. Cambridge Univ. Press, Cambridge, 2003. Chapter 20.

[125] D. N. Page, *Particle Emission Rates from a Black Hole. 2. Massless Particles from a Rotating Hole*, *Phys. Rev.* **D14** (1976) 3260–3273.

[126] E. Ayon-Beato, F. Canfora, and J. Zanelli, *Analytic self-gravitating Skyrmions, cosmological bounces and AdS wormholes*, *Phys. Lett.* **B752** (2016) 201–205, [arXiv:1509.0265].

[127] F. Canfora, N. Dimakis, and A. Paliathanasis, *Topologically nontrivial configurations in the 4d einstein-nonlinear σ-model system*, *Phys. Rev. D* **96** (Jul, 2017) 025021.

[128] A. C. Wall, *The Generalized Second Law implies a Quantum Singularity Theorem*, *Class. Quant. Grav.* **30** (2013) 165003, [arXiv:1010.5513]. [Erratum: Class. Quant. Grav.30,199501(2013)].

[129] M. Visser, *Lorentzian wormholes: From Einstein to Hawking*. 1995.

[130] F. S. N. Lobo, *Exotic solutions in General Relativity: Traversable wormholes and 'warp drive' spacetimes*, in *Classical and Quantum Gravity Research, 1-78, (2008), Nova Sci. Pub. ISBN 978-1-60456-366-5*. 2007. arXiv:0710.4474.

[131] J. Maldacena, D. Stanford, and Z. Yang, *Diving into traversable wormholes*, *Fortsch. Phys.* **65** (2017), no. 5 1700034, [arXiv:1704.0533].

[132] Z. Fu, B. Grado-White, and D. Marolf, *A perturbative perspective on self-supporting wormholes*, *Class. Quant. Grav.* **36** (2019), no. 4 045006, [arXiv:1807.0791].

[133] G. T. Horowitz, D. Marolf, J. E. Santos, and D. Wang, *Creating a Traversable Wormhole*, *Class. Quant. Grav.* **36** (2019), no. 20 205011, [arXiv:1904.0218].

[134] D. Marolf and S. McBride, *Simple Perturbatively Traversable Wormholes from Bulk Fermions*, *JHEP* **11** (2019) 037, [arXiv:1908.0399].

[135] R. Emparan and E. Teo, *Macroscopic and microscopic description of black diholes*, *Nucl. Phys.* **B610** (2001) 190–214, [hep-th/0104206].

[136] M. J. Manko V. S. and R. E., *Metric of two arbitrary Kerr-Newman sources. located on the symmetry axis*, *J. Math. Phys.* **35** (1995) 6644–6657.

[137] W. B. Bonnor, *An exact solution of the Einstein-Maxwell equations referring to a magnetic dipole*, *Z. Physik* **190** (1966) 444–445.

[138] S. Chandrasekhar and B. C. Xanthopoulos, *Two black holes attached to strings*, *Proc. Roy. Soc. Lond.* **A423** (1989) 387–400.

[139] A. Davidson and E. Gedalin, *Finite magnetic flux tube as a black and white dihole*, *Phys. Lett.* **B339** (1994) 304–308, [gr-qc/9408006].

[140] R. Emparan, *Black diholes*, *Phys. Rev.* **D61** (2000) 104009, [hep-th/9906160].

[141] J. McNamara, *Instability of Black Hole Inner Horizons*, *Proc. Roy. Soc. Lon.* **358** (1978) 499–517.

[142] P. Di Francesco, P. Mathieu, and D. Senechal, *Conformal Field Theory*. Graduate Texts in Contemporary Physics. Springer-Verlag, New York, 1997.

[143] S. Fischetti and D. Marolf, *Flowing Funnels: Heat sources for field theories and th AdS_3 dual of CFT_2 Hawking radiation*, *Class. Quant. Grav.* **29** (2012) 105004, [arXiv:1202.5069].

[144] S. Gao and R. M. Wald, *Theorems on Gravitational Time Delay and Related Issues*, *Class. Quant. Grav.* **17** (2000) 4999–5008, [gr-qc/0007021].

[145] R. Szmytkowski, *Closed forms of the green's function and the generalized green's function for the helmholtz operator on the n-dimensional unit sphere*, *Journal of Physics A: Mathematical and Theoretical* **40** (jan, 2007) 995–1009.

[146] S. Hirano, Y. Lei, and S. van Leuven, *Information Transfer and Black Hole Evaporation via Traversable BTZ Wormholes*, *JHEP* **09** (2019) 070, [arXiv:1906.1071].

[147] B. Freivogel, D. A. Galante, D. Nikolakopoulou, and A. Rotundo, *Traversable wormholes in AdS and bounds on information transfer*, arXiv:1907.1314.

[148] R. Bousso, Z. Fisher, S. Leichenauer, and A. C. Wall, *Quantum focusing conjecture*, *Phys. Rev.* **D93** (2016), no. 6 064044, [arXiv:1506.0266].

[149] Z. Fu, B. Grado-White, and D. Marolf, *Traversable Asymptotically Flat Wormholes with Short Transit Times*, *Class. Quant. Grav.* **36** (2019), no. 24 245018, [arXiv:1908.0327].

[150] J. Maldacena and A. Milekhin, *SYK wormhole formation in real time*, arXiv:1912.0327.

[151] M. Headrick, V. E. Hubeny, A. Lawrence, and M. Rangamani, *Causality and holographic entanglement entropy*, *Journal of High Energy Physics* **2014** (Dec, 2014).

[152] A. C. Wall, *The Generalized Second Law implies a Quantum Singularity Theorem*, *Class. Quant. Grav.* **30** (2013) 165003, [arXiv:1010.5513]. [Erratum: Class. Quant. Grav.30,199501(2013)].

[153] M. Melvin, *Pure magnetic and electric geons*, *Phys. Lett.* **8** (1964) 65–70.

[154] R. Emparan and M. Gutperle, *From p-branes to fluxbranes and back*, *JHEP* **12** (2001) 023, [hep-th/0111177].

[155] D. Marolf, H. Maxfield, A. Peach, and S. F. Ross, *Hot multiboundary wormholes from bipartite entanglement*, *Class. Quant. Grav.* **32** (2015), no. 21 215006, [arXiv:1506.0412].

[156] D. Berenstein, *Quenches on thermofield double states and time reversal symmetry*, *Phys. Rev. D* **100** (2019), no. 6 066022, [arXiv:1906.0829].

[157] G. J. Galloway, *Maximum principles for null hypersurfaces and null splitting theorems*, *Annales Henri Poincare* **1** (2000) 543–567, [math/9909158]. Theorem 4.1.

[158] P. Candelas and D. J. Raine, *General-relativistic quantum field theory: An exactly soluble model*, *Phys. Rev. D* **12** (Aug, 1975) 965–974.

[159] J. S. Dowker and R. Critchley, *Effective lagrangian and energy-momentum tensor in de sitter space*, *Phys. Rev. D* **13** (Jun, 1976) 3224–3232.